



A new odontocete (toothed cetacean) from the Early Miocene of Peru expands the morphological disparity of extinct heterodont dolphins

Journal:	<i>Journal of Systematic Palaeontology</i>
Manuscript ID	Draft
Manuscript Type:	Original Article
Keywords:	Cetacea, Odontoceti, heterodont, Miocene, Burdigalian, Peru
Note: The following files were submitted by the author for peer review, but cannot be converted to PDF. You must view these files (e.g. movies) online.	
Lambert et al_supplementary information.nex	

SCHOLARONE™
Manuscripts

1
2
3 **A new odontocete (toothed cetacean) from the Early Miocene of Peru**
4 **expands the morphological disparity of extinct heterodont dolphins**
5
6
7

8 Olivier Lambert^{a*}, Christian de Muizon^b, Elisa Malinverno^c, Claudio Di Celma^d,
9 Mario Urbina^e and Giovanni Bianucci^f
10
11

12
13 ^a*D.O. Terre et Histoire de la Vie, Institut Royal des Sciences Naturelles de Belgique,*
14 *Brussels, Belgium;* ^b*CR2P UMR 7207, (MNHN, CNRS, UPMC, Sorbonne-*
15 *Université), Muséum national d'Histoire naturelle, Département Origines et*
16 *Évolution, Paris, France;* ^c*Dipartimento di Scienze dell'Ambiente e della Terra,*
17 *Università di Milano-Bicocca, Milan, Italy;* ^d*Scuola di Scienze e Tecnologia,*
18 *Università di Camerino, Camerino, Italy;* ^e*Departamento de Paleontología de*
19 *Vertebrados, Museo de Historia Natural-UNMSM, Lima, Peru;* ^f*Dipartimento di*
20 *Scienze della Terra, Università di Pisa, Pisa, Italy*
21
22
23
24
25
26
27

28 *Corresponding author. Email: olivier.lambert@naturelsciences.be
29
30
31
32
33
34
35
36
37
38
39
40
41
42
43
44
45
46
47
48
49
50
51
52
53
54
55
56
57
58
59
60

1
2
3
4
5 A key step of the evolutionary history of Odontoceti (echolocating toothed cetaceans)
6 is the transition from the ancestral heterodont condition - characterized by the
7 presence of double-rooted cheek teeth bearing accessory denticles - to the homodont
8 dentition displayed by most extant odontocete species. During the last decades, new
9 finds and the reassessment of specimens in collections revealed an increased
10 morphological disparity among these Oligo-Miocene heterodont odontocetes. Based
11 on a partly articulated skeleton found in late Early Miocene (Burdigalian, 18.8-18.0
12 Ma, based on silicoflagellate assemblage) beds of the Chilcatay Formation from the
13 new marine vertebrate locality of Roca Negra, Pisco Basin, southern coast of Peru, we
14 describe a new genus and species of heterodont odontocete, *Inticetus vertizi*, in the
15 new family Inticetidae. This large dolphin is characterized, among others, by: a long
16 and robust rostrum bearing at least 18 teeth per tooth row; the absence of procumbent
17 anterior teeth; a high number of large, broad-based accessory denticles in double-
18 rooted posterior cheek teeth; a reduced ornamentation of dental crowns; the styliform
19 process of the jugal being markedly sturdy; a large fovea epitubaria on the periotic,
20 with a correspondingly voluminous accessory ossicle of the tympanic bulla; and a
21 shortened tuberculum of the malleus.
22

23
24
25
26
27
28
29
30
31
32
33 Several phylogenetic analyses (with and without molecular constraint, with
34 and without down-weighting of homoplastic characters) yielded contrasted results,
35 with *Inticetus* falling either as a stem Odontoceti or as an early branching member of
36 a large Platanistoidea clade.
37

38
39
40
41
42
43
44
45
46
47
48
49
50
51
52
53
54
55
56
57
58
59
60
With its large size, robust rostrum, unusual dental morphology, and the
absence of conspicuous tooth wear, *Inticetus* increases the morphological and
ecological disparity of Late Oligocene - Early Miocene heterodont odontocetes.
Finally, this new taxon calls for caution when attempting to identify isolated cetacean
cheek teeth, even at the suborder level.

[http://zoobank.org/urn:lsid:zoobank.org:pub:5B306B49-EB1B-42F9-B755-
B0B05B4F938F](http://zoobank.org/urn:lsid:zoobank.org:pub:5B306B49-EB1B-42F9-B755-B0B05B4F938F)

Keywords: Cetacea; Odontoceti; heterodont; Miocene; Burdigalian; Peru

Introduction

A vast majority of modern odontocetes (echolocating toothed cetaceans) are characterized by a roughly homodont and polydont dentition, resulting from the progressive simplification and multiplication of the teeth of their ancestors, in relation with major changes in predation techniques and food processing (Fordyce 1982; Uhen 2009; Armfield *et al.* 2013). Nevertheless, many Oligocene and Miocene odontocetes retain the plesiomorphic condition of double-rooted cheek teeth bearing accessory denticles. For a long time fragmentary fossil specimens displaying various degrees of heterodonty were generally referred to the waste-basket family Squalodontidae, often in the genus *Squalodon* (Fordyce & Muizon 2001; Marx *et al.* 2016; see for example the Paleobiology Database section on *Squalodon*, mostly compiled by M. D. Uhen, mentioning 23 species in the genus). The discovery and description of better-preserved specimens lead to the definition of several other families, highlighting a high morphological disparity and a complex evolutionary transition to crown odontocetes; heterodont odontocetes are now distributed in at least seven families: Agorophiidae, Ashleycetidae, Patriocetidae, Simocetidae, Squalodontidae, Waipatiidae, and Xenorophidae (see Whitmore & Sanders 1976; Fordyce 1981, 1994, 2002; Muizon 1991; Uhen 2008b; Geisler *et al.* 2014; Sanders & Geisler 2015; Godfrey *et al.* 2016). Among them, only Squalodontidae and Waipatiidae have been identified as members of the crown Odontoceti clade, in the superfamily Platanistoidea (e.g., Muizon 1991, 1994; Fordyce 1994; Tanaka & Fordyce 2016). However, such attributions did not yet reach a consensus (see Geisler *et al.* 2011; Aguirre-Fernández & Fordyce 2014; Tanaka & Fordyce 2014; Sanders & Geisler 2015; Godfrey *et al.* 2016). Furthermore, the familial affinities of several genera of heterodont and homodont, Late Oligocene - Early Miocene odontocetes are still debated (e.g., *Neosqualodon*, *Papahu*, *Prosqualodon*, and *Squaloziphius*), some of them even falling among stem Odontoceti in some analyses and among crown Odontoceti in others (e.g., Muizon 1991; Fordyce 1994; Geisler *et al.* 2011; Aguirre-Fernández & Fordyce 2014; Godfrey *et al.* 2016; Tanaka & Fordyce 2016; Lambert *et al.* in press).

In addition to the fossil-rich beds of the late Neogene Pisco Formation, the Pisco Basin, southern coast of Peru, includes older, marine vertebrate-bearing strata

1
2
3 ranging from the late Middle Eocene to the earliest Middle Miocene (Muizon &
4 DeVries 1985; Dunbar *et al.* 1990; DeVries 1998; Bianucci *et al.* 2016a). Dated from
5 the latest Oligocene - earliest Middle Miocene, the Chilcatay Formation already
6 yielded the remains of several homodont odontocetes (including kentriodontid-like
7 delphinidans, physeteroids, at least two squalodelphinids, and a member of an
8 unnamed new family), in a relatively poorly constrained stratigraphic context
9 (Lambert *et al.* 2014, 2015; Bianucci *et al.* 2015). Some years ago, the new fossil
10 locality of Roca Negra was discovered in the southern part of the basin, displaying
11 vast outcrops of the Chilcatay Formation. Based on an articulated cetacean skeleton,
12 including the cranium with ear bones, mandibles, teeth, sternum, vertebrae, and ribs,
13 discovered in late Early Miocene (Burdigalian) beds of this locality, we describe a
14 new genus and species of large heterodont odontocete. We compare the new taxon to
15 other forms from the Oligocene and Early Miocene worldwide, we investigate its
16 phylogenetic relationships, and we discuss the impact of this new genus and species
17 on our understanding of the stem-crown Odontoceti transition.
18
19
20
21
22
23
24
25
26
27
28
29

30 **Material and methods**

31 **Institutional abbreviations**

32
33
34 **MUSM:** Museo de Historia Natural, Universidad Nacional Mayor de San Marco,
35 Lima, Peru; **OU:** Geology Museum, University of Otago, Dunedin, New Zealand;
36
37 **ZMT:** Fossil mammals catalogue, Canterbury Museum, Christchurch, New Zealand.
38
39
40
41

42 **Anatomical terminology**

43 For cranial anatomical terminology we generally follow Mead & Fordyce (2009) and
44 we mention references when other terms are preferred. The specimen described here
45 being markedly polydont, teeth posterior to canines are named cheek teeth without
46 any attempt to distinguish between premolars and molars (e.g., Fordyce 1994). The
47 terminology for vertebrae follows Tanaka & Fordyce (2014). Due to the
48 incompleteness of the vertebral column, post-cervical vertebrae are tentatively
49 identified with Roman, instead of Arabic numbers.
50
51
52
53
54
55
56

57 **Systematic palaeontology**

Order **Cetacea** Brisson, 1762

Pelagiceti Uhen, 2008a

Neoceti Fordyce & Muizon, 2001

Suborder **Odontoceti** Flower, 1867

Inticetidae fam. nov.

Type genus. For now, only *Inticetus* gen. nov. is included in the family.

Diagnosis. As for the only included genus.

Inticetus gen. nov.

Type and only included species. *Inticetus vertizi* gen. et sp. nov.

Derivation of name. From *Inti*, the sun deity of the Inca Empire, and *cetus*, whale in Latin, for the typical, subcircular and ray-like arrangement of accessory denticles in posterior cheek teeth of MUSM 1980, reminiscent of artistic reconstructions of the rising sun.

Diagnosis. As for the only included species.

Inticetus vertizi gen. et sp. nov.

(Figs 3-25)

Holotype. MUSM 1980, partial skeleton including the cranium with ear bones, mandibles, teeth, cervical, thoracic, lumbar, and caudal vertebrae, two sternal elements, and ribs. The specimen was discovered by Á. Suárez Vértiz in 2008; the cranium, mandibles, and a few vertebrae were collected by a team lead by M. Urbina in February 2010; A. Altamirano, E. Díaz, G. Bianucci, O. Lambert, C. de Muizon, K. Post, and M. Urbina collected the rest of the skeleton on November 10, 2011.

1
2
3 **Type locality.** Roca Negra locality, Pisco Basin, 65 km SSE to the city of Ica and 2.4
4 km west to the Ica River (Fig. 1). Geographic coordinates: S14°39'02.6"-
5 W75°38'53.9"; elevation: 383 m.
6
7

8
9
10 **Type horizon.** The holotype of *Inticetus vertizi* MUSM 1980 was discovered in
11 layers of the Chilcatay Formation, the latter being dated based on diatoms,
12 foraminifers, and molluscs from the latest Oligocene - earliest Middle Miocene
13 (Macharé *et al.* 1988; Dunbar *et al.* 1990; DeVries 1998, 2001). The stratigraphic
14 section of the Roca Negra outcrop is dominated by fine- and medium-grained
15 sandstones with minor amounts of silts and two 0.2 m-thick volcanic ash layers (Fig.
16 2). By combining data from silicoflagellates (*Naviculopsis ponticula* zone of Bukry
17 1981) found in a sample located about 5.5 m above MUSM 1980 and diatoms from
18 beds containing *N. ponticula spinosa* in another section of the Chilcatay Formation in
19 the Pisco Basin (Pampa Chilcatay; Macharé *et al.* 1998), a time interval between 18.8
20 and 18.0 Ma can be provided, corresponding to the late early Burdigalian (late Early
21 Miocene) (see Biostratigraphy section below and Appendix 1).
22
23
24
25
26
27
28
29

30
31 **Derivation of name.** Honouring the discoverer of the holotype MUSM 1980, the
32 Peruvian artist Álvaro Suárez Vértiz.
33
34

35
36 **Diagnosis.** *Inticetus vertizi* differs from other odontocetes in the following possible
37 autapomorphies: presence of a high rim around the internal acoustic meatus of the
38 periotic; large fovea epitubaria on the periotic with a correspondingly voluminous
39 accessory ossicle of the tympanic bulla and short anterior bullar facet (also present in
40 physeteroids); shortened tuberculum of the malleus (also present in
41 eurhinodelphinids, physeteroids, and ziphiids); reduced ornamentation of dental
42 crowns; and relatively high number of large, broad-based accessory denticles (up to
43 four mesial and five distal denticles) in posterior cheek teeth (also present in
44 *Neosqualodon*). Other derived characters compared to early odontocetes include:
45 bony nares being located far posterior to level of antorbital notch and roughly vertical;
46 nasals being anteroposteriorly short; the intertemporal constriction being most likely
47 absent; lower tooth count being at least 18 teeth. Additional, probably plesiomorphic
48 characters include: absence of a pterygoid-maxilla contact on the palate; styliiform
49 process of the jugal being markedly sturdy; sutural contact of the jugal with the
50
51
52
53
54
55
56
57
58
59
60

zygomatic process of the squamosal being long; presence of a deep notch separating the basioccipital crest from the falcate process of the exoccipital; posterior increase of the height of the mandible being progressive; and incisors being not procumbent.

Description

Ontogeny

No vertebra from any region of the column could be found with a detached epiphysis. With suture lines between centrum and epiphysis occasionally clearly visible in some thoracic, lumbar, and anterior caudal vertebrae (intermediate between states C and D of Galatius & Kinze 2003), we consider this individual as young to fully adult, an interpretation further supported by the robust aspect of all cranial bones and the thick layer of cement covering dental roots.

Total body length estimate

To estimate the total body length (tbl) of MUSM 1980, we used two equations provided by Pyenson & Sponberg (2011) based on the bizygomatic width (bzw, estimated at 36 cm for MUSM 1980): one equation established for stem Odontoceti " $\log(\text{tbl}) = 0.92 * (\log(\text{bzw}) - 1.72) + 2.68$ " and the other for stem Platanistoidea " $\log(\text{tbl}) = 0.92 * (\log(\text{bzw}) - 1.51) + 2.49$ ". The two calculations yielded similar results for tbl, 3.38 and 3.41 m. This is slightly larger than the estimate for *Prosqualodon davidis* calculated by Pyenson & Sponberg (2011), in the upper part of the range for the extant delphinid *Tursiops truncatus* (Wells & Scott 1999). Measurements taken in the field indicate a length of the skeleton (from the apex of the rostrum to the last caudal vertebra) of about 4 m. Significantly higher than the values obtained using the Pyenson & Sponberg (2011) equations, such a value could be due, at least in part, to the slight disarticulation of the skeleton, which probably resulted in a minor shift of the skull compared to the postcranial skeleton (see below).

Skull

The cranium and mandible underwent some degree of deformation. On the one hand, the finely preserved rostrum and mandibles are moderately obliquely compressed, as indicated by the dorsal part of the right premaxilla being slightly below the left

1
2
3 premaxilla and the right mandible being markedly lower than the left in the
4 symphyseal region (Figs 3-5). On the other hand, the neurocranium is dorsoventrally
5 flattened, as indicated by the marked dorsoventral crushing of the left orbit, temporal
6 fossa, and mandibular ramus (Figs 4-8). In addition, the dorsal surface of the
7 neurocranium was exposed for some time at the surface of the outcrop. As a
8 consequence, bones of the facial region and supraoccipital shield are heavily worn
9 and partly dislocated (Fig. 3), rendering the interpretation of most sutures and other
10 morphological features from these regions dubious; this condition contrasts with the
11 much better preservation state of the basicranium. Most of the teeth are still in situ or
12 only slightly shifted from their original position in alveoli; the distance from the
13 original position is higher in upper teeth from the right side and all the lost/detached
14 teeth originate from the upper jaws. The left mandibular condyle is in connection with
15 the left mandibular fossa of the squamosal and the left lacrimojugal complex is
16 slightly shifted posteroventrally (Fig. 6). The right orbit is lost and the right part of the
17 basicranium is severely damaged.

28 29 30 **Cranium**

31 **General morphology.** The relatively large cranium is characterized by an elongated
32 rostrum, making 64 per cent of the condylobasal length (Table 1). The anterior part of
33 the rostrum is robust and the progressive posterior widening of the latter leads to a
34 broad rostrum base. The upper tooth count is at least 15, as seen on the right side
35 (three incisors, one canine, and at least 11 cheek teeth; see details below); this is at
36 least five teeth more than the basilosaurid condition, corresponding thus to moderate
37 polydonty. The mesorostral groove is widely open at rostrum base and the bony nares
38 are located far (c. 135 mm) posterior to the level of the antorbital notch. Whereas the
39 dorsoventral extent of the temporal fossa cannot be assessed, the fossa is
40 anteroposteriorly long (length estimated to 140-150 mm on the left side), longer than
41 the partly dislocated corresponding orbit.

42
43
44
45
46
47
48
49
50
51 **Premaxilla.** The anterior part of the rostrum is made of the premaxillae alone. Each
52 premaxilla bears alveoli for three non-procumbent, ventrolaterally directed incisors.
53 The ventral margin of each premaxilla converges anterodorsomedially, and the
54 maximum transverse width and dorsoventral height of each premaxilla in this region
55 is at the level of I³, with an oblique dorsomedial to ventrolateral width of more than
56
57
58
59
60

1
2
3 44 mm on the right side (Fig. 4). Right and left premaxillae are not fused
4 dorsomedially above the mesorostral groove, but they were probably originally either
5 contacting each other or only leaving a narrow medial gap for the anterior half of the
6 rostrum. In this region, the dorsolateral surface of each premaxilla is pierced by a
7 series of small to medium sized foramina (at least seven on the right side and six on
8 the left side), followed anteriorly by sulci of varying length. The dorsomedialmost
9 sulcus is the longer on each side (more than 80 mm). Visible throughout most of the
10 rostrum, the premaxilla-maxilla suture leaves from the ventrolateral margin of the
11 rostrum between I³ and the upper canine in a posterodorsomedial direction; the dorsal
12 and lateral exposures of the premaxilla decrease thus until about mid-length of the
13 rostrum. From this level, each premaxilla widens progressively posteriorly.
14 Unfortunately, the dorsal surface of the proximal part of the rostrum is damaged, and
15 sutures are more difficult to follow, especially on the right side. The convex lateral
16 margin of the left premaxilla posterior to the level of the antorbital notch is an
17 indication for the presence of a long and wide premaxillary sac fossa with a roughly
18 straight medial margin. However, no premaxillary foramen and associated sulci could
19 be detected. Left and right premaxillae are widely spaced anterior to the bony nares.
20 This wide dorsal opening of the mesorostral groove (c. 47 mm anterior to the
21 presphenoid) may have been slightly exaggerated by the dorsoventral flattening of
22 that region of the cranium. Based on the preserved parts, each premaxilla is wide in
23 front of the nasal and it most likely contacted the corresponding frontal (Fig. 3).
24
25
26
27
28
29
30
31
32
33
34
35
36
37
38
39

40 **Maxilla.** The upper surface of the maxilla is only well preserved along the anterior
41 half of the rostrum; its dorsal exposure progressively widens posteriorly due to the
42 oblique maxilla-premaxilla suture (Fig. 3). In this region, the lateral margin of the
43 maxilla is marked by notches corresponding to the wide spaces between maxillary
44 alveoli housing crowns of mandibular teeth (shallow embrasure pits). On the left side,
45 the six anteriormost maxillary alveoli (including the canine and five cheek teeth)
46 extend on a length of 210 mm; those alveoli open ventrolaterally. A laterally located
47 embrasure pit for the right C₆ is still visible between C⁵ and C⁶, whereas the
48 embrasure pit for C₇ extends less dorsolaterally between C⁶ and C⁷, and more
49 posterior embrasure pits (starting at C₈) are medial to the upper tooth row. In relation
50 to this pattern, the spacing between maxillary alveoli decreases progressively
51 posteriorly, from a distance of 16.4 mm between right C⁷ and C⁸ to less than 3 mm
52
53
54
55
56
57
58
59
60

1
2
3 between C¹⁰ and C¹¹. If present, more posterior maxillary alveoli are hidden by the
4 mandible.
5

6 The antorbital notch is better preserved on the left side, where it is followed
7 posteriorly by a wide sulcus (Fig. 3). The lateralmost part of the maxilla in the
8 supraorbital region is probably missing on the two sides, but less incomplete on the
9 left. The left maxilla reaches posteriorly the level of the occipital condyles. However,
10 this projection posterolateral to the supraoccipital shield is most likely exaggerated by
11 the dorsoventral crushing of the neurocranium. The presence of a left posterior dorsal
12 infraorbital foramen is suspected several centimeters posterolateral to the left
13 premaxilla.
14
15
16
17
18
19

20 On the palate, the joined maxillae form a wide, roughly flat surface anterior to
21 the palatines, well demarcated from the more posterodorsolateral regions by
22 posteriorly converging palatal ridges (Fig. 5). Each maxilla is pierced by at least one
23 foramen a short distance anterior to the anterolateral corner of the palatine.
24
25
26
27

28 **Presphenoid.** At the posterior end of the mesorostral groove, the ossified portion of
29 the presphenoid (= mesethmoid in many previous works; see Ichishima 2016) is short,
30 ending c. 90 mm posterior to the level of the antorbital notch, and transversely wide.
31 The preserved part of the nasal septum is surprisingly wide, broader than the
32 adjoining narrow bony naris (Fig. 3). Such a wide separation of the bony nares may
33 also be linked to the dorsoventral crushing and abrasion of this region, with the
34 artificial exposure of a more ventral region of the septum.
35
36
37
38
39
40

41 **Vomer.** The vomer could not be detected in the mesorostral groove. Ventrally, it
42 appears between the maxillae from a level 60 mm anterior to the palatine, widening
43 moderately anteriorly (Fig. 5). Posterior to the choanae, an undulating transverse
44 suture is interpreted as the vomer-basisphenoid suture.
45
46
47
48

49 **Nasal.** Two small, somewhat nodular bones posterior to the nasal septum and at a
50 longitudinal level just posterior to the tip of the zygomatic process of the squamosal
51 most likely correspond to the nasals (Fig. 3). Each nasal sends an anterolateral
52 projection, seemingly more pointed on the right side. Although the posterior portion
53 of the nasal is dorsoventrally thin, this may be a consequence of the superficial
54 abrasion of the dorsal surface.
55
56
57
58
59
60

1
2
3
4
5 **Frontal.** The vertex of the cranium being too damaged, no specific features of the
6 dorsal exposure of the frontals can be detected, except that they may have been
7 anteroposteriorly longer than the nasals.
8

9
10 Preserved on both sides, the massive and roughly vertical postorbital process
11 of the frontal has a dorsoventral height greater than 37 mm (Figs 4, 6). Due to the
12 shift of the lacrimojugal complex and the partial preservation of the maxilla and
13 frontal in the left antorbital region, the anteroposterior length of the orbit cannot be
14 estimated. There is nevertheless no indication for a reduced size of the latter.
15
16

17
18
19 **Palatine.** The anterior portion of well-defined palatine-maxilla suture zigzags with a
20 mean lateral direction until the palatal ridge, where it turns abruptly posterolaterally
21 (Fig. 5). The anterior end of the palatine is slightly anterior to the antorbital notch and
22 60 mm anterior to the tip of the pterygoid sinus fossa.
23
24
25

26
27
28 **Pterygoid.** Only a small part of the lateral lamina of the pterygoid may be visible on
29 the right side, forming the lateral wall of the pterygoid sinus fossa (Fig. 5).
30 Considering the great distance between the fragments of pterygoid around the fossa
31 and the palatine-maxilla suture, a contact between pterygoid and maxilla on the palate
32 can be ruled out in MUSM 1980, which differs on that point from many platanistoids
33 (e.g., *Pomatodelphis*, *Platanista*, *Squalodon*, and *Zarhachis*; see Muizon 1987, 1994).
34 Anterior to the choana, the pterygoid sinus fossa is wide and relatively long, with a
35 maximum ventromedial to dorsolateral width of 56 mm and an anterior tip 50 mm
36 before the choana, just posterior to the level of the antorbital process. The thin plates
37 of pterygoids anterolaterally margining the choanae are partly dislocated and slightly
38 shifted from their original position. Although partly crushed, the posterior lamina of
39 each pterygoid is preserved until its contact with the basioccipital crest.
40
41
42
43
44
45
46
47

48
49 **Lacrimal/jugal.** In the left orbital region, the lacrimojugal complex is shifted
50 posteroventrally from its original position (Figs 4, 6). Jugal and lacrimal are probably
51 fused and make a massive bone anteriorly limiting the orbit. The base of the styliform
52 process is wide and thick, whereas the process itself becomes thinner posteriorly, yet
53 retaining a great width (24 mm wide just anterior to the zygomatic process of the
54 squamosal, for a thickness of 3 mm for the lateralmost part of the process). The
55
56
57
58
59
60

1
2
3 contact surface of the jugal with the ventral margin of the zygomatic process is long,
4 c. 40 mm.
5
6
7

8 **Supraoccipital.** The outline of the fragmented and abraded dorsomedial part of the
9 supraoccipital shield cannot be reconstructed. Best seen in posterior view (Fig. 8),
10 only the ventrolateral region is partly preserved, with both temporal crests converging
11 anterodorsomedially, corresponding to widely posteriorly open temporal fossae.
12
13
14

15
16 **Squamosal.** In lateral view, the zygomatic process is anteriorly long; the
17 supramastoid crest rising slightly anterodorsally; and a bulge located at mid-length of
18 the ventral margin corresponds to the end of the jugal-squamosal suture (Figs 4, 6).
19 The maximum dorsoventral height of the process at the level of that bulge is 41 mm.
20 Best seen in anterior view, a deep longitudinal notch marking the anterior part of the
21 ventral margin originally housed the posterior part of the styliform process of the
22 jugal. The postglenoid process is ventrally long, with a vertical height of the
23 squamosal at that level reaching 98 mm. Distinctly curved anteroventrally, the apex of
24 the process makes a robust, yet anteroposteriorly flattened blade that ends ventrally
25 before the level of the ventral margin of the exoccipital (Figs 6, 7). The medial
26 surface of the postglenoid process is slightly concave, forming a shallow depression
27 possibly corresponding to an extension of the tympanosquamosal recess. The
28 posttympanic process is not much extended anteroposteriorly and is ventrally shorter
29 than the exoccipital. At least one sternomastoideus fossa excavates the posterolateral
30 surface of the bone. The external acoustic meatus is relatively wide and transversely
31 long. Better preserved on the left side, the falciform process is a large plate
32 (maximum length = 45 mm) with deeply indented margins.
33
34
35
36
37
38
39
40
41
42
43
44
45

46 **Basisphenoid.** A posteriorly convex suture halfway between the vomer and the
47 posterior end of the basioccipital crest in the basioccipital basin is tentatively
48 interpreted as the basisphenoid-basioccipital suture (Figs 5, 7) .
49
50
51
52

53 **Basioccipital.** Low anteriorly, the relatively thin ventral margin of the basioccipital
54 crest rises abruptly posteroventrolaterally. The ventralmost part of the crest is
55 anteroposteriorly short, smoothly curving posterolaterally and then posteromedially.
56 The crest is separated from the falcate process of the exoccipital by a deep oblique
57
58
59
60

1
2
3 notch (Figs 7, 8). Left and right crests diverge markedly, limiting a widely
4 posteroventrally open basioccipital basin.
5
6
7

8 **Exoccipital.** Posteromedial to the posttympanic process of the squamosal, the
9 exoccipital is bulky. In ventral view, the cylinder-shaped paroccipital process of the
10 exoccipital is robust, with transverse and anteroposterior diameters of the left process
11 of 61.0 and 41.5 mm, respectively (Fig. 7). The ventral surface of the process bears a
12 wide articulation facet for the stylohyal. The anterior surface of the process lacks any
13 paroccipital concavity for the posterior sinus. As in basilosaurids, the falcate process
14 of the exoccipital is distinct from the basioccipital crest; it is shorter ventrally than the
15 latter. A vestigial falcate process of the exoccipital is described in a few stem
16 physeteroids, much more reduced than in MUSM 1980 (Lambert *et al.* 2016). Best
17 preserved on the right side, the jugular notch is wide and deep, with an oval outline in
18 posterior view. The occipital condyles are robust, with a short condylar neck.
19
20
21
22
23
24
25
26
27

28 **Periotic.** Only the right periotic of MUSM 1980 could be observed (Fig. 9; Table 1),
29 as the left is still in situ, dorsal to the corresponding tympanic bulla attached to the
30 basicranium. The right periotic is nearly complete; only some small fragments are
31 missing at the apex of the posterior process and along the ventral surface of the
32 anterior process just anterior to the fovea epitubaria. The facial sulcus could not be
33 completely prepared, due to the presence of the stapes lying in the sulcus,
34 posterolateral to the fenestra vestibuli (= fenestra ovalis).
35
36
37
38
39

40 The ventral surface of the anterior process is excavated by a vast and deep
41 fovea epitubaria, housing the large, detached accessory ossicle of the tympanic bulla
42 (see below). The fovea epitubaria is defined (1) laterally by an acute, thin crest, (2)
43 medially by a slightly more robust crest, (3) posteriorly by the high anterior margin of
44 the malleolar fossa, and (4) anteriorly by a prominent tuberosity. This tuberosity is
45 margined laterally by a shallow groove just medial to the acute crest mentioned
46 above. Most likely housing part of the outer lip of the tympanic, this groove turns
47 anteromedially around the tuberosity and is followed by a small, roughly circular
48 fossa interpreted as a very small anterior bullar facet, as observed in many
49 physeteroids. The roughly flat ventrolateral surface of the anterior process is exposed
50 in ventral view, marked by a series of thin grooves (at least nine); posterior grooves
51 are transversely oriented whereas more anterior grooves are anterolaterally and then
52
53
54
55
56
57
58
59
60

1
2
3 anteriorly directed. No conspicuous parabullary sulcus (*sensu* Tanaka & Fordyce
4 2014) could be identified in this region. This ventrolateral surface is separated from
5 the lateral tuberosity by a wider, shallow groove, probably corresponding to the
6 anterolateral sulcus described in *Simocetus* (Fordyce 2002; anteroexternal sulcus
7 *sensu* Tanaka & Fordyce 2014). However, it should be noted that the posterolateral
8 part of the parabullary sulcus has been illustrated as nearly continuous with the
9 anteroexternal sulcus in some odontocetes (see Tanaka & Fordyce 2016), making the
10 distinction between these two features more difficult to define.

11
12
13
14
15
16 In medial view, the anteroventral apex of the anterior process is markedly
17 projected ventrally as compared to the proximal part of the process. The medial
18 surface of the process is weakly concave in the area dorsal to the prominent
19 tuberosity.
20
21
22

23 In lateral view, the apex of the anterior process is clearly inflated as compared
24 to its base, which is markedly constricted on its dorsolateral surface just anterior to
25 the lateral tuberosity (level of anteroexternal sulcus). This feature is partly related to
26 the presence of a wide, obliquely oriented depression on the dorsal surface of the
27 bone, separating the anterior process from the pars cochlearis. The anterodorsal region
28 of the anterior process is prominent, but no anterodorsal angle is observed (area
29 smoothly rounded in lateral view).
30
31
32
33

34 As a result of its complex morphology, the outline of the transverse section of
35 the anterior process changes markedly along its longitudinal axis: this section is
36 distinctly mediolaterally wider than dorsoventrally high at its base (17.4 vs. 11 mm),
37 roughly as mediolaterally wide as dorsoventrally high at mid-length (14 vs. 13 mm),
38 and much dorsoventrally high than mediolaterally wide in its anterior section. A small
39 tubercle is located medioventrally at the contact between anterior process and pars
40 cochlearis, anteroventral to the cerebral opening for the facial canal. It is followed
41 anterodorsally by a short crest.
42
43
44
45
46
47

48 The large, subrectangular ventral surface of the lateral tuberosity is flat to
49 slightly concave. Whereas the lateral surface of the tuberosity is only separated from
50 the lateral margin of the anterior process by a smooth concavity in ventral view, the
51 posteroventral margin of the tuberosity has an angular border with the moderately
52 deep hiatus epitympanicus. The vast, oval, and posteromedioventrally facing mallear
53 fossa has a maximum diameter of c. 7 mm. The well-defined fossa incudis has a
54 maximum diameter of c. 2 mm. It is separated from the mallear fossa by another
55
56
57
58
59
60

1
2
3 small, shallower, and anteroventrolaterally facing depression. Posterior to the fossa
4 incudis is a prominent small tubercle corresponding to the anterior end of the
5 posterior bullar facet.
6
7

8 The anterior margin of the ventral opening of the facial canal (= secondary
9 facial foramen) is slightly anterior to the anterior margin of the fenestra vestibuli. The
10 outline of the fenestra vestibuli is oval. The stapedius muscle fossa is dorsally deep,
11 but it does not excavate the medial surface of the posterior process. Between the
12 hiatus epitympanicus and the anterolateral surface of the posterior process, a wide,
13 oblique ridge extends in an anteromedial direction. Marked by a series of thin
14 grooves, this ridge probably corresponds to a low articular rim (see Muizon 1987,
15 1994). Although a small break surface limits the posterolateral extent of this ridge, a
16 hook-like articular process was most likely not present.
17
18
19
20
21
22

23 Whereas the long axis of the posterior process is directed
24 posteroventrolaterally, the surface of the posterior bullar facet is roughly flat, lacking
25 any longitudinal concavity (a feature observed for example in ziphiids) and any
26 transverse convexity (a feature observed in physeteroids). The surface of the proximal
27 region is marked by four to five shallow grooves, barely reaching half the length of
28 the process. In medial view, the dorsal margin of the posterior process curves
29 smoothly posteroventrally. The distal portion of this margin is keeled for at least 14
30 mm, displaying a triangular transverse section.
31
32
33
34
35

36 In ventral view, the pars cochlearis is proportionally wide and only moderately
37 medially elevated, not taking account of the high rim defining part of the internal
38 acoustic meatus (IAM); its outline is generally rounded, except for a barely marked
39 posteromedial angle. Ventral to the IAM, the dorsoventrally wide medial surface of
40 the pars cochlearis is nearly flat. The fenestra cochleae (= fenestra rotunda) is reniform
41 to crescent shaped, with a first groove leaving dorsally from the lateralmost tip and a
42 second groove leaving dorsomedially from the medialmost tip. Between the fenestra
43 cochleae and the stapedius muscle fossa, a thick bar of bone extends anteriorly along
44 the ventromedial edge of the fenestra vestibuli and floors the medial edge of the
45 stapedius muscle fossa. This crest represents the crista interfenestralis as identified by
46 O'Leary (2010), which is generally well developed in cetaceans. As mentioned by
47 Mead & Fordyce (2009, p. 115) "in *Tursiops* ... the crista interfenestralis merges back
48 into the indistinct caudal tympanic process". The structure labelled as "cochlear crest"
49 by Fordyce (2002, fig. 15) and "caudal tympanic process" by Tanaka & Fordyce
50
51
52
53
54
55
56
57
58
59
60

1
2
3 (2015b, fig. 13) is the posterior extension of the crista interfenestralis and corresponds
4 to the lateral caudal tympanic process as defined by MacPhee (1981, p.17-18). As
5 described by O'Leary (2010), the caudal tympanic process of cetaceans is a
6
7
8
9
10
11
12
13
14
15
16
17
18
19
20
21
22
23
24
25
26
27
28
29
30
31
32
33
34
35
36
37
38
39
40
41
42
43
44
45
46
47
48
49
50
51
52
53
54
55
56
57
58
59
60
mediolaterally broad and low thickening on the posterodorsal edge of the fenestra
cochleae and represents the medial caudal tympanic process (MacPhee, 1981, p. 17
and fig. 2; Muizon *et al.* 2015, figs. 37-39, 50). The medial caudal tympanic process
is generally low or absent in odontocetes. In *Inticetus*, however, the
posterodorsolateral edge of the fenestra cochleae is bordered by a thick ridge, which
extends posterodorsally and which is separated from the crista interfenestralis. We
interpret this ridge as a medial caudal tympanic process. The lateral caudal tympanic
process (*sensu* MacPhee 1981, fig. 2), which, in cetaceans, merges with the posterior
extension of the crista interfenestralis, is poorly developed in *Inticetus*: the crista
interfenestralis lacks a distinct posteroventral angle and only bears a tiny spine
directed posteroventrolaterally above the stapedius muscle fossa.

The small and transversely elongated aperture for the cochlear canaliculus (=
cochlear aqueduct) (2.5 x 1.2 mm) opens mediodorsally, but is more ventral than the
ventromedial margin of the IAM. Its dorsal margin is part of a prominent area
between this aperture and the aperture for the vestibular aqueduct (= endolymphatic
duct). Much larger (4.6 x 2.7 mm), the latter is closer to the IAM. In the IAM, the
large and anteriorly pointed opening for the facial canal (3.5 mm of diameter) is more
anterior than the tractus spiralis foraminosus, giving the IAM an anterolaterally
elongated outline. The thick transverse crest separating the opening for the facial
canal from the tractus spiralis foraminosus is moderately elevated, distinctly lower
than the surrounding dorsal surface of the periotic.

On the anterior flank of the transverse crest, posterior to the dorsal aperture of
the facial canal, is a small, circular depressed area, which probably represents the
anterior meatal pit, variably present in *Tursiops* (Mead & Fordyce 2009, p.112 and
fig. 25). On the posterior edge of the transverse crest is a large foramen singulare,
which was apparently partly open posteriorly. The margins of the IAM form a high
rim, thick at its base, around the tractus spiralis foraminosus; such a tube-like
mediodorsal extension of the tractus differs from the cochlear spine observed in the
ziphiids *Berardius* and *Ninoziphius*, both for its shape and position. A similar
condition is observed in *Remingtonocetus* and several protocetids (e.g., *Carolinacetus*
and *Georgiacetus*; Geisler *et al.* 2005), as well as in the tooth-bearing mysticete

1
2
3 *Mammalodon* (Fitzgerald 2010, fig. 23b); this character may thus be primitive among
4 neocetes, although it is not present in basilosaurids (see Kellogg 1936; Luo &
5 Gingerich 1999) and other archaic odontocetes for which this region is observable
6 (Park *et al.* 2016; pers. obs.).
7
8

9
10 The dorsal process forms a low dome with a top 10 mm distant from the
11 aperture for the vestibular aqueduct in a posterolateral direction. A small foramen
12 along the lateral surface of the dome may correspond to the posteroexternal foramen
13 identified medial to the incipient articular rim in *Waipatia* (Fordyce 1994). Medial to
14 the top of the dorsal process is another small opening, possibly a foramen too.
15
16
17
18

19
20 **Tympanic bulla.** The left tympanic bulla was kept in situ in the basicranium, where it
21 is probably somewhat anterodorsally shifted from its original position (Figs 5, 7); a
22 few measurements were taken on this side (Table 1), but most observations come
23 from the detached right tympanic (Fig. 10). The latter is nearly complete: only
24 fragments of the outer lip, dorsomedial fragments of the sigmoid process, the anterior
25 part of the posterior process, and a tiny part of the incipient anterior spine are missing.
26 The accessory ossicle is detached from the outer lip. In addition, the region of the
27 sigmoid process is slightly crushed over the conical process and the anterior part of
28 the outer lip is shifted slightly medially and separated from the posterior part of the lip
29 by a vertical break.
30
31
32
33
34
35

36 In ventral view, inner and outer posterior prominences have the same posterior
37 extent; the inner prominence is more pointed and somewhat narrower. A slight and
38 rather irregular ventral keel marks the ventral surface of the latter, extending
39 anteriorly on c. two-fifths of the length of the bone. The median furrow is wide and
40 shallow for its whole extent, being barely visible 8 mm from the anterior tip of the
41 bone. Based on the observation of the dorsoventrally thin anterior section, the anterior
42 spine was most likely incipient, forming a narrow and thin plate associated to a
43 distinct anterolateral concavity.
44
45
46
47
48

49 In medial view, the ventral margin of the involucrum is convex and somewhat
50 irregular, with a slight notch at the posterior fourth of its length. The dorsal margin
51 rises abruptly from the incipient anterior spine, reaching a shelf that rises only slightly
52 posterodorsally. The medial and dorsal surfaces of the involucrum are crossed by a
53 series of transverse grooves. In dorsal view, one of these grooves corresponds to a
54
55
56
57
58
59
60

1
2
3 clear step at the anterior third of the length of the bone, but this abrupt transverse
4 widening is not visible in medial view.
5

6 In lateral view, although the outer lip is somewhat damaged its original dorsal
7 extent was not much greater than the preserved condition. The lateral furrow is partly
8 obscured by hardened sediment. The sigmoid process is located high along the outer
9 lip and its posteroventral margin makes a smooth open curve, lacking any
10 posteroventral corner. Partly hidden by the sigmoid process, the conical process is
11 massive and transversely wide. In posterior view, the elliptical foramen is widely
12 open and vertically elongated.
13

14 On the posterior process, the surface of the facet for the posterior process of
15 the periotic faces posteromediodorsally. Its medial region is marked by a wide and
16 shallow, posterolaterally directed groove, perfectly matching a low ridge in the medial
17 part of the posterior bullar facet of the periotic. On the lateral part of the posterior
18 process, either some small fragments of the basicranium are attached (possibly
19 elements of the posterior meatal crest), or the surface of contact with the basicranium
20 is damaged.
21

22 The detached accessory ossicle is large, dorsoventrally flattened, and slightly
23 elongated (maximum length of 13.0 mm, including a fragment of outer lip attached,
24 maximum transverse width of 11.5 mm, and maximum dorsoventral thickness of 6.6
25 mm) (Fig. 9). Its outline is subcircular in ventral view (without the fragment of outer
26 lip) and oval in medial view. Positioned on the periotic, it projects
27 anteromedioventrally.
28

29
30
31
32
33
34
35
36
37
38
39
40
41 **Malleus.** Apart from fragments of the anterior and posterior facets for the incus and
42 the distal part of the anterior process, the right malleus of MUSM 1980 is finely
43 preserved (Fig. 11). Total height in posteroventromedial view is 8.0 mm, including
44 5.1 mm for the articular head (bearing the facets for the incus). The tuberculum is thus
45 markedly reduced compared to other odontocetes except eurhinodelphinids,
46 physeteroids, and ziphiids (Muizon 1985; Lambert 2005; Bianucci *et al.* 2010).
47 Maximum width of the bone across the articular head is 6.8 mm, including 4.9 mm
48 for the joined anterior and posterior facets. The posterior facet is slightly higher and
49 transversely narrower than the anterior facet. On the same side as the anterior facet,
50 the tuberculum bears the well-defined muscular process (for insertion of tendon for
51 muscle tensor tympani); the latter is lower than the manubrium (the vertical being
52
53
54
55
56
57
58
59
60

1
2
3 taken along the line separating anterior and posterior facets), a condition reminiscent
4 of platanistoids (e.g., *Notocetus*, *Pomatodelphis*, and *Squalodelphis*; Muizon 1985,
5 1987) and differing from delphinidans, physeteroids, and ziphiids. At the top of the
6 tuberculum, the manubrium makes a massive cone. The base of the broken anterior
7 process is high relative to the posterior facet.
8
9

10
11
12
13 **Stapes.** The small bone preserved in the facial sulcus of the right periotic
14 posterolateral to the fenestra vestibuli is most likely the right stapes (Fig. 9). Apart
15 from the oval umbo visible in anteroventral view, no further morphological features
16 can be observed.
17
18

20 21 **Mandibles**

22 Although the symphyseal portion of the two mandibles is finely preserved, due to
23 dorsoventral compression both rami are more fragmented and, for the better-preserved
24 left ramus, partly obscured by the lacrimojugal complex and squamosal. As a result,
25 the dorsal outline of the ramus could not be reconstructed.
26
27

28 The long symphyseal portion of the mandible makes 44 per cent of the total
29 length, ending at a level between C₆ and C₇ (Fig. 5; Table 1). Right and left mandibles
30 are not ankylosed and the flat ventral part of the symphyseal surface is visible along
31 the ventrally shifted right mandible. In lateral view the ventral margin of the mandible
32 makes a straight line for most of its length, rising abruptly anterodorsally from the
33 level of I₂. The ventromedial margin of each mandible is marked by a longitudinal
34 crest for 30 mm distally. Numerous mental foramina are observed on each side,
35 followed anteriorly by sulci; a total of about 13-14 foramina are counted on the right
36 side, with anterior foramina concentrated along the ventral margin of the bone and
37 more posterior foramina rising posterodorsally. Mental foramina extend posteriorly
38 beyond the level of C¹¹, as seen on the right side.
39
40
41
42
43
44
45
46
47

48 Matching tooth counts on the upper jaw, alveoli for three lower incisors and
49 one canine are identified, with I₁ being located anterior to I¹. Posterior to the lower
50 canine, alveoli for right cheek teeth C₁-C₉ are visible in lateral view (Fig. 4), whereas
51 alveoli for right C₇-C₁₄ are visible in medial view. The total lower tooth count is thus
52 at least 18 teeth. The alveolus for I₁ opens dorsally and slightly anteriorly, but it does
53 not correspond to a procumbent tooth. Alveoli for more other teeth open dorsally and
54 slightly laterally. Whereas anterior lower teeth are widely spaced, alternating with
55
56
57
58
59
60

1
2
3 upper teeth, spacing decreases from the level of C₇; from C₈ to C₁₄, interalveolar
4 space is highly reduced, with crowns of succeeding teeth nearly contacting each other.
5 Although the left angular process is fragmented and titled under the mandibular
6 condyle, its extent indicates that the condyle was originally at some distance from the
7 ventral margin of the mandible, differing on this point from physeteroids. The
8 mandibular condyle is robust; its marked lateral projection (27 mm) may have been
9 exaggerated due to partial dislocation. The outline of the left coronoid process is
10 visible in medial view. This process rises only progressively and moderately
11 posterodorsally. The anterior and anterodorsal margin of the enlarged mandibular
12 foramen is preserved on both sides.
13
14
15
16
17
18
19

20 21 **Teeth**

22 As detailed above, the upper dental formula is three incisors, one canine, and more
23 than 11 cheek teeth, totalling more than 15 teeth, and the lower dental formula is three
24 incisors, one canine, and at least 14 cheek teeth, totalling at least 18 teeth.
25
26
27
28

29
30 **Incisors.** The right I¹ is detached (Fig. 12A-F) and all other incisors are in situ in the
31 premaxillae and mandibles (Figs 13-15). All incisors are moderately curved, with the
32 root projecting distolingually; for in situ teeth the long axis of the crown is
33 approximately vertical. The root is considerably longer than the crown (Table 2). The
34 height of the conical crown increases slightly posteriorly along the incisor row and the
35 mesiodistal diameter at crown base is slightly greater in upper incisors as compared to
36 lower incisors. When available, the labiolingual diameter at crown base is lower than
37 the mesiodistal diameter. The crown of all the incisors bears a clear mesial keel; the
38 distal keel is less distinct, constituted by a slightly more developed longitudinal ridge
39 as compared to the rest of the crown. None of the keels is serrated. All surfaces of the
40 nearly smooth enameled crown are ornamented by slightly undulating, low
41 longitudinal ridges. In I¹, the ornamentation is slightly more conspicuous along the
42 lingual and distolingual surfaces and towards crown base, most likely due to
43 differential abrasion wear.
44
45
46
47
48
49
50
51
52

53 Along a break section close to the root-crown boundary of right I², a thick
54 layer of cement (c. 0.5 mm) is measured. Additionally, the root of right and left I¹ is
55 marked by a distinct mesial bulge close to the root-crown boundary.
56
57
58
59
60

1
2
3 **Canines.** The right upper canine is detached, with the lingual surface damaged (Fig.
4 12G-L) and all other canines are in situ in the maxillae and mandibles (Figs 13-15).
5 The root of the right upper canine is proportionally slightly shorter, stockier than the
6 root of I¹. No significant size differences are noted for canine crowns as compared to
7 incisors, and the labiolingual diameter at crown base is similarly lesser than the
8 mesiodistal diameter (Table 2). As in incisors, the mesial keel is somewhat more
9 conspicuous than the distal keel.
10
11
12
13
14
15

16 **Cheek teeth.** Antermost cheek teeth do not differ significantly from canines. From
17 C¹ and C₁, the mesiodistal diameter at crown base increases progressively posteriorly,
18 with the maximum size attained in C¹⁰ (C¹¹ incomplete) and C₉ (decrease of size in
19 C₁₀ and next lower teeth partly obscured). In a similar way, the height of the crown
20 increases until C⁵ (more posterior upper cheek teeth obscured) and, in a less regular
21 way along the lower row, until C₁₀ (C₁₁ obscured) (Table 2). For the better observable
22 lower tooth rows, the mesiodistal diameter at crown base becomes greater than crown
23 height in the interval between C₅ and C₉, with a ratio between the two measurements
24 of 0.94 in C₅, 1.72 in C₉, and 1.60 in C₁₀.
25
26
27
28
29
30

31 Along the upper tooth row, a tiny accessory denticle may have occurred at the
32 base of the distal keel of C⁴ (area slightly damaged) (Fig. 14). On the left C⁵ (better-
33 preserved than the right; Fig. 15), a slight bulge at the base of the mesial keel bears
34 two tiny denticles, whereas the widened base of the distal keel bears about six tiny
35 denticles. The base of the mesial keel of C⁶ bears at least one small denticle, whereas
36 at least three distinctly larger accessory denticles, decreasing in size towards crown
37 base, are observed along the distal keel (Table 2). As in the next cheek teeth of the
38 upper tooth row, these large and labiolingually robust accessory denticles display a
39 mesiodistally broad base and these considerably increase the labial/lingual surface of
40 the proportionally wide crown. The condition in C⁷ is nearly identical to C⁶, with two-
41 three tiny denticles along the mesial keel and three larger accessory denticles along
42 the distal keel (Fig. 16); a tiny denticle is observed at the base of distal keel of the
43 most apical of these distal accessory denticles. The mesial keel of C⁸ bears three large
44 accessory denticles, with one tiny denticle at the base of the medial keel of the two
45 basalmost accessory denticles, and the distal keel bears at least three large accessory
46 denticles. In C⁹, three large accessory denticles are present along the mesial keel, and
47 at least two along the distal keel (base damaged). In C¹⁰, three accessory denticles are
48
49
50
51
52
53
54
55
56
57
58
59
60

1
2
3 visible along the mesial keel: the basalmost is small and an additional mesial denticle
4 may be present before the apical denticle. At least two accessory denticles are present
5 along the distal keel (apex of the tooth obscured by the mandible). C^{11} is nearly
6 completely hidden by the mandible. Only the labial surface of the crown is available
7 for these upper cheek teeth; no cingulum or other labial ornamentations are present.
8 Only the lower part of the roots of upper cheek teeth is visible. C^3 is single-rooted,
9 and although a partial separation of mesial and distal roots by a longitudinal groove
10 appears in C^4 , we could not identify the level at which two apically separated roots
11 appear.
12

13
14 Along the lower tooth row, a distinct widening is observed at the base of the
15 crown in C_2 , C_3 , and C_4 , with mesioventral and distoventral bulges of the enamel
16 becoming larger posteriorly (Figs 14, 15). In C_5 , the base of the mesial keel may bear
17 a tiny denticle; a better-defined, larger denticle is present at the base of the distal keel,
18 possibly bearing several tiny denticles as suggested by the observation of several
19 longitudinal ridges in this area. Several tiny denticles are most likely present at the
20 base of the mesial keel of C_6 , and one larger accessory denticle bears about four tiny
21 denticles at the base of the distal keel. The crown of the right C_7 is partly hidden in
22 labial view, but shows at least two large accessory denticles along the distal keel.
23 Better seen in lingual view (Fig. 17), C_8 bears three large accessory denticles along
24 the mesial keel and four along the distal keel, with an additional smaller denticle at
25 the base. As for posterior upper cheek teeth, the broad-based large denticles increase
26 the labial/lingual surface of the crown; a line passing through the apices of succeeding
27 denticles gives a broadly open ogival outline. The mesial keel of C_9 bears an
28 additional small denticle at the base of the mesial keel, and five denticles along the
29 distal keel. Four denticles are present along the mesial keel of C_{10} , and five along the
30 distal keel. Partly obscured by C_{10} , the mesial keel of C_{11} bears at least three denticles,
31 whereas five denticles are present along the distal keel. In both C_{12} and C_{13} , the distal
32 keel bears at least three denticles.
33

34
35 The labial surface of C_1 - C_7 and the lingual surface of C_8 - C_{13} lack any
36 indication of a cingulum; only fine, shallow longitudinal ridges are observed.
37 As for upper cheek teeth, roots are only partly visible. A slight depression between
38 mesial and distal roots appears in C_4 ; the groove separating the two roots is deeper in
39 C_5 , with a mesiodistally broader exposure of the roots; lower cheek teeth are probably
40 double-rooted from C_6 (more conspicuous in C_7).
41
42
43
44
45
46
47
48
49
50
51
52
53
54
55
56
57
58
59
60

1
2
3 None of the upper and lower teeth displays unambiguous wear facets; when
4 preserved, the apex of the crown and accessory denticles is intact; only the fine
5 longitudinal grooves ornamenting the labial and lingual surfaces of teeth are
6 occasionally slightly attenuated, most likely due to abrasion.
7
8
9

10 11 **Vertebrae**

12 The preservation state of the vertebrae is in general not good; due to a long period of
13 exposure at the surface, many processes and even parts of centra were worn away.
14 Furthermore, part of the vertebrae display clues for post-burial deformation, which
15 leads to some degree of uncertainty for the measurements. The vertebral series is most
16 likely not complete. The posterior half portion of the vertebral column was still nearly
17 perfectly articulated in the field. Consequently, for this part it was easy to reconstruct
18 the original position of the vertebrae. Instead, the anterior half portion was partly
19 disarticulated prior to collection and the original sequence was tentatively
20 reconstructed after measuring and comparing the vertebrae. Therefore, the sequence
21 as presented here and in Table 3 for thoracics (ThI, ThII, ...), lumbar (LuI, LuII, ...),
22 and caudals (CaI, CaII, ...) should be considered as tentative (and therefore indicated
23 with Roman numbers instead of Arabic numbers).
24
25
26
27
28
29
30
31
32
33

34 **Cervicals.** Only the right side of the atlas is preserved, including the anterior and
35 posterior articular facets, the transverse processes, and part of the neural arch (Fig.
36 18). The maximum anteroposterior length as preserved is 59 mm; the maximum
37 height of the posterior articular facet is 55 mm. The dorsal transverse process is not as
38 well preserved as the ventral process; both processes were most likely not much
39 elongated with a roughly similar lateral extent. Atlas and axis were not ankylosed.
40 The right side and the ventral portion of the free axis are preserved in a single block
41 together with cervicals C3-C5 (Fig. 19). The maximum anteroposterior length of the
42 axis as preserved is 41 mm; the maximum width is estimated at 142 mm. The
43 transverse process forms a dorsoventrally high, subrectangular and posterolaterally
44 projected plate, pierced by a small vertebrarterial canal (maximum diameter = 6 mm).
45 The partly preserved odontoid process is robust.
46
47
48
49
50
51
52
53
54

55 The somewhat more pointed transverse process of C3 is slightly longer than
56 the transverse process of the axis. Both the dorsal and ventral transverse processes of
57 C4 are incomplete; it cannot be ascertained if the large vertebrarterial canal
58
59
60

1
2
3 (maximum diameter = at least 19 mm) was originally laterally closed in the latter. The
4 ventral transverse process of C5 curves laterodorsally and most likely originally
5 joined the dorsal process. C6 and C7 are preserved together. The dorsoventrally thin,
6 blade-like ventral transverse process of C6 is long (58 mm along its anterior surface)
7 and directed ventrolateroposteriorly; its apex is moderately thickened. The centrum of
8 C6 and C7 is transversely wider than dorsoventrally high. C7 probably lacks a
9 genuine lower transverse process, only retaining a short prominence; its dorsal
10 transverse process is a thin, incompletely preserved plate.
11
12
13
14
15
16
17

18 **Thoracics.** Eleven vertebrae are identified as thoracics. The centrum length and
19 height progressively increase posteriorly, with the transverse process becoming lower
20 along the centrum in the posteriormost thoracics (Table 3). With proportions of the
21 epiphyses close to the last cervicals, ThI is probably the first thoracic, bearing a
22 transverse process projected far posterolaterodorsally (Fig. 20). The neural arch is
23 only well preserved in ThIV, with an anteroposteriorly long neural spine, probably
24 somewhat posteriorly projected. The transverse process of ThIV is higher than the
25 floor of the neural canal and extends far anteriorly, bearing a large fovea for the
26 articulation of the rib. ThX and ThXI are most likely close to the thoracic-lumbar
27 transition, with ThXI only tentatively identified as a thoracic.
28
29
30
31
32
33
34
35

36 **Lumbar.** Nine lumbar are identified. When available, the centrum length is
37 generally longer than in thoracics (Table 3). Most lumbar are too fragmentary to
38 allow an informative description; only the ventral portion of the centrum is partly
39 preserved in several of them, sometimes with the broad base of the transverse process
40 (Fig. 21). The ventral surface of the centrum is marked by a medial keel in several
41 lumbar (e.g., LuVII and LuVIII).
42
43
44
45
46
47

48 **Caudals.** Seventeen caudals are identified (CaI-CaXVII). The facets for the chevron
49 (hemal arch) are barely marked in CaI, which is probably close to the lumbar-caudal
50 transition. The centrum length decreases progressively posteriorly, with a more abrupt
51 reduction from CaXI (Table 3; Fig. 22). Centrum height is greater than length at least
52 in the CaVIII-CaX section; those caudals may correspond to the tail stock, supporting
53 the laterally compressed peduncle region (Buchholtz & Schur 2004). The length of
54 the transverse process is strongly reduced from CaVII; from the same level, the base
55
56
57
58
59
60

1
2
3 of the transverse process is pierced by a vertical vertebrarterial canal. The transverse
4 process is roughly absent in CaIX, only making a low and thick crest, also pierced by
5 a vertical canal. A second, oblique foramen leaves from the ventral side of this crest,
6 reaching the ventromedial surface of the centrum, a condition also observed in CaX.
7
8 The much shorter centrum of CaXI remains dorsoventrally higher than transversely
9 wide.
10

11
12
13 The five posteriormost caudals (CaXIII-CaXVII) are markedly wider than
14 long or high, corresponding to the fluke region. The lateral surface of these last
15 caudals is incised by a deep longitudinal notch, separating dorsal and lateral swollen
16 regions. On the ventral surface, a depressed medial region is separated by two
17 longitudinal crests; the latter are medial to the vertical vertebrarterial canals. CaXVI
18 and CaXVII were found in tight connection and could not be separated.
19
20
21
22
23

24
25 **Changes in proportions of vertebral centra along the vertebral column.** Plotting
26 the dimensions of the vertebral centrum of the best-preserved vertebrae in charts
27 allows visualizing changes in the proportions of the centra along the vertebral column
28 (see Buchholtz 2001). Although many vertebrae are missing or too incomplete to be
29 measured (resulting in artificially steeper slopes for all the curves), when combining
30 central length, width and height in a single chart (Fig. 23) the result for *Inticetus*
31 *vertizi* contrasts markedly with the basilosaurid *Cynthiacetus peruvianus*, the latter
32 showing a more progressive, parallel increase for all the dimensions of the centra
33 towards the posterior lumbar and anterior caudals (Martínez-Cáceres *et al.* in press).
34 Among extant cetaceans, the pattern in *I. vertizi* is more similar to the beluga
35 *Delphinapterus leucas* (see Buchholtz 2001, fig. 5c), characterized by proportionally
36 long posterior thoracics and lumbar. Similarities are even stronger with the large
37 Middle Miocene delphinidan *Hadrodelphis calvertense* (see Buchholtz 2001, fig. 7e).
38 The latter displays a similar increase of the width of cervicals (slightly more posterior
39 in MUSM 1980) and a high peak for the length of posterior lumbar. The available
40 dimensions of the centra match thus well the anatomical pattern 2 as defined by
41 Buchholtz (2001), suggesting a greater flexibility in the anterior torso for *I. vertizi*,
42 more similar to extant Iniioidea, Lipotidae, Monodontidae, and Ziphiidae. Finally,
43 similarities with the tooth-bearing mysticete *Aetiocetus cotylalveus* (Buchholtz 2001,
44 fig. 7c) suggest that the condition of *I. vertizi* could be relatively close to the ancestral
45 neocete condition.
46
47
48
49
50
51
52
53
54
55
56
57
58
59
60

1
2
3
4
5
6
7
8
9
10
11
12
13
14
15
16
17
18
19
20
21
22
23
24
25
26
27
28
29
30
31
32

Sternum. Two elements of the sternum are preserved, the manubrium and the second sternebra (Fig. 24). The considerably dorsoventrally flattened manubrium (as compared to basilosaurids, see Uhen 2004; Martínez-Cáceres *et al.* in press) is 163 mm long (maximum anteroposterior length), for a sagittal length of 110 mm and an estimated maximum width of 132 mm. A groove separating the right and left parts is visible on the dorsal and ventral surfaces. The two posterior articular surfaces (for intersternbral cartilage) are slightly dorsoventrally thickened (12-13 mm), compared to the generally thin aspect of all other edges, and separated by a 21 mm deep V-shaped notch. A posteromedial bulge is also observed on the ventral surface, more developed on the left side. The anterolateral region is also slightly thickened. The Y-shaped second sternebra is smaller, with a maximum anteroposterior length of 91 mm, a sagittal length of 80 mm, and an estimated maximum width of 84 mm, and even more slender than the manubrium. The anterior margin is smoothly concave and the anterolateral region is barely thickened. The posterior surface of articulation is regularly convex and slightly dorsoventrally thickened. Apart from an opening in the centre of the bone, no trace of a sagittal suture is visible.

33
34
35
36
37
38
39
40

Ribs. Many rib fragments are preserved, but most are poorly informative. The proximal part of a left anterior rib is well preserved, being wide and flat. Other fragments, either with the articular region or with a slightly more complete body, are illustrated in Figure 25.

41 42 43 44

Comparison

45
46
47
48
49
50
51
52
53
54
55
56
57
58
59
60

Inticetus vertizi differs from most other odontocete lineages in a series of skull characters; the most striking differences concern the ear bones and teeth (ornamentation and number and shape of accessory denticles in cheek teeth, see below). Among the ear bone differences, the shortened tuberculum of the malleus is only shared with eurhinodelphinids, physeteroids, and ziphiids (Muizon 1985; Bianucci *et al.* 2010), and the large fovea epitubaria with a correspondingly voluminous accessory ossicle and short anterior bullar facet is seen to a roughly similar extent in physeteroids (e.g., Bianucci & Landini 2006; Lambert *et al.* 2016).

1
2
3 However, *Inticetus* differs from all these clades in being heterodont. It further lacks
4 the main cranial synapomorphies of eurhinodelphinids (extreme elongation of the
5 edentulous premaxillary part of the rostrum; e.g., Abel 1901; Lambert 2005),
6 physeteroids (vast supracranial basin and high asymmetry of the bony nares and
7 surrounding bones; e.g., Muizon 1991; Heyning 1997; Lambert *et al.* 2016), and
8 ziphiids (high vertex with transverse premaxillary crests and pterygoid sinus fossa
9 extending anteriorly beyond the level of the antorbital notch and ventrally beyond the
10 ventralmost level of the basicranium; e.g., Lambert *et al.* 2013; Bianucci *et al.*
11 2016b).

12
13 Compared to other heterodont odontocetes, the teeth of *Inticetus* differ from
14 many taxa (e.g., *Agorophius*, *Patriocetus*, *Simocetus*, *Squalodon*, and *Waipatia*) in
15 the reduced ornamentation of the crown (no cingulum and low longitudinal ridges),
16 the relatively high number of large, broad-based accessory denticles (up to four
17 mesial and five distal denticles), and the less triangular outline of the crown in
18 posterior cheek teeth. The best match for the morphology of cheek teeth is with the
19 poorly known *Neosqualodon*, from the Early Miocene of Italy (see Dal Piaz 1904;
20 Fabiani 1949; Rothausen 1968; G. B. pers. obs.). However, MUSM 1980 differs from
21 *Neosqualodon* in: its much larger size, with larger teeth; the styliform process of its
22 jugal being markedly more sturdy; the posterior increase of the height of the mandible
23 being less abrupt; its lower tooth count; incisors being not procumbent; and the
24 number of accessory denticles in posterior cheek teeth being higher. Unfortunately,
25 only fragmentary ear bones were figured for one specimen of *Neosqualodon gastaldii*
26 (Capellini 1881) and these ear bones could not be later found in the Bologna
27 collection.

28
29 Another poorly known taxon is *Kekenodon onamata* Hector, 1881 from the
30 Late Oligocene of New Zealand. It has been referred to archaeocetes (Kellogg 1936;
31 Fordyce 2004; Clementz *et al.* 2014), or to basal toothed mysticetes (Fordyce and
32 Muizon, 2001). The holotype of this taxon consists in several isolated teeth, a
33 fragment of lower jaw, a tympanic and a periotic apparently belonging to the same
34 individual. Among the seven teeth illustrated by Hector (1881), five of them are
35 double-rooted, triangular, and bear up to four broad-based accessory denticles. In this
36 respect, they resemble the posterior cheek teeth of *Inticetus* (C_8 to C_{11}). However,
37 they distinctly differ from *Inticetus* in the following features: they are ca. 30% larger,
38 they have higher crowns, they do not present anteroposterior asymmetry (in lateral
39
40
41
42
43
44
45
46
47
48
49
50
51
52
53
54
55
56
57
58
59
60

1
2
3 view), and their enamel apparently bears marked longitudinal ridges. The periotic
4 figured by Hector resembles that of *Inticetus* in its large fovea epitubaria and the well-
5 developed ventrolateral tuberosity. The tympanic of *Kekenodon* essentially differs
6 from that of *Inticetus* in its inner posterior prominence being wider than the outer
7 prominence, while it is narrower in *Inticetus*. An undescribed, subcomplete skull
8 recently attributed to *Kekenodon* sp. (Clementz *et al.* 2014) differs markedly from
9 *Inticetus*, retaining many plesiomorphic features as compared to neocetes.
10

11
12
13
14
15 Among more fragmentarily known cetacean taxa, several isolated teeth
16 display similarities with posterior cheek teeth of *Inticetus*. The species *Phococetus*
17 *vasconum* is based on a single cheek tooth from the Burdigalian of Saint-Médart-en-
18 Jalle, SW France (Delfortrie 1873; Kellogg 1936), a locality that also yielded the
19 holotype of the squalodelphinid *Medocinia tetragorhina*, isolated odontocete teeth,
20 and many fish remains (Delfortrie 1872, 1875; Priem 1914; Muizon 1988). With four
21 mesial and five distal broad-based denticles, relatively smooth enamel, a mesiodistal
22 length of the crown of 35.5 mm (as measured on a cast; Kellogg, 1936), and a long
23 isthmus between mesial and distal roots, this tooth strongly resembles C₉₋₁₀ of MUSM
24 1980. The only difference we could note is the proportionally higher crown in *P.*
25 *vasconum*. The latter was earlier proposed as an archaeocete (Kellogg 1936), possibly
26 a kekenodontid archaeocete (Uhen 2008b; Fitzgerald 2010), and an enigmatic
27 probable mysticete (Fordyce & Barnes 1994). Based on the morphological similarities
28 and shared Burdigalian age, we think that systematic affinities of *P. vasconum* with
29 *Inticetus* cannot be ruled out.
30

31
32
33
34
35
36
37
38
39
40
41
42
43
44
45
46
47
48
49
50
51
52
53
54
55
56
57
58
59
60
61
62
63
64
65
66
67
68
69
70
71
72
73
74
75
76
77
78
79
80
81
82
83
84
85
86
87
88
89
90
91
92
93
94
95
96
97
98
99
100
101
102
103
104
105
106
107
108
109
110
111
112
113
114
115
116
117
118
119
120
121
122
123
124
125
126
127
128
129
130
131
132
133
134
135
136
137
138
139
140
141
142
143
144
145
146
147
148
149
150
151
152
153
154
155
156
157
158
159
160
161
162
163
164
165
166
167
168
169
170
171
172
173
174
175
176
177
178
179
180
181
182
183
184
185
186
187
188
189
190
191
192
193
194
195
196
197
198
199
200
201
202
203
204
205
206
207
208
209
210
211
212
213
214
215
216
217
218
219
220
221
222
223
224
225
226
227
228
229
230
231
232
233
234
235
236
237
238
239
240
241
242
243
244
245
246
247
248
249
250
251
252
253
254
255
256
257
258
259
260
261
262
263
264
265
266
267
268
269
270
271
272
273
274
275
276
277
278
279
280
281
282
283
284
285
286
287
288
289
290
291
292
293
294
295
296
297
298
299
300
301
302
303
304
305
306
307
308
309
310
311
312
313
314
315
316
317
318
319
320
321
322
323
324
325
326
327
328
329
330
331
332
333
334
335
336
337
338
339
340
341
342
343
344
345
346
347
348
349
350
351
352
353
354
355
356
357
358
359
360
361
362
363
364
365
366
367
368
369
370
371
372
373
374
375
376
377
378
379
380
381
382
383
384
385
386
387
388
389
390
391
392
393
394
395
396
397
398
399
400
401
402
403
404
405
406
407
408
409
410
411
412
413
414
415
416
417
418
419
420
421
422
423
424
425
426
427
428
429
430
431
432
433
434
435
436
437
438
439
440
441
442
443
444
445
446
447
448
449
450
451
452
453
454
455
456
457
458
459
460
461
462
463
464
465
466
467
468
469
470
471
472
473
474
475
476
477
478
479
480
481
482
483
484
485
486
487
488
489
490
491
492
493
494
495
496
497
498
499
500
501
502
503
504
505
506
507
508
509
510
511
512
513
514
515
516
517
518
519
520
521
522
523
524
525
526
527
528
529
530
531
532
533
534
535
536
537
538
539
540
541
542
543
544
545
546
547
548
549
550
551
552
553
554
555
556
557
558
559
560
561
562
563
564
565
566
567
568
569
570
571
572
573
574
575
576
577
578
579
580
581
582
583
584
585
586
587
588
589
590
591
592
593
594
595
596
597
598
599
600
601
602
603
604
605
606
607
608
609
610
611
612
613
614
615
616
617
618
619
620
621
622
623
624
625
626
627
628
629
630
631
632
633
634
635
636
637
638
639
640
641
642
643
644
645
646
647
648
649
650
651
652
653
654
655
656
657
658
659
660
661
662
663
664
665
666
667
668
669
670
671
672
673
674
675
676
677
678
679
680
681
682
683
684
685
686
687
688
689
690
691
692
693
694
695
696
697
698
699
700
701
702
703
704
705
706
707
708
709
710
711
712
713
714
715
716
717
718
719
720
721
722
723
724
725
726
727
728
729
730
731
732
733
734
735
736
737
738
739
740
741
742
743
744
745
746
747
748
749
750
751
752
753
754
755
756
757
758
759
760
761
762
763
764
765
766
767
768
769
770
771
772
773
774
775
776
777
778
779
780
781
782
783
784
785
786
787
788
789
790
791
792
793
794
795
796
797
798
799
800
801
802
803
804
805
806
807
808
809
810
811
812
813
814
815
816
817
818
819
820
821
822
823
824
825
826
827
828
829
830
831
832
833
834
835
836
837
838
839
840
841
842
843
844
845
846
847
848
849
850
851
852
853
854
855
856
857
858
859
860
861
862
863
864
865
866
867
868
869
870
871
872
873
874
875
876
877
878
879
880
881
882
883
884
885
886
887
888
889
890
891
892
893
894
895
896
897
898
899
900
901
902
903
904
905
906
907
908
909
910
911
912
913
914
915
916
917
918
919
920
921
922
923
924
925
926
927
928
929
930
931
932
933
934
935
936
937
938
939
940
941
942
943
944
945
946
947
948
949
950
951
952
953
954
955
956
957
958
959
960
961
962
963
964
965
966
967
968
969
970
971
972
973
974
975
976
977
978
979
980
981
982
983
984
985
986
987
988
989
990
991
992
993
994
995
996
997
998
999
1000

With its smooth enamel and relatively large accessory denticles, an isolated
cheek tooth from Late Oligocene deposits of Australia identified as *Squalodon*
gambierensis (Glaessner 1955; Pledge & Rothausen 1977) displays similarities with
posterior cheek teeth of MUSM 1980, for example C₈. This Australian tooth has been
attributed to a kekenodontid archaeocete (Fordyce 2004; Fitzgerald 2010).

The marked dental similarities of the heterodont odontocete *Inticetus* with
fragmentary remains tentatively attributed to non-odontocete cetaceans urges to be
cautious in the identification of isolated cetacean cheek teeth from the Oligocene-
early Miocene. In several cases those may not be diagnostic at the suborder level.

In addition to the differences mentioned above at the level of ear bones and
cheek teeth, *Inticetus* differs from the stem odontocete families Agorophiidae,
Ashleycetidae, Mirocetidae, Simocetidae, and Xenorophidae (see Fordyce 2002;

1
2
3 Uhen 2008b; Sanders & Geisler 2015; Geisler *et al.* 2014; Churchill *et al.* 2016;
4 Godfrey *et al.* 2016) in: its larger size, the bony nares being located far posterior to
5 level of antorbital notch and roughly vertical, the nasals being anteroposteriorly
6 shorter, and the intertemporal constriction being most likely absent.
7
8

9
10 It further differs from Squalodontidae (see Kellogg 1923; Pilleri 1985; Muizon
11 1991; Dooley 2005) in: the absence of a pterygoid-maxilla contact on the palate, the
12 styliiform process of jugal being markedly more sturdy, the sutural contact of the jugal
13 with the zygomatic process of the squamosal being longer, the presence of a deep
14 notch separating the basioccipital crest from the falcate process of the exoccipital, the
15 presence of a high rim around the internal acoustic meatus, and the incisors being not
16 procumbent, with the crown being not fluted.
17
18

19
20 It further differs from Patriocetidae (see Dubrovo & Sanders 2000) in: its
21 larger size, the bony nares being located far posterior to level of antorbital notch, the
22 intertemporal constriction being most likely absent, and the zygomatic process of
23 squamosal being proportionally shorter.
24
25

26
27 It further differs from *Waipatia* (see Fordyce 1994; Tanaka & Fordyce 2015a)
28 in: its larger size, the styliiform process of jugal being markedly more sturdy, the
29 presence of a high rim around the internal acoustic meatus, the posterior increase of
30 the height of the mandible being less abrupt; the incisors being not procumbent, and
31 the presence of mesial denticles on upper and lower posterior cheek teeth.
32
33

34
35 It shares with *Papahu* (see Aguirre-Fernández & Fordyce 2014) the large
36 fovea epitubaria with a correspondingly short anterior bullar facet (although more
37 marked in MUSM 1980), but it differs from this homodont odontocete in: its larger
38 size, the styliiform process of jugal being markedly more sturdy, an inconspicuous
39 parabullary sulcus on the periotic, and the posterior increase of the height of the
40 mandible being less abrupt.
41
42

43
44 Although *Inticetus* shares with *Prosqualodon davidis* a voluminous accessory
45 ossicle, it further differs from *Prosqualodon* spp. (see Lydekker 1893; True 1909;
46 Flynn 1948) in: the rostrum being proportionally longer, the posterior increase of the
47 height of the mandible being less abrupt, a higher tooth count (compared to *P.*
48 *davidis*), and incisors being not procumbent.
49
50
51
52
53
54

55 56 57 58 59 60 **Phylogeny**

1
2
3
4
5 To investigate the phylogenetic relationships of *Inticetus vertizi* we coded the
6 specimen MUSM 1980 in the matrix of Tanaka & Fordyce (2016) (see character-
7 taxon matrix as online Supplemental material). Four heuristic searches were
8 performed using Paup 4.0 (Swofford 2001), with the protocetid *Georgiacetus*
9 *vogtlensis* and the basilosaurid *Zygorhiza kochii* as outgroups, all characters treated as
10 unordered, TBR branch swapping, and ACCTRAN optimization: (analysis 1) with
11 equally weighted characters and no molecular constraint; (analysis 2) with down-
12 weighted homoplastic characters, following the method of Goloboff (1993) with the
13 constant $k = 3$ and no molecular constraint; (analysis 3) with equally weighted
14 characters and with a backbone molecular constraint taken from the analysis of
15 McGowen *et al.* (2009), as performed by Tanaka & Fordyce (2016), and (analysis 4)
16 with down-weighted homoplastic characters and with a backbone molecular
17 constraint.
18
19
20
21
22
23
24
25
26
27

28 Results

29 Analysis 1 resulted in 6480 most parsimonious trees with tree length 1828; CI 0.24;
30 RI 0.64; the strict consensus is shown in Figure 26. Analysis 2 resulted in 9 most
31 parsimonious trees with CI 0.24; RI 0.64; the strict consensus is partly shown in
32 Figure 27A (without details for the clade Delphinida). Analysis 3 resulted in 135 most
33 parsimonious trees with tree length 1914; CI 0.23; RI 0.62; the strict consensus is
34 partly shown in Figure 27B. Analysis 4 resulted in 9 most parsimonious trees with CI
35 0.23; RI 0.62; the strict consensus is partly shown in Figure 27C.
36
37
38
39
40
41

42 Without any molecular constraint, analyses 1 and 2 identify the superfamily
43 Platanistoidea as the most stemward crown odontocete clade, with Physterioidea and
44 Ziphiidae forming a more crownward clade, itself sister-group to Delphinida. The
45 content of Platanistoidea differs in these two analyses: in the analysis with equally
46 weighted characters (analysis 1) it only includes *Squalodon*, *Prosqualodon*, a
47 monophyletic Squalodelphinidae and a monophyletic Platanistidae, with *Inticetus* and
48 a clade including *Otekaikea* and *Waipatia* being the last stem odontocete lineages to
49 branch off, whereas in the analysis with down-weighted homoplastic characters
50 (analysis 2) Platanistoidea also includes *Inticetus*, *Otekaikea* and *Waipatia*, and
51 Squalodelphinidae is paraphyletic.
52
53
54
55
56
57
58
59
60

1
2
3 The molecular constraint (in analyses 3 and 4) places Physterioidea as the first
4 stem odontocete clade to branch off, followed by Platanistoidea and Ziphiidae. Here
5 again the content of Platanistoidea differs if homoplastic characters are down-
6 weighted or not. In the analysis with equally weighted characters (analysis 3), it only
7 includes Platanistidae, a paraphyletic Squalodelphinidae, OU 22670 and *Papahu* sp.
8 ZMT 73, with *Inticetus*, *Waipatia*, and *Otekaikea* forming a clade stemward to the
9 successive branches of *Squalodon*, *Prosqualodon*, and Physterioidea. In the analysis
10 with down-weighted homoplastic characters (analysis 4), Platanistoidea makes a
11 much larger clade, also including *Prosqualodon* + *Squalodon*, *Inticetus*, *Otekaikea*,
12 and *Waipatia*, but not *Papahu* sp. ZMT 73.
13
14
15
16
17
18
19
20

21 Discussion

22 Down-weighting homoplastic characters has a profound impact on both the content of
23 the superfamily Platanistoidea and the relationships of *Inticetus*; indeed, in the two
24 analyses with equally weighted characters (analyses 1 and 3, without and with a
25 molecular constraint), the clade Platanistoidea is less inclusive and *Inticetus* falls as a
26 stem odontocete. Interestingly, the two analyses with down-weighted homoplastic
27 characters (analyses 2 and 4) resulted in a larger clade Platanistoidea, which includes
28 Platanistidae, Squalodelphinidae, *Inticetus*, *Otekaikea*, *Squalodon*, and *Waipatia*. The
29 only difference between the two results is the position of *Prosqualodon*, which is
30 either a stem taxon to Platanistoidea (analysis 2) or included in the Platanistoidea
31 (analysis 4). Therefore, down-weighting homoplastic characters tends to tighten the
32 clade Platanistoidea, and in both cases *Inticetus* is included in the superfamily.
33
34
35
36
37
38
39
40

41 A molecular constraint was applied for the two analyses performed by Tanaka
42 & Fordyce (2016); those can thus only be compared to analyses 3 and 4. Interestingly,
43 the inclusion of *Inticetus* in analysis 3 'attracts' *Otekaikea*, *Prosqualodon*, *Squalodon*,
44 and *Waipatia* outside the Platanistoidea clade, and even outside the crown Odontoceti,
45 a result that is not found in any of Tanaka & Fordyce's results. Nevertheless,
46 *Prosqualodon*, *Squalodon*, and in some cases *Waipatia* fell outside crown Odontoceti
47 in several past phylogenetic analyses (e.g., Geisler *et al.* 2011, 2014; Aguirre-
48 Fernández & Fordyce 2014; Tanaka & Fordyce 2014, 2015b; Sanders & Geisler
49 2015; Godfrey *et al.* 2016). Analysis 4 yields a general topology similar to the
50 analysis of Tanaka & Fordyce (2016) with down-weighted homoplastic characters,
51
52
53
54
55
56
57
58
59
60

1
2
3 meaning that in this case, reducing the impact of homoplastic characters tends to
4 stabilize a topology when new taxa are added.
5

6 Based on our different results, there is no consensus about the phylogenetic
7 relationships of *Inticetus*. It is either a stem odontocete more crownward than
8 *Agorophius* and *Patriocetus* (in a separate lineage or in a clade with *Otekaikea* and
9 *Waipatia*), or a crown odontocete branching off relatively early in a large
10 Platanistoidea clade. In all our analyses, *Inticetus* is close to the node defining crown
11 Odontoceti, and its most recurrent phylogenetic affinities are with (1) *Otekaikea* and
12 *Waipatia*, either as sister-groups or as successive branches, and (2) *Squalodon*, as
13 successive branches in two analyses (in one case with *Prosqualodon* as sister-group to
14 *Squalodon*). However, *Inticetus* does not match any of the families, or genera from
15 undetermined families, of Oligocene and Miocene odontocetes, displaying
16 morphological features departing markedly from any other known taxon, including
17 Squalodontidae and Waipatiidae. Because it differs strikingly from all the other
18 heterodont odontocetes (see comparison above), and although the generally highly
19 diagnostic facial region, including the vertex, is not optimally preserved in the
20 holotype and only known specimen, we think that the diagnostic features of *Inticetus*
21 should lead to the erection of a higher rank taxon, the new family Inticetidae.
22
23
24
25
26
27
28
29
30
31
32
33

34 **Geological context, biostratigraphy and taphonomy**

35 **Geological context**

36
37
38 The Meso-Cenozoic tectonics of the Peruvian margin was controlled by the oblique
39 subduction of the oceanic Nazca-Farallon Plate beneath the continental South
40 American Plate. This resulted in a composite transform-convergent margin
41 characterized by normal and strike-slip faults that formed a number of extensional and
42 pull apart basins along the western margin of Peru (e.g., Thornburg & Kulm 1981;
43 León *et al.* 2008; Zúñiga-Rivero *et al.* 2010). The Cenozoic stratigraphy of the Pisco
44 Basin in southern Peru consists of Eocene to Pliocene nearshore and shelf sediments
45 that occur in repetitive successions and are separated by basin-wide, conglomerate-
46 mantled unconformities (Dunbar *et al.* 1990; DeVries 1998). Based on the currently
47 existing stratigraphic framework, the basin fill comprises the middle to upper Eocene
48 Paracas Formation, the uppermost Eocene to lower Oligocene Otuma Formation, the
49
50
51
52
53
54
55
56
57
58
59
60

1
2
3 uppermost Oligocene to middle Miocene Chilcatay Formation, and the upper Miocene
4 to Pliocene Pisco Formation (DeVries *et al.* 2006).

5
6 The Roca Negra locality is along the western side of the Ica River valley,
7 where the Chilcatay Formation consists of two main sediment units separated by an
8 intraformational unconformity. The lower unit includes a sub-horizontal package of
9 medium- to fine-grained sandstones and siltstones that underlie and, locally, landward
10 interfinger (from southwest to northeast) with a seaward-dipping clinofomed package
11 of coarse-grained biocalcarenites. This lower unit is unconformably overlain by a
12 fining-upward unit composed of basal sandstones gradually overlain by massive
13 siltstones. An ash layer sampled in the fine-grained unit of the Chilcatay Formation,
14 just 1 m below the erosional contact with the overlying Pisco Formation, yielded a
15 $^{40}\text{Ar}/^{39}\text{Ar}$ age of 17.99 ± 0.10 Ma (Di Celma *et al.* in press).

23 24 25 **Biostratigraphy**

26 The Chilcatay sedimentary succession exposed in the locality of MUSM 1980 (Roca
27 Negra) is part of the sub-horizontal package of sandstones and siltstones occurring in
28 the lower portion of the lower unit. Most of the samples recovered for biostratigraphic
29 analysis along the measured section had a lithogenic composition. Sample PN2 (see
30 Fig. 2) contained a well preserved siliceous assemblage (see Appendix 1).

31 Silicoflagellates were rare but yielded a diverse assemblage, represented, in order of
32 abundance, by *N. obtusarca*, *Distephanopsis crux* subsp. *scutulata*, *Corbisema*
33 *triacantha*, *N. ponticula* subsp. *ponticula*, *N. obtusarca* var. *acicula* and *Naviculopsis*
34 sp. 2 (described by Cisielsky 1991 from the Early Miocene of the sub-Antarctic South
35 Atlantic). Accordingly, this assemblage is assigned to the *Naviculopsis ponticula* zone
36 of Bukry (1981), correlated by Bukry (1982) to the coccolith *Sphenolithus belemnos*
37 Zone at DSDP Site 495 offshore Guatemala, that, in turn, has been dated between 19
38 and 18 Ma (Bukry, 1982), early Burdigalian. Bukry (1985) described this biozone
39 across the equatorial Pacific and showed that it is dominated sequentially by *N.*
40 *obtusarca*, *N. contraria*, and *N. ponticula* var. *spinosa*. In our sample, given the
41 dominance of the former and the absence of the latter two species, we can speculate
42 that it is located in the lower part of the *N. ponticula* biozone. Macharé *et al.* (1998)
43 indicated the presence of *N. ponticula spinosa* in one sample (84407) at the Pampa
44 Chilcatay section, along with a diatom assemblage including *Triceratium pileus*,
45 *Thalassiosira fraga*, and *T. spinosa*; according to Barron (1985), this diatom

1
2
3 assemblage indicates an age of 18.8 to 17.9 Ma. *N. ponticula* is otherwise reported
4 from the eastern Equatorial Pacific (Engel & McCartney 1990), the eastern Equatorial
5 Atlantic (Schellpeper & Watkins 1998), and outcrops of the temperate North Atlantic
6 (Wetmore & Andrews 1991).
7
8
9

10 11 **Taphonomy**

12 Although the fossil skeleton MUSM 1980 was only partly articulated, all the bones
13 were found associated, roughly near their original anatomical position, and with the
14 axial skeleton (both the forelimbs are lost) forming on the whole an arc (Fig. 28). The
15 disarticulation mainly concerns the ribcage (thoracic vertebrae, ribs, and sternal
16 bones). Except for slight displacement due to wind for exposed bones included in soft,
17 uncemented sediment, most disarticulation probably occurred before the burial of the
18 skeleton and could be due to: 1) collapse of the ribcage after decomposition of soft
19 tissues, 2) explosion resulting from the accumulation of gases generated during the
20 decay of the carcass, 3) water currents on the sea bottom, or 4) scavenging by sharks
21 and other marine vertebrates. This last possibility is strongly supported by the finding
22 on the one side of three isolated shark teeth near the bones of the odontocete and, on
23 the other side, of shark bite marks along the rostrum of the cranium and along the left
24 mandible. Discovered near the sternum and near the anteriormost lumbar vertebrae,
25 the shark teeth belong to three distinct species already recorded in the late Miocene
26 strata of the Pisco Formation: *Cosmopolitodus hastalis*, *Galeocerdo aduncus*, and
27 *Pysogaleous contortus*, (Muizon & DeVries 1985; Collareta *et al.* 2017; Landini *et al.*
28 2017). Considering the trophic spectrum of the extant relatives of these sharks, and/or
29 of other similar extant sharks (Klymley 1994; Long & Jones 1996; Heithaus 2001;
30 Curtis *et al.* 2006), it is reasonable to suggest that these teeth indicate the partial
31 consumption of the carcass by sharks of these three species. Such an occurrence is
32 relatively common during the excavation of fossil cetacean skeletons and it was also
33 well documented for a whale skeleton from the Pisco Formation (Takakuwa 2014).
34 Most of the bite marks are observed in the left dorsolateral side of the rostrum. They
35 consist in some pseudo-parallel incisions about 2 cm long. These shallow grooves
36 lacking serrated margins could correspond to scraping marks caused by one or more
37 sharks biting the carcass of the odontocete. Scavenging, rather than active predation,
38 is supported by the fact that the incisions are not deep, in relatively small number, and
39 located in a portion of the skeleton (skull and mandibles) usually not damaged during
40
41
42
43
44
45
46
47
48
49
50
51
52
53
54
55
56
57
58
59
60

1
2
3 a shark attack. Indeed, data about the well-documented feeding behaviour of the
4 extant white shark *Carcharodon carcharias* indicate that sharks usually do not target
5 the head region of dolphins in order to avoid sonar detection (Long & Jones 1996).
6 For this reason a direct predation, conceivable for other fossil odontocetes with
7 several deep shark bites in the ribcage region (Cigala Fugosi 1992, Bianucci *et al.*
8 2010), cannot be proposed for the fossil examined here. Scavenging by sharks could
9 also explain the absence of both forelimbs, possibly removed when the carcass was
10 still floating, or after it sank to the seafloor (Shäfer 1972; Bianucci & Gingerich
11 2011). Re-floating of the carcass, due to a buildup of gases during initial
12 decomposition (Shäfer 1972), did most likely not occur, or for only a short time,
13 before it sank to the bottom, considering the preservation of the mandibles firmly
14 articulated to the cranium, of most of the teeth inside their alveoli, and of the last
15 caudal vertebrae.
16
17
18
19
20
21
22
23
24
25

26 **General discussion and conclusions**

27
28
29
30 With such unusual tooth morphology, the feeding ecology of *Inticetus* is worth briefly
31 discussing. First, among heterodont odontocetes the general outline of the long and
32 robust rostrum is most similar to *Squalodon*, contrasting with the much shorter
33 rostrum of *Prosqualodon* and the more slender rostrum of e.g. *Waipatia*. Combined
34 with strong, but not procumbent, conical anterior teeth, this condition suggests the
35 ability to grasp relatively large prey with the incisors, canines, and anterior cheek
36 teeth, as proposed for at least part of the basilosaurids (Uhen 2004; Snively *et al.*
37 2015). However, contrasting with basilosaurids (Uhen 2004; Fahlke *et al.* 2013), the
38 absence of conspicuous attritional tooth wear facets in cheek teeth may indicate only a
39 limited use of the posterior dentition for processing food (namely cutting or tearing
40 larger prey in smaller pieces), a hypothesis further supported by the highly reduced
41 ornamentation of tooth crowns. Furthermore, the enlarged, broad-based accessory
42 denticles displayed by the closely spaced posterior cheek teeth leads to a better
43 closure of the lateral wall of the posterior buccal cavity. Differing from most other
44 heterodont odontocetes, such a condition may correspond to higher suction-feeding
45 abilities, with rigid lateral walls of the cavity allowing the production of higher
46 intraoral pressure during suction and with broad dental crowns allowing the retention
47
48
49
50
51
52
53
54
55
56
57
58
59
60

1
2
3 of food items when water is expelled laterally from the cavity during the recovery
4 phase (see Werth 2006). A similar conclusion has been experimentally confirmed for
5 pinnipeds showing enlarged accessory denticles in cheek teeth (Hocking *et al.* 2013).
6
7

8 In addition to its dental morphology, *Inticetus* differs from many other Late
9 Oligocene - Early Miocene odontocetes in its larger body size; except from the larger,
10 homodont physeteroids *Diaphorocetus poucheti* and *Idiorophus patagonicus* (Moreno
11 1892; Lydekker 1894), *Inticetus* is only in the same size category as *Phoberodon*
12 *arctirostris*, *Prosqualodon* spp. and the homodont *Macrodelphinus kelloggi*
13 (Lydekker 1893; Flynn 1948; Cabrera 1926; Wilson 1935).
14
15
16
17

18 Combining the skull morphology, dental features, and size of *Inticetus*, this
19 heterodont odontocete further increases the morphological disparity of Late Oligocene
20 - Early Miocene odontocetes; it most likely occupied a relatively specific ecological
21 niche.
22
23

24 From a phylogenetic viewpoint, the relationships of *Inticetus* are not fully
25 resolved, this new taxon being either a stem odontocete or an early diverging
26 platanistoid. The addition of other Late Oligocene - Early Miocene heterodont
27 odontocetes to the analysed sample and the reassessment of *Prosqualodon* spp. and
28 the family Squalodontidae may prove useful to further characterize the stem-to-crown
29 odontocete transition.
30
31
32
33

34 Finally, from a taxonomic perspective, the description of an unusual
35 morphotype of odontocete cheek teeth, sharing similarities with the dentition of a few
36 other, non-odontocete fossil cetaceans, urges to be cautious in the identification of
37 isolated cetacean teeth, even at the suborder level.
38
39
40
41
42

43 **Supplemental material**

44
45
46 Supplemental material for the phylogenetic analysis, including the character-taxon
47 matrix and the constraint tree based on molecular analysis is available online at doi: ...
48
49

50 **Acknowledgements**

51
52
53
54
55 We wish to warmly thank A. Altamirano, E. Díaz, and K. Post for their help during
56 fieldwork, W. Aguirre for the preparation of the skull and postcranial remains, R.
57
58
59
60

1
2
3 Salas-Gismondi and R. Varas-Malca for providing access to the MUSM collection
4 and for facilitating our work there, W. Miseur for the photographs of ear bones. This
5 research was supported by funding from the Muséum national d'Histoire naturelle,
6 Paris (Action Transversale "Biodiversité actuelle et fossile" 2011) to C.M. and O.L., a
7 grant of the Italian Ministero dell'Istruzione dell'Università e della Ricerca (PRIN
8 Project 2012YJSBMK) to C.D.C., E.M. and G.B., and a National Geographic Society
9 Committee for Research Exploration grant (9410–13) to G.B.
10
11
12
13
14
15

16 References

- 17
18
19
20 **Abel, O.** 1901. Les dauphins longirostres du Boldérien (Miocène supérieur) des
21 environs d'Anvers. I. *Mémoires du Musée Royal d'Histoire Naturelle de*
22 *Belgique*, **1**, 1-95.
23
24 **Aguirre-Fernández, G. & Fordyce, R. E.** 2014. *Papahu taitapu*, gen. et sp. nov., an
25 early Miocene stem odontocete (Cetacea) from New Zealand. *Journal of*
26 *Vertebrate Paleontology*, **34**, 195-210.
27
28 **Armfield, B. A., Zheng, Z., Bajpai, S., Vinyard, C. J. & Thewissen, J. M. G.**
29 2013. Development and evolution of the unique cetacean dentition. *PeerJ*, **1**,
30 e24.
31
32 **Barron, J. A.** 1985. Miocene to Holocene planktic diatom stratigraphy. Pp. 413-456
33 in H. M. Bolli, J. B. Saunders & K. Perch-Nielsen (eds.) *Plankton*
34 *Stratigraphy*. Cambridge University Press, UK.
35
36 **Bianucci, G. & Gingerich, P. D.** 2011. *Aegyptocetus tarfa*, n. gen. et sp. (Mammalia,
37 Cetacea), from the middle Eocene of Egypt: clinorhynch, olfaction, and
38 hearing in a protocetid whale. *Journal of Vertebrate Paleontology*, **31**, 1173-
39 1188.
40
41 **Bianucci, G. & Landini, W.** 2006. Killer sperm whale: a new basal physeteroid
42 (Mammalia, Cetacea) from the Late Miocene of Italy. *Zoological Journal of*
43 *the Linnean Society*, **148**, 103-131.
44
45 **Bianucci, G., Lambert, O. & Post, K.** 2010. High concentration of long-snouted
46 beaked whales (genus *Messapicetus*) from the Miocene of Peru.
47 *Palaeontology*, **53**, 1077-1098.
48
49
50
51
52
53
54
55
56
57
58
59
60

- 1
2
3 **Bianucci, G., Sorce, B., Storai, T. & Landini, W.** 2010. Killing in the Pliocene:
4 shark attack on a dolphin from Italy. *Palaeontology*, **53**, 457-470.
- 5
6 **Bianucci, G., Urbina, M. & Lambert, O.** 2015. A new record of *Notocetus*
7 *vanbenedeni* (Squalodelphinidae, Odontoceti, Cetacea) from the early
8 Miocene of Peru. *Comptes Rendus Palevol*, **14**, 5-13.
- 9
10
11 **Bianucci, G., Di Celma, C., Landini, W., Post, K., Tinelli, C., de Muizon, C.,**
12 **Gariboldi, K., Malinverno, E., Cantalamessa, G., Gioncada, A., Collareta,**
13 **A., Salas-Gismondi, R., Varas-Malca, R., Urbina, M. & Lambert, O.**
14 2016a. Distribution of fossil marine vertebrates in Cerro Colorado, the type
15 locality of the giant raptorial sperm whale *Livyatan melvillei* (Miocene, Pisco
16 Formation, Peru). *Journal of Maps*, **12**, 543-557.
- 17
18 **Bianucci, G., Di Celma, C., Urbina, M. & Lambert, O.** 2016b. New beaked whales
19 from the late Miocene of Peru and evidence for convergent evolution in stem
20 and crown Ziphiidae (Cetacea, Odontoceti). *PeerJ*, **4**, e2479.
- 21
22 **Brisson, M.-J.** 1762. *Regnum Animale in classes IX distributum, sine synopsis*
23 *methodica*. Theodorum Haak, Paris, 296 pp.
- 24
25 **Buchholtz, E. A.** 2001. Vertebral osteology and swimming style in living and fossil
26 whales (Order Cetacea). *Journal of Zoology*, **253**, 175-190.
- 27
28 **Buchholtz, E. A. & Schur, S. A.** 2004. Vertebral osteology in Delphinidae (Cetacea).
29 *Zoological Journal of the Linnean Society*, **140**, 383-401.
- 30
31 **Bukry, D.** 1978. Cenozoic coccolith, silicoflagellate, and diatom stratigraphy, Deep
32 Sea Drilling Project Leg 44. *Initial Reports, DSDP*, **44**, 807-863.
- 33
34 **Bukry, D.** 1981. Synthesis of silicoflagellate stratigraphy for Maastrichtian to
35 Quaternary marine sediments. Pp. 433-444 in T. E. Warme, R. C. Douglas &
36 E. L. Winterer (eds.) *The deep sea drilling project: a decade of*
37 *progress*. Special Publication - SEPM, 32.
- 38
39 **Bukry, D.** 1982. Cenozoic silicoflagellates from offshore Guatemala, Deep Sea
40 Drilling Project site 495. *Initial Reports, DSDP*, **67**, 425-445.
- 41
42 **Bukry, D.** 1985. Tropical Pacific silicoflagellate zonation and paleotemperature
43 trends of the late Cenozoic. *Initial Reports, DSDP*, **85**, 477-497.
- 44
45
46 **Cabrera, A.** 1926. Cetaceos fosiles del Museo de La Plata. *Revista del Museo de La*
47 *Plata*, **29**, 363-411.
- 48
49
50
51
52
53
54
55
56
57
58
59
60

- 1
2
3 **Capellini, G.** 1881. Avanzi di Squalodonte nella mollassa marnosa miocenica del
4 Bolognese. *Memorie della Accademia delle Scienze dell'Istituto di Bologna*,
5 *ser. 4, 2*, 413-419.
6
7
8 **Churchill, M., Martinez-Caceres, M., de Muizon, C., Mnieckowski, J. & Geisler,**
9 **J. H.** 2016. The origin of high-frequency hearing in whales. *Current Biology*,
10 **26**, 2144-2149.
11
12 **Ciesielski, P.F.** 1991. Biostratigraphy of diverse silicoflagellate assemblages from the
13 early Paleocene to early Miocene of holes 698A, 700B, 702B, AND 703A:
14 Subantarctic South Atlantic. *Proceedings of the Ocean Drilling Program*,
15 *Scientific Results*, **114**, 49-96.
16
17 **Cigala Fulgosi, F.** 1990. Predation (or possible scavenging) by a great white shark on
18 an extinct species of bottlenosed dolphin in the Italian Pliocene. *Tertiary*
19 *Research*, **12**, 17-36.
20
21 **Clementz, M. T., Fordyce, R. E., Peek, S. L. & Fox, D. L.** 2014. Ancient marine
22 isoscapes and isotopic evidence of bulk-feeding by Oligocene cetaceans.
23 *Palaeogeography, Palaeoclimatology, Palaeoecology*, **400**, 28-40.
24
25 **Collareta, A., Landini, W., Chacaltana, C., Valdivia, W., Altamirano-Sierra, A.,**
26 **Di Celma, C., Urbina, M. & Bianucci, G.** 2017. A well preserved skeleton of
27 the fossil shark *Cosmopolitodus hastalis* from the late Miocene of Peru,
28 featuring fish remains as fossilized stomach contents. *Rivista Italiana di*
29 *Paleontologia e Stratigrafia*, **123**, 11-22.
30
31 **Curtis, T. H., Kelly, J. T., Menard, K. L., Laroche, R. K., Jones, R. E. & Klimley,**
32 **A. P.** 2006. Observations on the behavior of white sharks scavenging from a
33 whale carcass at Point Reyes, California. *California Fish and Game*, **92**, 113-
34 124.
35
36 **Dal Piaz, G.** 1904. *Neosqualodon*, nuovo genere della famiglia degli Squalodontidi.
37 *Mémoires de la Société Paléontologique Suisse*, **31**, 1-19.
38
39 **Delfortrie, E.** 1872. Les phoques du falun aquitainien. *Actes de la Société Linnéenne*
40 *de Bordeaux*, **28**, 383-386.
41
42 **Delfortrie, E.** 1873. Un Zeuglodon dans les faluns du sud-ouest de la France. *Journal*
43 *de Zoologie*, **9**, 113-117.
44
45 **Delfortrie, E.** 1875. Un dauphin d'espèce nouvelle dans les faluns du Sud-Ouest.
46 *Actes de la Société Linnéenne de Bordeaux*, **30**, 3-7.
47
48
49
50
51
52
53
54
55
56
57
58
59
60

- 1
2
3 **Desikachary, T. V. & Prema, P.** 1996. Silicoflagellates (Dictyochophyceae).
4 *Bibliotheca Phycologica*, **100**, 1–298
- 5
6 **DeVries, T. J.** 1998. Oligocene deposition and Cenozoic sequence boundaries in the
7 Pisco Basin (Peru). *Journal of South American Earth Sciences*, **11**, 217-231.
- 8
9 **DeVries, T. J.** 2001. Molluscan evidence for an Oligocene-Miocene age of 'Paracas'
10 beds in Southern Peru. *Boletín de la Sociedad Geológica del Perú*, **92**, 57-65.
- 11
12 **DeVries, T. J., Navarez, Y., Sanfilippo, A., Malumian, N. & Tapia, P.** 2006. New
13 microfossil evidence for a late Eocene age of the Otuma Formation (Southern
14 Peru). *XIII Congreso Peruano de Geología, Lima, Peru*, 615-618.
- 15
16
17 **Di Celma, C., Malinverno, E., Bosio, G., Collareta, A., Gariboldi, K., Gioncada,**
18 **A., Molli, G., Basso, D., Varas-Malca, R., Pierantoni, P.P., Villa, I.M.,**
19 **Lambert, O., Landini, W., Sarti, G., Cantalamessa, G., Urbina, M. &**
20 **Bianucci, G.** In press. Allostratigraphy and palaeontology of the upper
21 Miocene Pisco Formation along the western side of the lower Ica Valley (Ica
22 Desert, Peru). *Rivista Italiana di Paleontologia e Stratigrafia*.
- 23
24
25 **Dooley, A. C., Jr.** 2005. A new species of *Squalodon* (Mammalia, Cetacea) from the
26 Middle Miocene of Virginia. *Virginia Museum of Natural History Memoir*, **8**,
27 1-43.
- 28
29 **Dubrovo, I. A. & Sanders, A. E.** 2000. A new species of *Patriocetus* (Mammalia,
30 Cetacea) from the late Oligocene of Kazakhstan. *Journal of Vertebrate*
31 *Paleontology*, **20**, 577-590.
- 32
33
34 **Dunbar, R. B., Marty, R. C. & Baker, P. A.** 1990. Cenozoic marine sedimentation
35 in the Sechura and Pisco basins, Peru. *Palaeogeography, Palaeoclimatology,*
36 *Palaeoecology*, **77**, 235-261.
- 37
38
39 **Engel, R. & McCartney, K.** 1990. Silicoflagellates recovered from Deep Sea, ODP
40 Leg 199 site 1219, east Equatorial Pacific. *Proceedings of the Ocean Drilling*
41 *Program, Scientific Results*, **199**, 1-29.
- 42
43
44 **Fahlke, J. M., Bastl, K. A., Semprebon, G. M. & Gingerich, P. D.** 2013.
45 Paleocology of archaeocete whales throughout the Eocene: Dietary
46 adaptations revealed by microwear analysis. *Palaeogeography,*
47 *Palaeoclimatology, Palaeoecology*, **386**, 690-701.
- 48
49
50 **Fitzgerald, E. M. G.** 2010. The morphology and systematics of *Mammalodon*
51 *colliveri* (Cetacea: Mysticeti), a toothed mysticete from the Oligocene of
52 Australia. *Zoological Journal of the Linnean Society*, **158**, 367-476.
- 53
54
55
56
57
58
59
60

- 1
2
3 **Flower, W. H.** 1867. Description of the skeleton of *Inia geoffrensis* and the skull of
4 *Pontoporia blainvillii*, with remarks on the systematic position of these
5 animals in the Order Cetacea. *Transactions of the Zoological Society of*
6 *London*, **6**, 87-116.
7
8
9
10 **Flynn, T. T.** 1948. Description of *Prosqualodon davidi* Flynn: A fossil cetacean from
11 Tasmania. *Transactions of the Zoological Society of London*, **26**, 153-197.
12
13 **Fordyce, R. E.** 1981. Systematics of the odontocete whale *Agorophius pygmaeus* and
14 the family Agorophiidae (Mammalia: Cetacea). *Journal of Paleontology*, **55**,
15 1028-1045.
16
17
18 **Fordyce, R. E.** 1982. Dental anomaly in a fossil squalodont dolphin from New
19 Zealand, and the evolution of polydonty in whales. *New Zealand Journal of*
20 *Zoology*, **9**, 419-426.
21
22
23 **Fordyce, R. E.** 1994. *Waipatia maerewhenua*, new genus and new species
24 (Waipatiidae, new family), an archaic late Oligocene dolphin from New
25 Zealand. Pp. 147-178 in A. Berta & T. A. Deméré (eds.) *Contributions in*
26 *marine mammal paleontology honoring Frank C. Whitmore, Jr.* Proceedings
27 of the San Diego Society of Natural History, 29.
28
29
30
31 **Fordyce, R. E.** 2002. *Simocetus rayi* (Odontoceti: Simocetidae) (new species, new
32 genus, new family), a bizarre new archaic Oligocene dolphin from the eastern
33 North Pacific. *Smithsonian Contributions to Paleobiology* 93: 185-222.
34
35
36
37 **Fordyce, R. E.** 2004. The transition from Archaeoceti to Neoceti: Oligocene
38 archaeocetes in the southwest Pacific. *Journal of Vertebrate Paleontology* 24
39 (suppl. to 3): 59A.
40
41
42 **Fordyce, R. E. & Barnes, L. G.** 1994. The evolutionary history of whales and
43 dolphins. *Annual Review of Earth and Planetary Science* 22: 419-455.
44
45
46 **Fordyce, R. E. & Muizon, C., de.** 2001. Evolutionary history of cetaceans: a review.
47 Pp. 169-233 in J.-M. Mazin & V. de Buffrénil (eds.) *Secondary adaptation of*
48 *tetrapods to life in water*. Verlag Dr. Friedrich Pfeil, München.
49
50
51 **Galatius, A. & Kinze, C. C.** 2003. Ankylosis patterns in the postcranial skeleton and
52 hyoid bones of the harbour porpoise (*Phocoena phocoena*) in the Baltic and
53 North Sea. *Canadian Journal of Zoology*, **81**, 1851-1861.
54
55
56 **Geisler, J. H., Sanders, A. E. & Luo, Z.-X.** 2009. A new protocetid whale (Cetacea:
57 Archaeoceti) from the late middle Eocene of South Carolina. *American*
58 *Museum Novitates*, **3480**, 1-65.
59
60

- 1
2
3 **Geisler, J. H., McGowen, M. R., Yang, G. & Gatesy, J.** 2011. A supermatrix
4 analysis of genomic, morphological, and paleontological data for crown
5 Cetacea. *BMC Evolutionary Biology*, **11**, 1-22.
6
7
8 **Geisler, J. H., Colbert, M. W. & Carew, J. L.** 2014. A new fossil species supports
9 an early origin for toothed whale echolocation. *Nature*, **508**, 383-386.
10
11 **Glaessner, M.** 1955. Pelagic fossils (Aturia, penguins, whales) from the Tertiary of
12 South Australia. *Records of the South Australian Museum*, **11**, 353-372.
13
14 **Godfrey, S. J., Uhen, M. D., Osborne, J. E. & Edwards, L. E.** 2016. A new
15 specimen of *Agorophius pygmaeus* (Agorophiidae, Odontoceti, Cetacea) from
16 the early Oligocene Ashley Formation of South Carolina, USA. *Journal of*
17 *Paleontology*, **90**, 154-169.
18
19
20
21 **Goloboff, P. A.** 1993. Estimating character weights during tree search. *Cladistics*, **9**,
22 83-91.
23
24
25 **Hanna, G. D.** 1931. Diatoms and silicoflagellates of the Kreyenhagen shale.
26 *California Division of Mines Report*, **27**, 187-201.
27
28 **Hector, J.** 1881. Notes on New Zealand Cetacea, recent and fossil. *Transactions and*
29 *Proceedings of the New Zealand Institute*, **13**, 434-437.
30
31 **Heithaus, M. R.** 2001. Predator-prey and competitive interactions between sharks
32 and dolphins: a review. *Journal of Zoology*, **253**, 53-68.
33
34
35 **Heyning, J. E.** 1997. Sperm whale phylogeny revisited: analysis of the morphological
36 evidence. *Marine Mammal Science*, **13**, 596-613.
37
38 **Hocking, D. P., Evans, A. R. & Fitzgerald, E. M. G.** 2013. Leopard seals
39 (*Hydrurga leptonyx*) use suction and filter feeding when hunting small prey
40 underwater. *Polar Biology*, **36**, 211-222.
41
42
43 **Ichishima, H.** 2016. The ethmoid and presphenoid of cetaceans. *Journal of*
44 *Morphology*, **277**, 1661-1674.
45
46 **Kellogg, R.** 1923. Description of two squalodonts recently discovered in the Calvert
47 Cliffs, Maryland; and notes on the shark-toothed dolphins. *Proceedings of the*
48 *United States National Museum*, **62**, 1-69.
49
50
51 **Kellogg, R.** 1936. A review of the Archaeoceti. *Carnegie Institute of Washington*
52 *Publication*, **482**, 1-366.
53
54
55 **Klimley, A. P.** 1994. The predatory behavior of the white shark. *American Scientist*,
56 **82**, 122-133.
57
58
59
60

- 1
2
3 **Lambert, O.** 2005. Phylogenetic affinities of the long-snouted dolphin
4 *Eurhinodelphis* (Cetacea, Odontoceti) from the Miocene of Antwerp.
5 *Palaeontology*, **48**, 653-679.
6
7
8 **Lambert, O., Bianucci, G. & Urbina, M.** 2014. *Huaridelphis raimondii*, a new early
9 Miocene Squalodelphinidae (Cetacea, Odontoceti) from the Chilcatay
10 Formation, Peru. *Journal of Vertebrate Paleontology*, **34**, 987-1004.
11
12 **Lambert, O., Muizon, C., de & Bianucci, G.** 2015. A new archaic homodont
13 toothed whale (Mammalia, Cetacea, Odontoceti) from the early Miocene of
14 Peru. *Geodiversitas*, **37**, 79-108.
15
16
17 **Lambert, O., Bianucci, G. & Muizon, C., de.** 2016. Macroraptorial sperm whales
18 (Cetacea, Odontoceti, Physeteroidea) from the Miocene of Peru. *Zoological*
19 *Journal of the Linnean Society*. doi: 10.1111/zoj.12456
20
21
22 **Lambert, O., Bianucci, G., Urbina, M. & Geisler, J. H.** In press. A new inioid
23 (Cetacea, Odontoceti, Delphinida) from the Miocene of Peru and the origin of
24 modern dolphin and porpoise families. *Zoological Journal of the Linnean*
25 *Society*.
26
27
28
29 **Landini, W., Altamirano-Sierra, A., Collareta, A., Di Celma, C., Urbina, M. &**
30 **Bianucci, G.** 2017. The late Miocene elasmobranch assemblage from Cerro
31 Colorado (Pisco Formation, Peru). *Journal of South American Earth Sciences*,
32 **73**, 168-190.
33
34
35
36 **León, W., Aleman, A., Torres, V., Rosell, W. & De La Cruz, O.** 2008.
37 Estratigrafía, sedimentología y evolución tectónica de la cuenca Pisco
38 Oriental. *Boletín INGEMMET*, **27**, 1-144.
39
40
41 **Long, D. J. & Jones, R. E.** 1996. White shark predation and scavenging on cetaceans
42 in the eastern North Pacific Ocean. Pp. 293-307 in A. P. Klimley & D. G.
43 Ainley (eds.) *Great white sharks: the biology of Carcharodon carcharias*.
44 Academic Press, San Diego.
45
46
47 **Luo, Z.-X. & Gingerich, P. D.** 1999. Terrestrial Mesonychia to aquatic Cetacea:
48 transformation of the basicranium and evolution of hearing in whales.
49 *University of Michigan Papers on Paleontology*, **31**, 1-98.
50
51
52 **Lydekker, R.** 1893. Contribution to the knowledge of the fossil vertebrates of
53 Argentina. Part II. Cetacean skulls from Patagonia. *Anales del Museo de La*
54 *Plata*, **1893**, 1-14.
55
56
57
58
59
60

- 1
2
3 **MacPhee, R. D.** 1981. Auditory regions of primates and eutherian insectivores.
4 *Contributions to Primatology*, **18**, 1-282.
- 5
6 **Macharé, J., DeVries, T., Barron, J. & Fourtanier, E.** 1988, Oligo-Miocene
7 transgression along the Pacific margin of South America: new paleontological
8 and geological evidence from the Pisco basin (Peru). *Géodynamique*, **3**, 25-37.
- 9
10 **Martínez-Cáceres, M., Lambert, O. & Muizon, C. de.** In press. The anatomy and
11 phylogenetic affinities of *Cynthiacetus peruvianus*, a large dorudontine
12 basilosaurid (Cetacea, Mammalia) from the late Eocene of Peru.
13 *Geodiversitas*.
- 14
15 **Marx, F. G., Lambert, O. & Uhen, M. D.** 2016. *Cetacean paleobiology*. John Wiley
16 & Sons, Chichester, UK, 319 pp.
- 17
18 **McGowen, M. R., Spaulding, M. & Gatesy, J.** 2009. Divergence date estimation
19 and a comprehensive molecular tree of extant cetaceans. *Molecular*
20 *Phylogenetics and Evolution*, **53**, 891-906.
- 21
22 **Mead, J. G. & Fordyce, R. E.** 2009. The therian skull: a lexicon with emphasis on
23 the odontocetes. *Smithsonian Contributions to Zoology*, **627**, 1-248.
- 24
25 **Moreno, F. P.** 1892. Noticias sobre algunos cetáceos fósiles y actuales de la
26 República Argentina. *Revista del Museo de La Plata*, **3**, 383-400.
- 27
28 **Muizon, C., de.** 1985. Nouvelles données sur le diphylétisme des Dauphins de rivière
29 (Odontoceti, Cetacea, Mammalia). *Comptes Rendus de l'Académie des*
30 *Sciences, Paris*, **301**, 359-361.
- 31
32 **Muizon, C., de.** 1987. The affinities of *Notocetus vanbenedeni*, an Early Miocene
33 platanistoid (Cetacea Mammalia) from Patagonia, southern Argentina.
34 *American Museum Novitates*, **2904**, 1-27.
- 35
36 **Muizon, C., de.** 1988. Le polyphylétisme des Acrodelphidae, odontocètes
37 longirostres du Miocène européen. *Bulletin du Muséum National d'Histoire*
38 *Naturelle, Paris*, **10**, 31-88.
- 39
40 **Muizon, C., de.** 1991. A new Ziphiidae (Cetacea) from the Early Miocene of
41 Washington State (USA) and phylogenetic analysis of the major groups of
42 odontocetes. *Bulletin du Muséum National d'Histoire Naturelle, Paris*, **12**,
43 279-326.
- 44
45 **Muizon, C., de.** 1994. Are the squalodonts related to the platanistoids? Pp. 135-146
46 in A. Berta & T. Deméré (eds.) *Contributions in marine mammal paleontology*
47
48
49
50
51
52
53
54
55
56
57
58
59
60

1
2
3 honoring Frank Whitmore Jr. Proceedings of the San Diego Society of
4 Natural History, 29.

5
6 **Muizon, C., de & DeVries, T. J.** 1985. Geology and paleontology of late Cenozoic
7 marine deposits in the Sacaco area (Peru). *Geologische Rundschau*, **74**, 547-
8 563.

9
10
11 **Muizon, C., de, Billet, G., Argot, C., Ladevèze, S. & Goussard, F.** 2015.
12 *Alcidedorbignya inopinata*, a basal pantodont (Placentalia, Mammalia) from
13 the early Palaeocene of Bolivia: anatomy, phylogeny and palaeobiology.
14 *Geodiversitas*, **37**, 397-634.

15
16
17
18 **O'Leary, M. A.** 2010. An anatomical and phylogenetic study of the osteology of the
19 petrosal of extant and extinct artiodactylans (Mammalia) and relatives.
20 *Bulletin of the American Museum of Natural History*, **335**, 1-206.

21
22
23 **Park, T., Fitzgerald, E. M. G. & Evans, A. R.** 2016. Ultrasonic hearing and
24 echolocation in the earliest toothed whales. *Biology Letters*, **12**, 20160060.

25
26 **Pilleri, G.** 1985. The Miocene Cetacea of the Belluno sandstones (eastern southern
27 Alps). *Memorie di Scienze Geologiche*, **36**, 1-87.

28
29
30 **Pledge, N. S. & Rothausen, K.** 1977. *Metasqualodon Harwoodi* (Sanger, 1881) - a
31 redescription. *Records of the South Australian Museum*, **17**, 285-297.

32
33 **Priem, M. F.** 1914. Sur les poissons fossiles des terrains tertiaires supérieurs du Sud-
34 Ouest de la France. *Bulletin de la Société Géologique de France*, **14**, 118-131.

35
36
37 **Pyenson, N. D. & Sponberg, S. N.** 2011. Reconstructing body size in extinct crown
38 Cetacea (Neoceti) using allometry, phylogenetic methods and tests from the
39 fossil record. *Journal of Mammalian Evolution*, **18**, 269-288.

40
41
42 **Rothausen, K.** 1968. Die systematische Stellung der europäischen Squalodontidae
43 (Odontoceti, Mammalia). *Palaeontologische Zeitschrift*, **42**, 83-104.

44
45 **Sanders, A. E. & Geisler, J. H.** 2015. A new basal odontocete from the upper
46 Rupelian of South Carolina, USA, with contributions to the systematics of
47 *Xenorophus* and *Mirocetus* (Mammalia, Cetacea). *Journal of Vertebrate*
48 *Paleontology*, **35**, e890107.

49
50
51 **Schäfer, W.** 1972. *Ecology and palaeoecology of marine environments*. The
52 University of Chicago Press, Chicago, 568 pp.

53
54
55 **Schellpeper, M. E. & Watkins, D. K.** 1998. Oligocene to early Miocene
56 silicoflagellates from the Ivorian Basin, eastern equatorial Atlantic, site 959.
57 *Proceedings of the Ocean Drilling Program, Scientific Results*, 159, 493-508.
58
59
60

- 1
2
3 **Snively, E., Fahlke, J. M. & Welsh, R. C.** 2015. Bone-breaking bite force of
4 *Basilosaurus isis* (Mammalia, Cetacea) from the Late Eocene of Egypt
5 estimated by Finite Element Analysis. *PLoS ONE*, **10**, e0118380.
6
7
8 **Swofford, D. L.** 2001. *PAUP**. *Phylogenetic analysis using parsimony (*and other*
9 *methods)*. Version 4b10. Sinauer Associates, Sunderland, Massachusetts.
10
11 **Takakuwa, Y.** 2014. A dense occurrence of teeth of fossil “mako” shark (“*Isurus*”
12 *hastalis*: Chondrichthyes, Lamniformes), associated with a balaenopterid-
13 whale skeleton of the late Miocene Pisco Formation, Peru, South America.
14 *Bulletin of the Gumma Museum of Natural History*, **18**, 77-86.
15
16 **Tanaka, Y. & Fordyce, R. E.** 2014. Fossil dolphin *Otekaikea marplei* (latest
17 Oligocene, New Zealand) expands the morphological and taxonomic diversity
18 of Oligocene cetaceans. *PLoS ONE*, **9**, e107972.
19
20 **Tanaka, Y. & Fordyce, R. E.** 2015a. Historically significant late Oligocene dolphin
21 *Microcetus hectori* Benham 1935: a new species of *Waipatia* (Platanistoidea).
22 *Journal of the Royal Society of New Zealand*, **45**, 135-150.
23
24 **Tanaka, Y. & Fordyce, R. E.** 2015b. A new Oligo-Miocene dolphin from New
25 Zealand: *Otekaikea huata* expands diversity of the early Platanistoidea.
26 *Palaeontologia Electronica*, **18**, 1-71.
27
28 **Tanaka, Y. & Fordyce, R. E.** 2016. *Papahu*-like fossil dolphin from Kaikoura, New
29 Zealand, helps to fill the Early Miocene gap in the history of Odontoceti. *New*
30 *Zealand Journal of Geology and Geophysics*, **59**, 551-567.
31
32 **Thornburg T. M. & Kulm L. D.** 1981. Sedimentary basins of the Peru continental
33 margin: Structure, stratigraphy, and Cenozoic tectonics from 6°S to 16°S
34 latitude. Pp. 393-422 in: L. D. Kulm, J. Dymond, E. J. Dasch & D. M.
35 Hussong (eds.) *Nazca plate: Crustal formation and Andean convergence*.
36 Geological Society of America, Memoir 154, Boulder, CO.
37
38 **True, F.W.** 1909. A new genus of fossil cetaceans from Santa Cruz Territory,
39 Patagonia; and description of a mandible and vertebrae of *Prosqualodon*.
40 *Smithsonian Miscellaneous Collections*, **52**, 441-456.
41
42 **Uhen, M. D.** 2004. Form, function, and anatomy of *Dorudon atrox* (Mammalia,
43 Cetacea): an archaeocete from the middle to late Eocene of Egypt. *University*
44 *of Michigan Papers on Paleontology*, **34**, 1-222.
45
46
47
48
49
50
51
52
53
54
55
56
57
58
59
60

- 1
2
3 **Uhen, M. D.** 2008a. New protocetid whales from Alabama and Mississippi, and a
4 new cetacean clade, Pelagiceti. *Journal of Vertebrate Paleontology*, **28**, 589-
5 593.
6
7
8 **Uhen, M. D.** 2008b. A new *Xenorophus*-like odontocete cetacean from the Oligocene
9 of North Carolina and a discussion of the basal odontocete radiation. *Journal*
10 *of Systematic Palaeontology*, **6**, 433-452.
11
12 **Uhen, M. D.** 2009. Dental morphology, evolution of. Pp. 302-307 in W. F. Perrin, B.
13 Würsig & J. G. M. Thewissen (eds.) *Encyclopedia of Marine Mammals*,
14 *second edition*. Academic Press, San Diego.
15
16
17
18 **Wells, R. S. & Scott, M. D.** 1999. Bottlenose dolphin *Tursiops truncatus* (Montagu,
19 1821). Pp. 137-182 in S. H. Ridgway & R. Harrison (eds.) *Handbook of*
20 *marine mammals, vol. 6: The second book of dolphins and the porpoises*.
21 Academic Press, London.
22
23
24
25 **Werth, A. J.** 2006. Mandibular and dental variation and the evolution of suction
26 feeding in Odontoceti. *Journal of Mammalogy*, **87**, 579-588.
27
28 **Wetmore, K. L. & Andrews, G. W.** 1991. Silicoflagellate and diatom
29 biostratigraphy in successive Burdigalian transgressions, middle Atlantic
30 coastal plain. *Micropaleontology*, **36**, 283-295.
31
32
33 **Whitmore, F. C., Jr. & Sanders, A. E.** 1976. Review of the Oligocene Cetacea.
34 *Systematic Biology*, **25**, 304-320.
35
36
37 **Wilson, L. E.** 1935. Miocene marine mammals from the Bakersfield region,
38 California. *Bulletin of the Peabody Museum of Natural History*, **4**, 1-143.
39
40 **Zúñiga-Rivero F. J., Klein G. D., Hay-Roe H. & Álvarez-Calderon E.** 2010. *The*
41 *hydrocarbon potential of Peru*. BPZ Exploración & Producción S.R.L., Lima,
42 Peru, 338 pp.
43
44
45
46
47
48
49
50
51
52
53
54
55
56
57
58
59
60

1
2
3 **Appendix 1.** List of silicoflagellate taxa from sample PN2.

4 *Corbisema triacantha* (Ehrenberg 1844) Hanna 1931

5
6 *Distephanopsis crux* subsp. *scutulata* (Bukry) Desikachary & Prema 1996

7
8 *Naviculopsis obtusarca* Bukry 1978 (DSDP44-37)

9
10 *Naviculopsis obtusarca* Bukry var. *acicula* Bukry 1985

11 *N. ponticula* subsp. *ponticula* (Ehrenberg) Bukry 1982

12
13 *Naviculopsis* sp. 2 Cisielsky 1991

14
15
16
17
18
19
20
21
22
23
24
25
26
27
28
29
30
31
32
33
34
35
36
37
38
39
40
41
42
43
44
45
46
47
48
49
50
51
52
53
54
55
56
57
58
59
60

For Review Only

Table captions

Table 1. Measurements (in mm) of the skull of *Inticetus vertizi* MUSM 1980 (holotype). e estimate, + incomplete, - missing data.

Table 2. Measurements (in mm) and number of accessory denticles for the upper and lower teeth of *Inticetus vertizi* MUSM 1980 (holotype). e estimate, + incomplete, - missing data.

Table 3. Measurements (in mm) of the vertebrae of *Inticetus vertizi* MUSM 1980 (holotype). e estimate, + incomplete, ++ very incomplete, - missing data. Roman numbers for post-cervical vertebrae indicate that the identification is only tentative.

Figure captions

Figure 1. Map of the northern part of the Pisco Basin, southern coast of Peru, indicating several fossil-rich localities of the Pisco Formation (Cerro Colorado, Cerro los Quesos, and Cerro la Bruja) and Chilcatay Formation (Roca Negra, Ullujaya, and Zamaca). Roca Negra (black star) is the locality where *Inticetus vertizi* MUSM 1980 (holotype) was found. Modified from Lambert *et al.* (2014).

Planned for column width.

Figure 2. Stratigraphic column of part of the lower unit of the Chilcatay Formation in the Roca Negra locality, providing the relative position of *Inticetus vertizi* MUSM 1980 (holotype) and of the sample PN2 having yielded a biostratigraphically informative silicoflagellate assemblage (Early Miocene, late early Burdigalian).

Planned for column width.

Figure 3. Cranium and mandibles of *Inticetus vertizi* MUSM 1980 (holotype). **A**, dorsal view; **B**, corresponding explanatory linear drawing; **C**, detail of the posterior part with a different lighting. Scale bars equal 200 mm.

1
2
3 **Figure 4.** Cranium and mandibles of *Inticetus vertizi* MUSM 1980 (holotype). **A**, left
4 lateral view; **B**, corresponding explanatory linear drawing. Scale bar equals 200 mm.
5
6

7
8 **Figure 5.** Cranium and mandibles of *Inticetus vertizi* MUSM 1980 (holotype). **A**,
9 ventral view; **B**, corresponding explanatory linear drawing. Scale bar equals 200 mm.
10
11

12
13 **Figure 6.** Cranium and mandibles of *Inticetus vertizi* MUSM 1980 (holotype). **A**,
14 detail of the neurocranium region in left lateral view; **B**, corresponding explanatory
15 linear drawing. Scale bar equals 100 mm.
16
17

18
19 **Figure 7.** Cranium and mandibles of *Inticetus vertizi* MUSM 1980 (holotype). **A**,
20 detail of the left side of the basicranium in ventrolateral view; **B**, corresponding
21 explanatory linear drawing. Grey areas for sediment; hatched areas for break surfaces.
22 Scale bar equals 100 mm.
23
24
25
26

27
28 **Figure 8.** Cranium of *Inticetus vertizi* MUSM 1980 (holotype) in posterior view.
29 Scale bar equals 100 mm.
30
31

32
33 **Figure 9.** Right periotic of *Inticetus vertizi* MUSM 1980 (holotype). **A**, ventral view;
34 **B**, corresponding explanatory linear drawing; **C**, ventral view with accessory ossicle
35 removed; **D**, medial view; **E**, dorsomedial and slightly anterior view; **F**,
36 corresponding explanatory linear drawing; **G**, dorsal view; **H**, lateral view.
37 Abbreviations: crista interfen, crista interfenestralis; lateral ctp; lateral caudal
38 tympanic process; medial ctp, medial caudal tympanic process. Grey areas for main
39 openings; hatched areas for break surfaces. Periotic whitened with ammonium
40 chloride. Scale bar equals 30 mm.
41
42
43
44
45
46

47
48 **Figure 10.** Right tympanic bulla of *Inticetus vertizi* MUSM 1980 (holotype). **A**,
49 medial view; **B**, corresponding explanatory linear drawing; **C**, ventral view; **D**, dorsal
50 view; **E**, lateral view; **F**, corresponding explanatory linear drawing; **G**, posterior view;
51 **H**, anterior view. Grey areas for sediment; hatched areas for break surfaces. Tympanic
52 whitened with ammonium chloride. Scale bar equals 30 mm.
53
54
55
56
57
58
59
60

1
2
3 **Figure 11.** Right malleus of *Inticetus vertizi* MUSM 1980 (holotype). **A**, explanatory
4 linear drawing in posteromedial view; **B**, corresponding photo; **C**,
5 posteroventrolateral view. Scale bar equals 2 mm.
6
7

8
9
10 **Figure 12.** Detached upper teeth of *Inticetus vertizi* MUSM 1980 (holotype). **A-F**,
11 right I¹ in labial (A), lingual (B), mesial (C), and distal (D) view, and detail of the
12 crown in distolingual (E) and mesiolingual (F) view; **G-L**, right canine in labial (G),
13 lingual (H), mesial (I), and distal (J) view, and detail of the crown in distolingual (K)
14 and mesial (L) view. Scale bar equals 10 mm.
15
16
17

18
19
20 **Figure 13.** Cranium and mandibles of *Inticetus vertizi* MUSM 1980 (holotype). Detail
21 of the anterior part of the rostrum and mandible in oblique right anterolateral and
22 slightly dorsal view, showing upper and lower anterior teeth. For the size of elements,
23 refer to more orthogonal views.
24
25
26 Planned for column width.
27
28

29
30 **Figure 14.** Cranium and mandibles of *Inticetus vertizi* MUSM 1980 (holotype). **A**,
31 detail of the anterior part of the rostrum and mandible in right lateral view; **B**,
32 corresponding explanatory linear drawing; **C-E**, enlarged views of anterior cheek
33 teeth and incisors. Scale bar for A-B equals 100 mm.
34
35
36

37
38 **Figure 15.** Cranium and mandibles of *Inticetus vertizi* MUSM 1980 (holotype). **A**,
39 detail of the anterior part of the rostrum and mandible in left lateral view; **B-E**,
40 enlarged views of incisors, upper canine, and anterior cheek teeth C₂ and C⁵; **F**, detail
41 of the accessory denticles on the distal keel of C⁵. Scale bar for A equals 100 mm.
42
43
44
45

46
47 **Figure 16.** Cranium and mandibles of *Inticetus vertizi* MUSM 1980 (holotype). **A**,
48 detail of the posterior part of the rostrum and mandible in right lateral view, with
49 anterior part of the rostrum removed; **B-D**, detail of cheek teeth C⁹, C⁸, C⁷, and C₆.
50 Scale bar for A equals 50 mm.
51
52
53

54
55 **Figure 17.** Cranium and mandibles of *Inticetus vertizi* MUSM 1980 (holotype). **A**,
56 detail of the posterior part of the right lower tooth row including cheek teeth C₈₋₁₂, in
57 medial view; **B**, corresponding explanatory linear drawing. Scale bar equals 50 mm.
58
59
60

1
2
3
4
5 **Figure 18.** Fragment of the atlas of *Inticetus vertizi* MUSM 1980 (holotype). **A**,
6 anterior view; **B**, posterior view. Scale bar equals 20 mm.
7

8
9
10 **Figure 19.** Axis and cervicals C3-C7 of *Inticetus vertizi* MUSM 1980 (holotype). **A-**
11 **D**, axis and C3-C5 in anterior view (A), corresponding explanatory linear drawing
12 (B), right anterodorsolateral (C), and ventral (D) view; **E-F**, C6-C7 in anterior (E) and
13 ventral (F) view. Scale bar equals 20 mm.
14
15

16
17
18 **Figure 20.** Thoracic vertebrae of *Inticetus vertizi* MUSM 1980 (holotype). **A-B**, ThI
19 in posterior (A) and dorsal (B) view; **C-D**, ThII in anterior (C) and left lateral (D)
20 view; **E**, ThIII in anterior/posterior view; **F**, ThIV in right lateral view; **G**, ThIV-VI in
21 a single block with a rib fragments; **H-J**, ThVII in posterior (H), right lateral (I), and
22 dorsal (J) view; **K**, ThIX in right lateral view; **L-M**, ThXI in anterior/posterior (L)
23 and lateral (M) view. Scale bar equals 20 mm.
24
25
26
27

28
29
30 **Figure 21.** Lumbar vertebrae of *Inticetus vertizi* MUSM 1980 (holotype). **A**, LuIII in
31 ventral view; **B**, LuVI in dorsal view; **C**, LuVII in ventral view; **D-E**, LuVIII in
32 ventral (D) and anterior/posterior (E) view; **F**, LuIX in ventral view. Scale bar equals
33 20 mm.
34
35

36 Planned for column width.
37

38
39
40 **Figure 22.** Caudal vertebrae of *Inticetus vertizi* MUSM 1980 (holotype). **A**, CaI in
41 ventral view; **B**, CaII in ventral view; **C**, CaIII in ventral view; **D**, CaVI in ?right
42 lateral view; **E**, CaVII in ?left lateral view; **F**, CaVIII in ?left lateral view; **G**, CaIX in
43 lateral view; **H**, CaX in lateral view; **I-J**, CaXI in anterior/posterior (I) and lateral (J)
44 view; **K-M**, CaXII in anterior/posterior (K), lateral (L), and ventral (M) view; **N-O**,
45 CaXIII in anterior/posterior (N) and ?ventral (O) view; **P-Q**, CaXIV in
46 anterior/posterior (P) and ?ventral (Q) view; **R-S**, CaXV in anterior/posterior (R) and
47 ?ventral (S) view; **T**, CaXVI in anterior view; **U-V**, CaXVI + CaXVII in left lateral
48 (U) and ventral (V) view. Scale bar equals 20 mm.
49
50
51
52
53
54

55
56 **Figure 23.** Chart showing changes in the dimensions (in mm) of vertebral central
57 (namely length, height and width) along the vertebral column of *Inticetus vertizi*
58
59
60

1
2
3 MUSM 1980 (holotype). Numbers on the horizontal axis correspond to a sequence
4 from cervical C3 on the left to the last preserved caudals on the right, as listed in
5 Table 3. Some vertebrae could be missing and several centra were too incomplete to
6 be measured for one or more of their dimensions.
7
8
9

10
11 **Figure 24.** Sternum of *Inticetus vertizi* MUSM 1980 (holotype). **A-B**, manubrium in
12 dorsal (A), ventral (B), and right lateral (C) view; **D-F**, second sternebra in ?dorsal
13 (D), ?ventral (E), and anterior (F) view. Scale bar equals 20 mm.
14
15
16

17
18 **Figure 25.** Ribs of *Inticetus vertizi* MUSM 1980 (holotype). The rib fragments are
19 organized in an anteroposterior sequence from the lower part of the figure to the top,
20 except for the two lower distal fragments. Scale bar equals 50 mm.
21
22
23

24
25 **Figure 26.** Strict consensus tree for the phylogenetic analysis with equally weighted
26 characters and without molecular constraint (analysis 1), resulting in the placement of
27 *Inticetus vertizi* as a stem Odontoceti.
28
29
30

31
32 **Figure 27.** Alternative relationships of *Inticetus vertizi* resulting from other
33 phylogenetic analyses. **A**, strict consensus tree for the analysis with down-weighted
34 homoplastic characters and without molecular constraint (analysis 2), placing *I. vertizi*
35 in a large Platanistoidea clade; **B**, strict consensus tree for the analysis with equally
36 weighted homoplastic characters and with molecular constraint (analysis 3), placing *I.*
37 *vertizi* as a stem Odontoceti; **C**, strict consensus tree for the analysis with down-
38 weighted homoplastic characters and with molecular constraint (analysis 4), placing *I.*
39 *vertizi* in a large Platanistoidea clade.
40
41
42
43
44
45

46
47 **Figure 28.** Schematic drawing showing the position of the partly articulated skeleton
48 of *Inticetus vertizi* MUSM 1980 (holotype) as found in the field, together with three
49 shark teeth (black triangles). Detail photograph and interpretive drawing of the
50 rostrum and mandible of MUSM 1980 in left lateral view, with shallow shark bite
51 marks indicated. Scale bar for the skeleton equals 500 mm, scale bar for detail of the
52 rostrum and mandible equals 50 mm, and scale bars for shark teeth equal 10 mm.
53
54
55
56
57
58
59
60

	MUSM 1980
Cranium	
Condylobasal length	940
Rostrum length	600
Length of anterior premaxillary portion of rostrum (left/right)	81.5/79
Width of rostrum at base	e254
Distance from apex of rostrum to anterior margin of left bony naris	734
Bizygomatic width	e360
Distance between ventromedial margins of exoccipitals (lateral to jugular notch)	184
Distance between ventrolateral margins of basioccipital crests	161
Width of occipital condyles	e120
Width of foramen magnum	e47
Maximum width of nasals	+67
Distance between anterior tip of left zygomatic process and ventral tip of left postglenoid process	130
Periotic (right)	
Total length	50.3
Maximum mediolateral width (between medial top of pars cochlearis and lateral margin of lateral tuberosity)	32.9
Maximum thickness between ventral margin of pars cochlearis and dorsal process (taken perpendicular to horizontal surface)	20.4
Length of anterior process from apex to anterior margin of pars cochlearis)	17
Length of pars cochlearis until anteromedial margin of fenestra rotunda	17.8
Length of pars cochlearis until posteromediodorsal margin of stapedial muscle fossa	24.6
Length of posterior process from apex to posterior margin of fossa incudis	20
Tympanic bulla	
Maximum length (without posterior process) (left/right)	+57/56.7
Maximum width (left/right)	35/36.2
Maximum dorsoventral height of involucrum	-/23
Maximum width of facet for periotic on posterior process	-/13.7
Maximum length of facet for periotic on posterior process	+20/+19.1
Mandible	
Total length of left mandible	830
Length of symphyseal portion	366
Height of mandible at posterior end of symphysis	48

1
2
3
4
5
6
7
8
9
10
11
12
13
14
15
16
17
18
19
20
21
22
23
24
25
26
27
28
29
30
31
32
33
34
35
36
37
38
39
40
41
42
43
44
45
46
47
48
49
50
51
52
53
54
55
56
57
58
59
60

Width of each mandible at posterior end of symphysis	37
Distance between anterior tip of mandibular foramen and posterior surface of mandibular condyle	183
Height of mandibular condyle	+46

For Review Only

	Mesiodist. diameter at crown base	Bucco-lingual diameter at crown base	Height of crown (at mid-width)	Maximum mesiodist. diameter of root	Maximum buccolingual diameter of root	Total length of tooth	Number of large access. denticles mesial/distal
Incisors							
I ¹ r	10.8	9	17.2	14.1	11.8	56.6	0/0
I ¹ l	10.7	-	+16.5	-	-	-	0/0
I ² r	11	-	17	13.7	-	-	0/0
I ² l	11.1	-	+17.4	-	-	-	0/0
I ³ r	10.8	-	19	13.7	-	-	0/0
I ³ l	-	-	+18	-	-	-	0/0
I ₁ r	9.8	8.8	+14.3	-	-	-	0/0
I ₁ l	9.4	8.1	+14.3	-	-	-	0/0
I ₂ r	10.3	-	+11.9	-	-	-	0/0
I ₂ l	9.4	-	+14.3	-	-	-	0/0
I ₃ r	10.2	-	+15.8	-	-	-	0/0
I ₃ l	10.5	-	-	-	-	-	0/0
Canines							
Ca ¹ r	11.1	-	17.1	14.1	-	+54.7	0/0
Ca ¹ l	10.3	-	17	-	-	-	0/0
Ca ₁ r	+9.8	-	17.3	-	-	-	0/0
Ca ₁ l	10.9	8.9	18.7	-	-	-	0/0
Cheek teeth							
C ¹ r	11.25	-	+16.3	14.3	-	-	0/0
C ¹ l	11.4	-	+13.5	-	-	-	0/0
C ³ r	12.6	-	16.5	16.8	-	-	0/0
C ⁴ r	14.2	-	17.8	19	-	-	0/0
C ⁵ r	-	-	-	-	-	-	-/0
C ⁵ l	16.5	-	18.6	-	-	-	0/0
C ⁶ r	-	-	-	-	-	-	0/3
C ⁷ r	+24	-	-	-	-	-	0/3
C ⁸ r	27.5	-	-	-	-	-	3/+3
C ⁹ r	29.9	-	-	-	-	-	3/+2
C ¹⁰ r	31.9	-	-	-	-	-	3/+2
C ¹¹ r	+30	-	-	-	-	-	-
C ₁ r	11.3	-	+15.1	-	-	-	0/0
C ₁ l	11.5	9.2	?19.2	-	-	-	0/0
C ₂ r	12.5	-	+14.2	-	-	-	0/0
C ₂ l	12.3	-	16	-	-	-	0/0
C ₃ r	13	-	+15.6	-	-	-	0/0
C ₃ l	13.4	-	+15.3	-	-	-	0/0
C ₄ r	14.7	-	16.3	-	-	-	0/0
C ₄ l	14.5	-	15.8	-	-	-	0/0
C ₅ r	16.5	-	17.6	-	-	-	0/0
C ₅ l	16.3	-	17.3	-	-	-	0/0
C ₆ r	-	-	-	-	-	-	0/1
C ₈ r	32.2	-	+16.7	-	-	-	3/4
C ₉ r	35.7	-	20.8	-	-	-	3/5
C ₁₀ r	35.5	-	22.2	-	-	-	4/5
C ₁₁ r	+33.6	-	+17.2	-	-	-	+3/5
C ₁₂ r	+32	-	-	-	-	-	-/+3
C ₁₃ r	+32	-	-	-	-	-	-/+3

	Centrum length	Centrum height	Width anterior epiphysis	Width posterior epiphysis	Width neural canal	Total width	Field number
Cervicals							
C3	e19	-	-	-	-	-	-
C4	e15.5	-	-	-	-	-	-
C5	-	-	-	-	-	-	-
C6	e20	52	e60.5	-	-	-	-
C7	23	51	-	e74	-	-	-
Thoracics							
ThI	37	48	68	66	-	-	T1
ThII	+31	51	-	58	e52	-	32
ThIII	+43	51	e61	-	-	-	31
ThIV	63	e55	-	-	29	-	A
ThV	+52	53.5	63	-	-	-	B
ThVI	+43	-	-	-	-	-	C
ThVII	-	60.5	-	69	e34	-	*
ThVIII	+50	59	66	-	e34	-	24
ThIX	71	e56	-	-	-	-	30
ThX	+64	e63	e75	-	-	-	23
ThXI	+56	+63	76	-	+27	-	29
Lumbar							
LuI	+58	e72	+67	-	-	-	22
LuII	+71	++66	-	-	-	-	28
LuIII	87	+60	e75	-	-	-	27
LuIV	67	+48	+69	-	-	-	26
LuV	+64	-	++73	-	-	-	25
LuVI	94	-	-	-	-	-	21
LuVII	+85	-	+80	-	-	-	20
LuVIII	98	++56	++75	-	-	-	19
LuIX	101	-	-	-	-	-	18
Caudals							
CaI	96	-	++67	-	-	-	17
CaII	++83	-	83	-	-	-	16
CaIII	89	-	e2x43	-	-	-	15
CaIV	-	-	-	-	-	-	14
CaV	+81	+95	-	-	-	-	13
CaVI	+80	81	-	-	-	-	12
CaVII	+76	-	-	-	-	-	11
CaVIII	82	+86	-	-	-	-	10
CaIX	77	+74	-	-	-	-	9
CaX	66	+66	-	-	-	-	8
CaXI	43	-	-	-	-	-	7
CaXII	31	-	-	-	-	-	4
CaXIII	e28	-	-	-	-	e65	5
CaXIV	25	28	-	-	-	e67	3
CaXV	21	40	-	-	-	68	6
CaXVI	21	22	-	-	-	56	2

CaXVII	19	14.5	-	-	-	e46	1
--------	----	------	---	---	---	-----	---

For Review Only

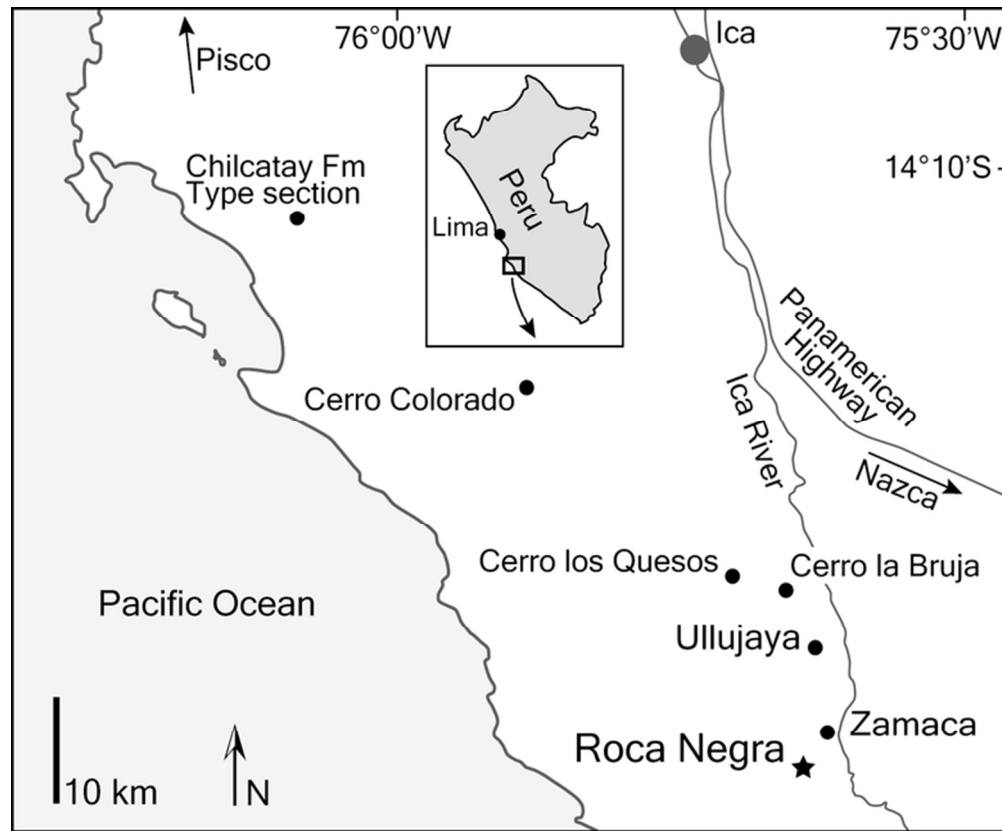


Figure 1. Map of the northern part of the Pisco Basin, southern coast of Peru, indicating several fossil-rich localities of the Pisco Formation (Cerro Colorado, Cerro los Quesos, and Cerro la Bruja) and Chilcatay Formation (Roca Negra, Ullujaya, and Zamaca). Roca Negra (black star) is the locality where *Inticetus vertizi* MUSM 1980 (holotype) was found. Modified from Lambert et al. (2014).
Planned for column width.

66x54mm (300 x 300 DPI)

1
2
3
4
5
6
7
8
9
10
11
12
13
14
15
16
17
18
19
20
21
22
23
24
25
26
27
28
29
30
31
32
33
34
35
36
37
38
39
40
41
42
43
44
45
46
47
48
49
50
51
52
53
54
55
56
57
58
59
60

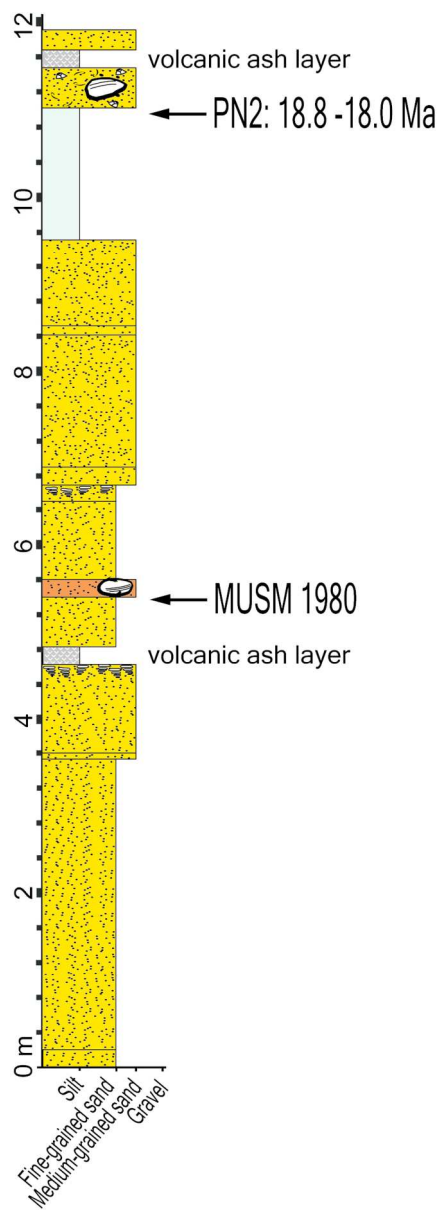


Figure 2. Stratigraphic column of part of the lower unit of the Chilcatay Formation in the Roca Negra locality, providing the relative position of *Inticetus vertizi* MUSM 1980 (holotype) and of the sample PN2 having yielded a biostratigraphically informative silicoflagellate assemblage (Early Miocene, late early Burdigalian). Planned for column width.

99x276mm (300 x 300 DPI)

1
2
3
4
5
6
7
8
9
10
11
12
13
14
15
16
17
18
19
20
21
22
23
24
25
26
27
28
29
30
31
32
33
34
35
36
37
38
39
40
41
42
43
44
45
46
47
48
49
50
51
52
53
54
55
56
57
58
59
60

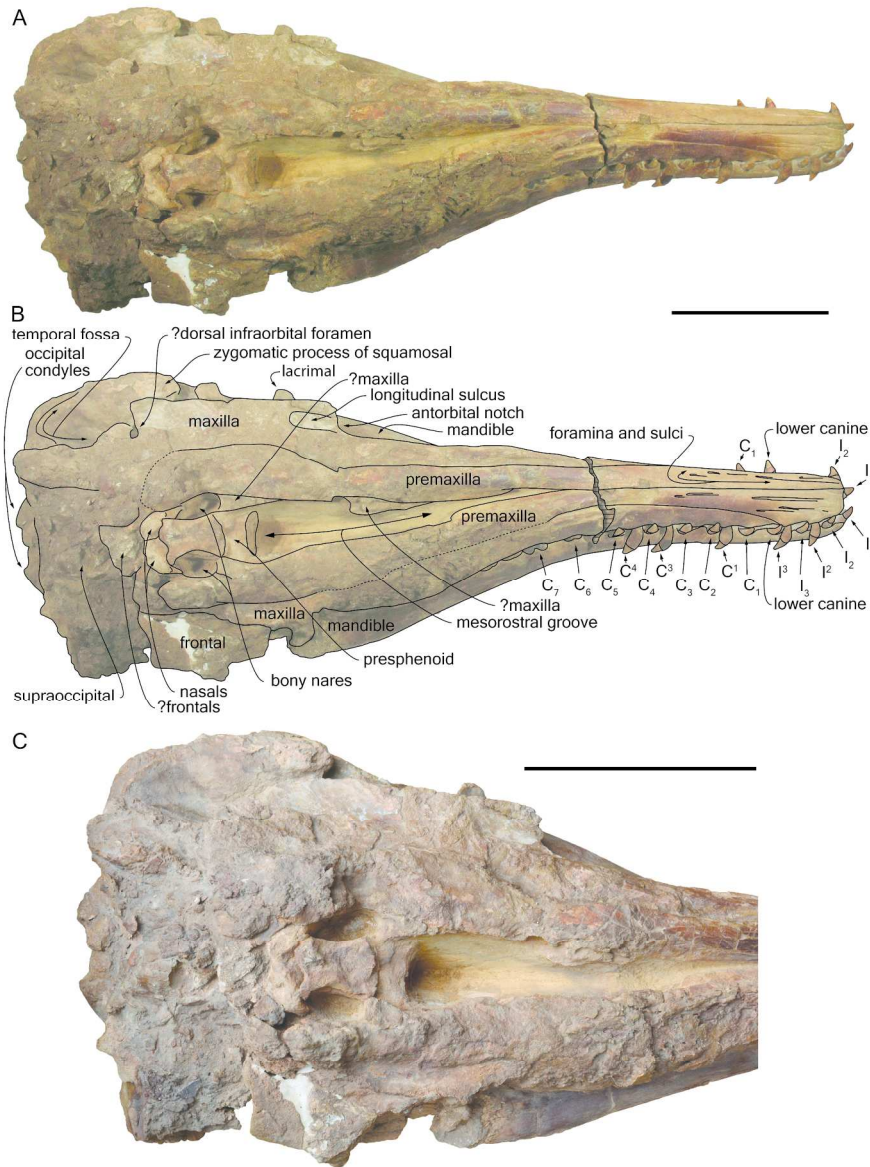
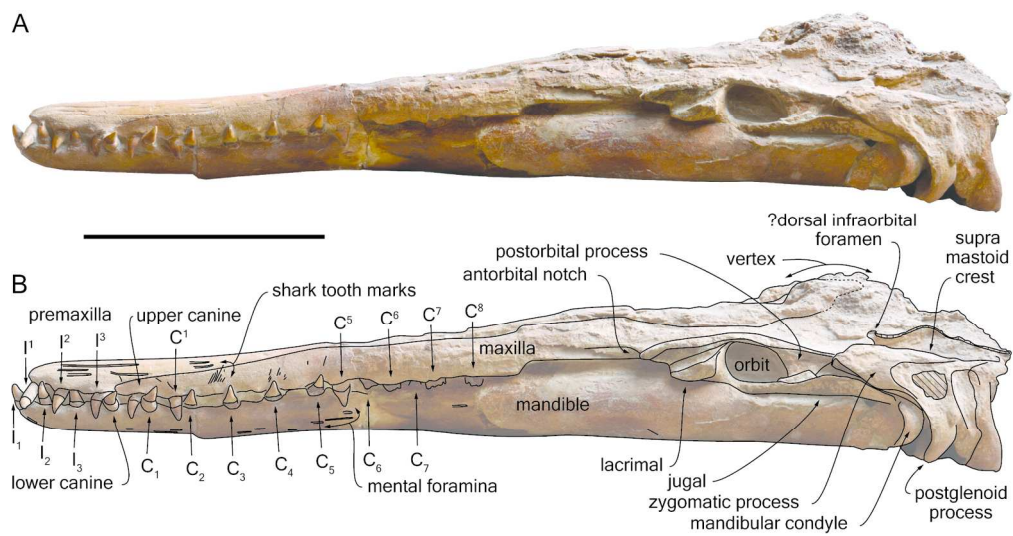


Figure 3. Cranium and mandibles of *Inticetus vertizi* MUSM 1980 (holotype). A, dorsal view; B, corresponding explanatory linear drawing; C, detail of the posterior part with a different lighting. Scale bars equal 200 mm.

168x231mm (300 x 300 DPI)



25 Figure 4. Cranium and mandibles of *Inticetus vertizi* MUSM 1980 (holotype). A, left lateral view; B,
26 corresponding explanatory linear drawing. Scale bar equals 200 mm.

27 165x86mm (300 x 300 DPI)

1
2
3
4
5
6
7
8
9
10
11
12
13
14
15
16
17
18
19
20
21
22
23
24
25
26
27
28
29
30
31
32
33
34
35
36
37
38
39
40
41
42
43
44
45
46
47
48
49
50
51
52
53
54
55
56
57
58
59
60

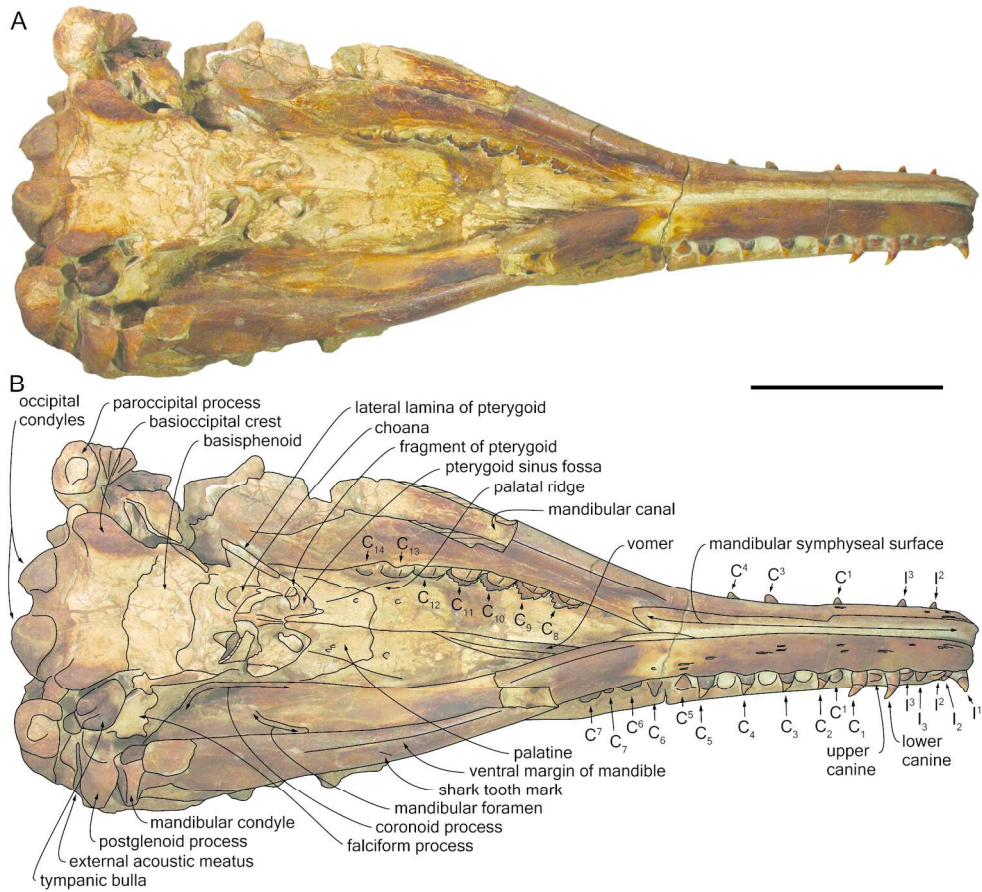


Figure 5. Cranium and mandibles of *Inticetus vertizi* MUSEM 1980 (holotype). A, ventral view; B, corresponding explanatory linear drawing. Scale bar equals 200 mm.

169x153mm (300 x 300 DPI)

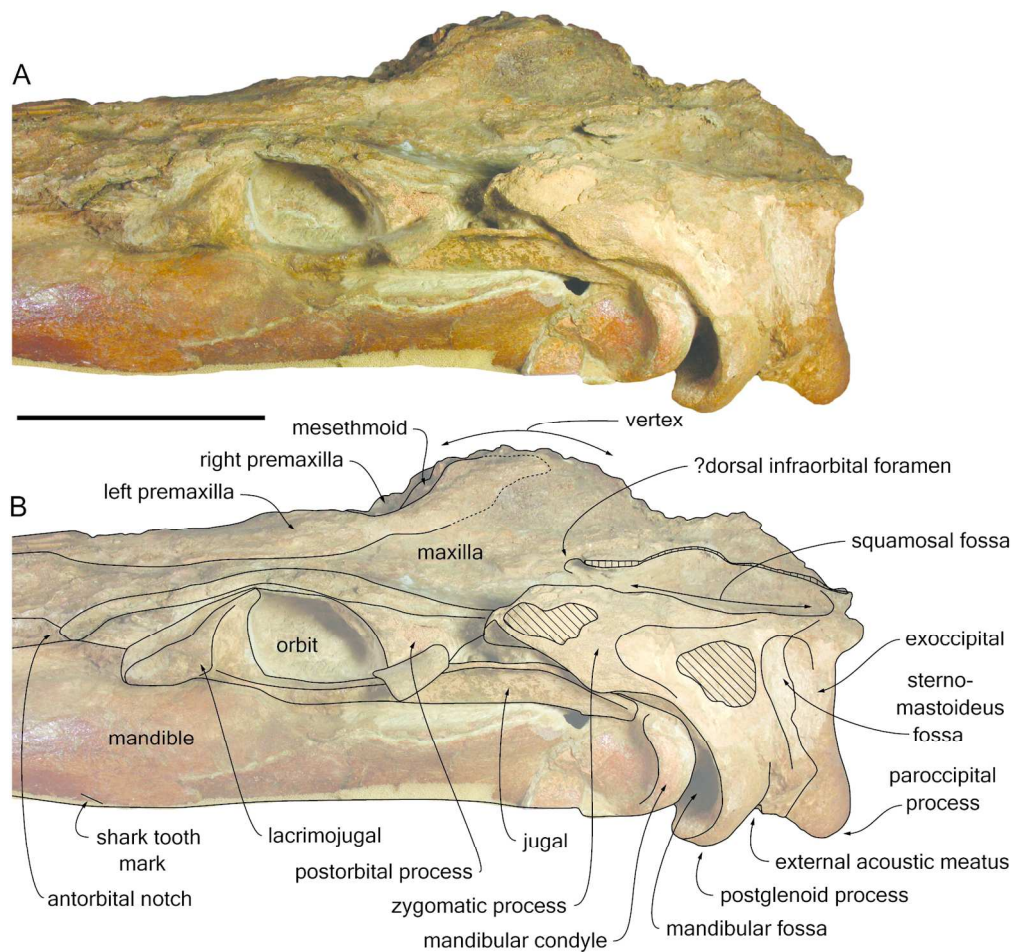


Figure 6. Cranium and mandibles of *Inticetus vertizi* MUSM 1980 (holotype). A, detail of the neurocranium region in left lateral view; B, corresponding explanatory line drawing. Scale bar equals 100 mm.

149x142mm (300 x 300 DPI)

1
2
3
4
5
6
7
8
9
10
11
12
13
14
15
16
17
18
19
20
21
22
23
24
25
26
27
28
29
30
31
32
33
34
35
36
37
38
39
40
41
42
43
44
45
46
47
48
49
50
51
52
53
54
55
56
57
58
59
60

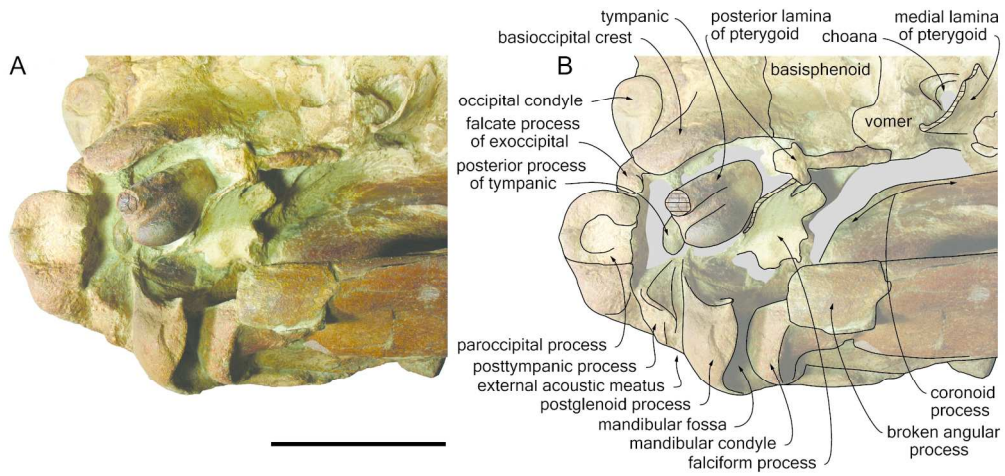


Figure 7. Cranium and mandibles of *Inticetus vertizi* MUSM 1980 (holotype). A, detail of the left side of the basicranium in ventrolateral view; B, corresponding explanatory linear drawing. Grey areas for sediment; hatched areas for break surfaces. Scale bar equals 100 mm.

166x77mm (300 x 300 DPI)

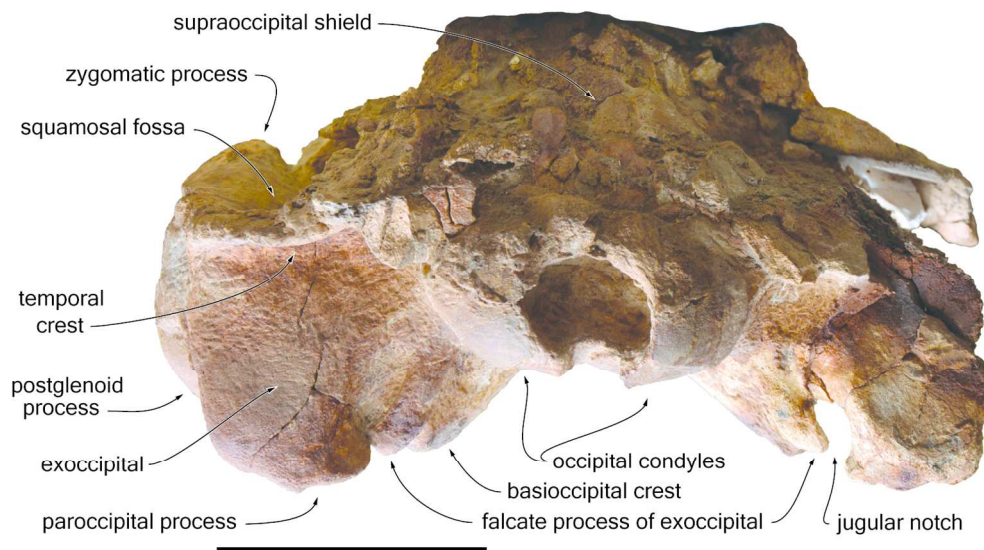


Figure 8. Cranium of *Inticetus vertizi* MUSM 1980 (holotype) in posterior view. Scale bar equals 100 mm.

144x78mm (300 x 300 DPI)

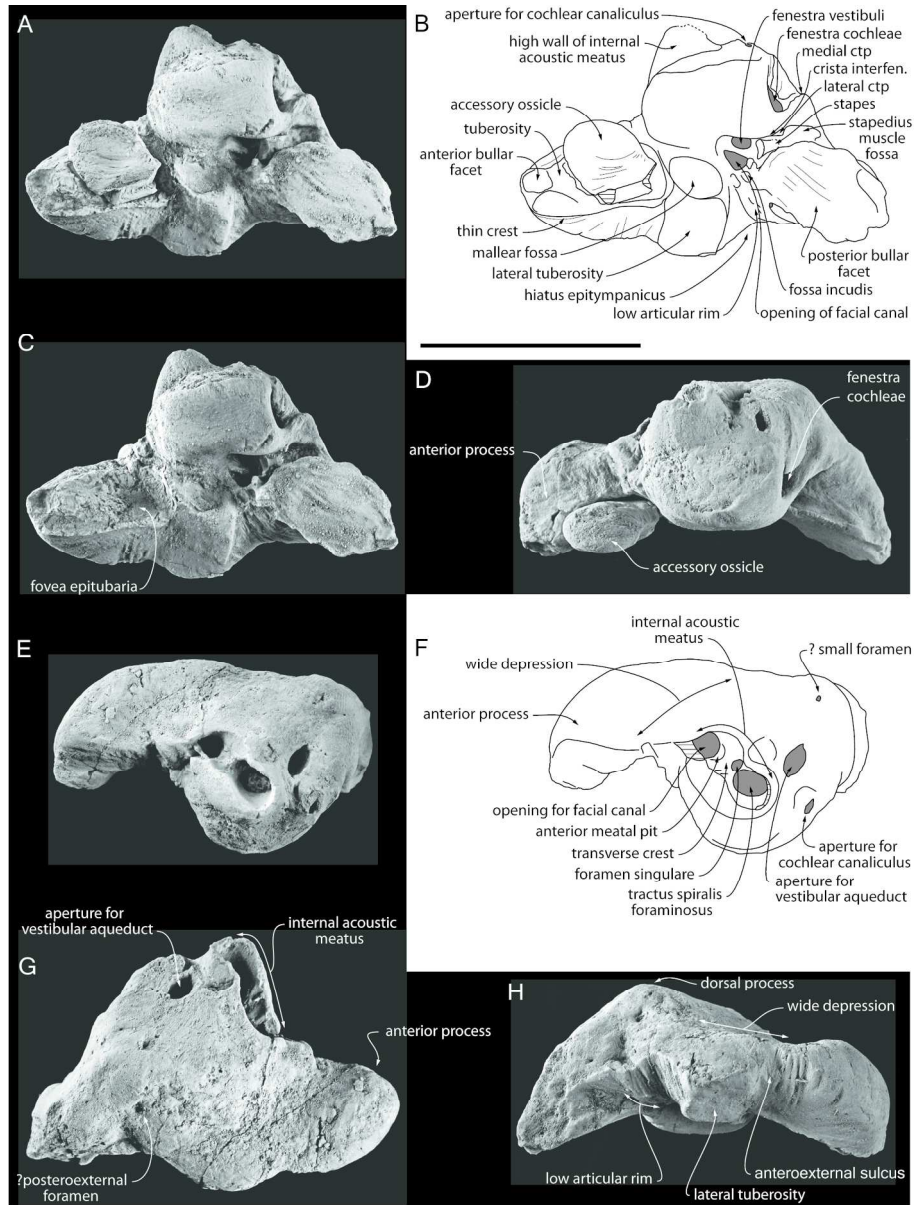


Figure 9. Right periotic of *Inticetus vertizi* MUSM 1980 (holotype). A, ventral view; B, corresponding explanatory linear drawing; C, ventral view with accessory ossicle removed; D, medial view; E, dorsomedial and slightly anterior view; F, corresponding explanatory linear drawing; G, dorsal view; H, lateral view. Abbreviations: crista interfen, crista interfenestralis; lateral ctp; lateral caudal tympanic process; medial ctp, medial caudal tympanic process. Grey areas for main openings; hatched areas for break surfaces. Periotic whitened with ammonium chloride. Scale bar equals 30 mm.

161x214mm (300 x 300 DPI)

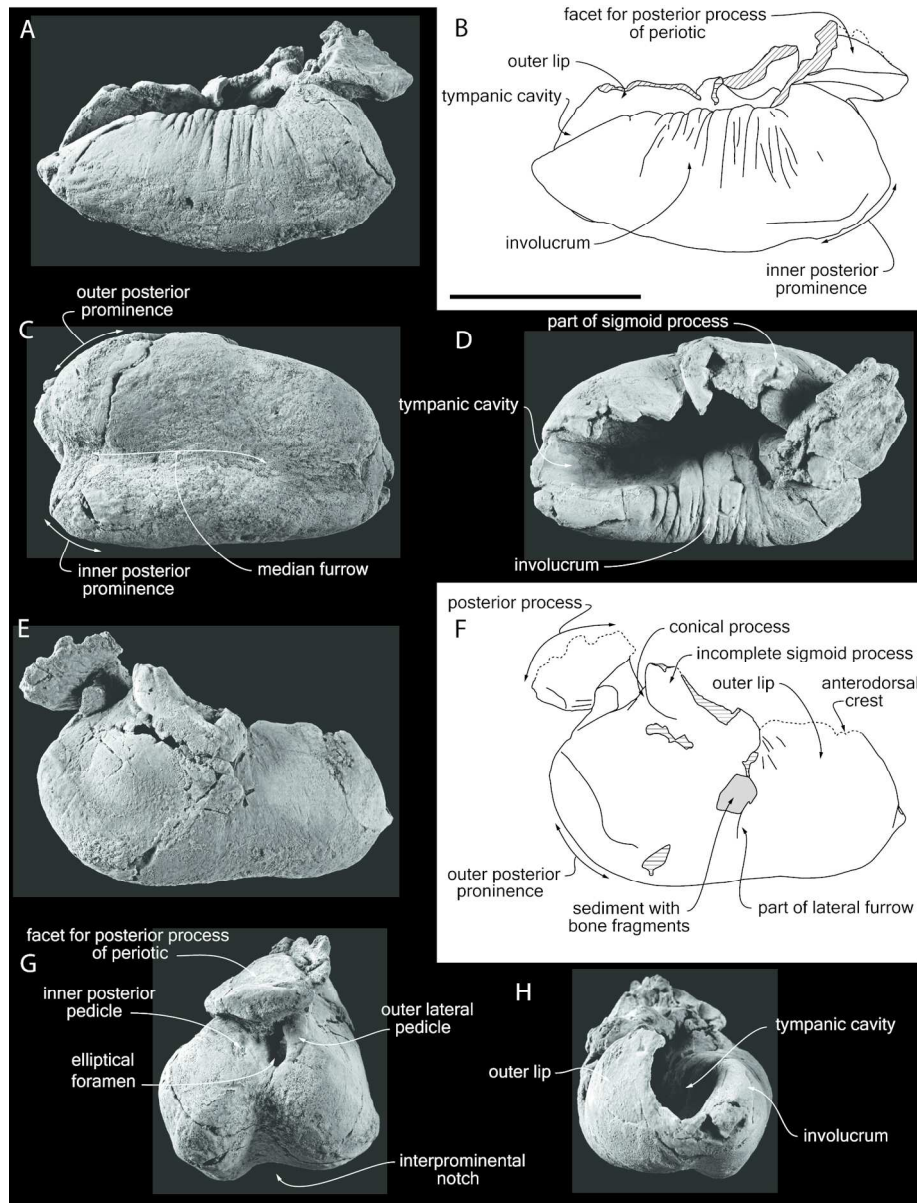


Figure 10. Right tympanic bulla of *Inticetus vertizi* MUSM 1980 (holotype). A, medial view; B, corresponding explanatory linear drawing; C, ventral view; D, dorsal view; E, lateral view; F, corresponding explanatory linear drawing; G, posterior view; H, anterior view. Grey areas for sediment; hatched areas for break surfaces. Tympanic whitened with ammonium chloride. Scale bar equals 30 mm.

147x193mm (300 x 300 DPI)

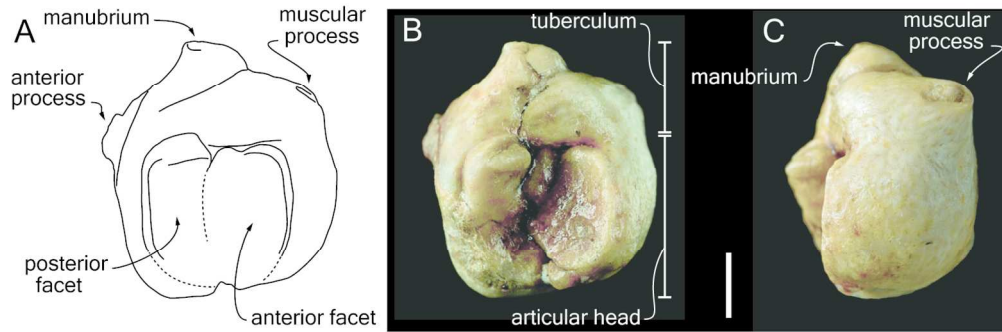


Figure 11. Right malleus of *Inticetus vertizi* MUSM 1980 (holotype). A, explanatory linear drawing in posteromedial view; B, corresponding photo; C, posteroventrolateral view. Scale bar equals 2 mm.

131x43mm (300 x 300 DPI)

Review Only



Figure 12. Detached upper teeth of *Inticetus vertizi* MUSEM 1980 (holotype). A-F, right I1 in labial (A), lingual (B), mesial (C), and distal (D) view, and detail of the crown in distolingual (E) and mesiolingual (F) view; G-L, right canine in labial (G), lingual (H), mesial (I), and distal (J) view, and detail of the crown in distolingual (K) and mesial (L) view. Scale bar equals 10 mm.

149x141mm (300 x 300 DPI)

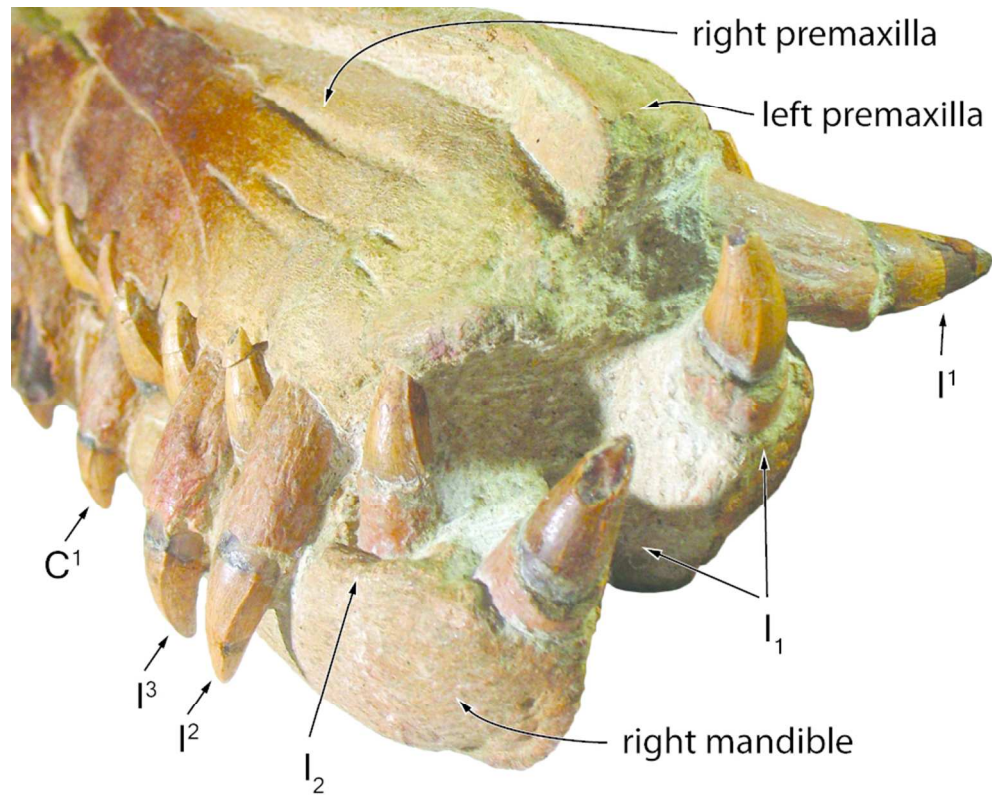


Figure 13. Cranium and mandibles of *Inticetus vertizi* MUSEM 1980 (holotype). Detail of the anterior part of the rostrum and mandible in oblique right anterolateral and slightly dorsal view, showing upper and lower anterior teeth. For the size of elements, refer to more orthogonal views.
Planned for column width.

84x67mm (300 x 300 DPI)



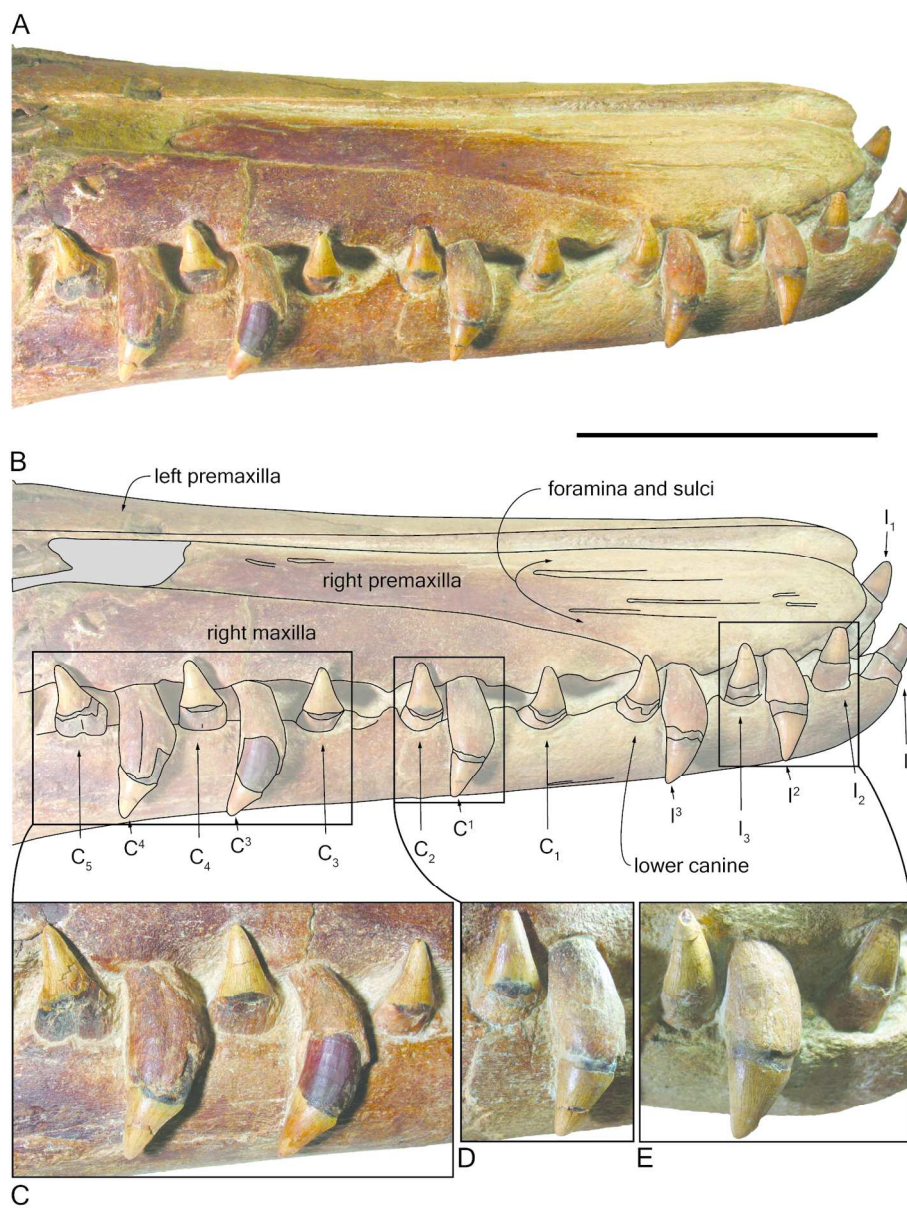


Figure 14. Cranium and mandibles of *Inticetus vertizi* MUSM 1980 (holotype). A, detail of the anterior part of the rostrum and mandible in right lateral view; B, corresponding explanatory linear drawing; C-E, enlarged views of anterior cheek teeth and incisors. Scale bar for A-B equals 100 mm.

141x185mm (300 x 300 DPI)

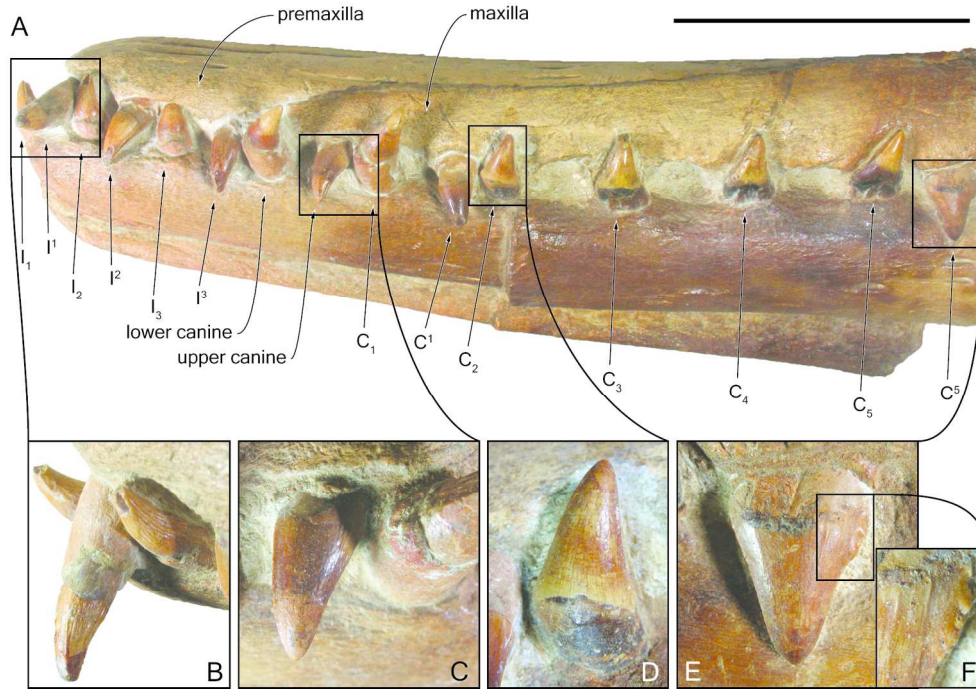


Figure 15. Cranium and mandibles of *Inticetus vertizi* MUSM 1980 (holotype). A, detail of the anterior part of the rostrum and mandible in left lateral view; B-E, enlarged views of incisors, upper canine, and anterior cheek teeth C2 and C5; F, detail of the accessory denticles on the distal keel of C5. Scale bar for A equals 100 mm.

160x109mm (300 x 300 DPI)

Only

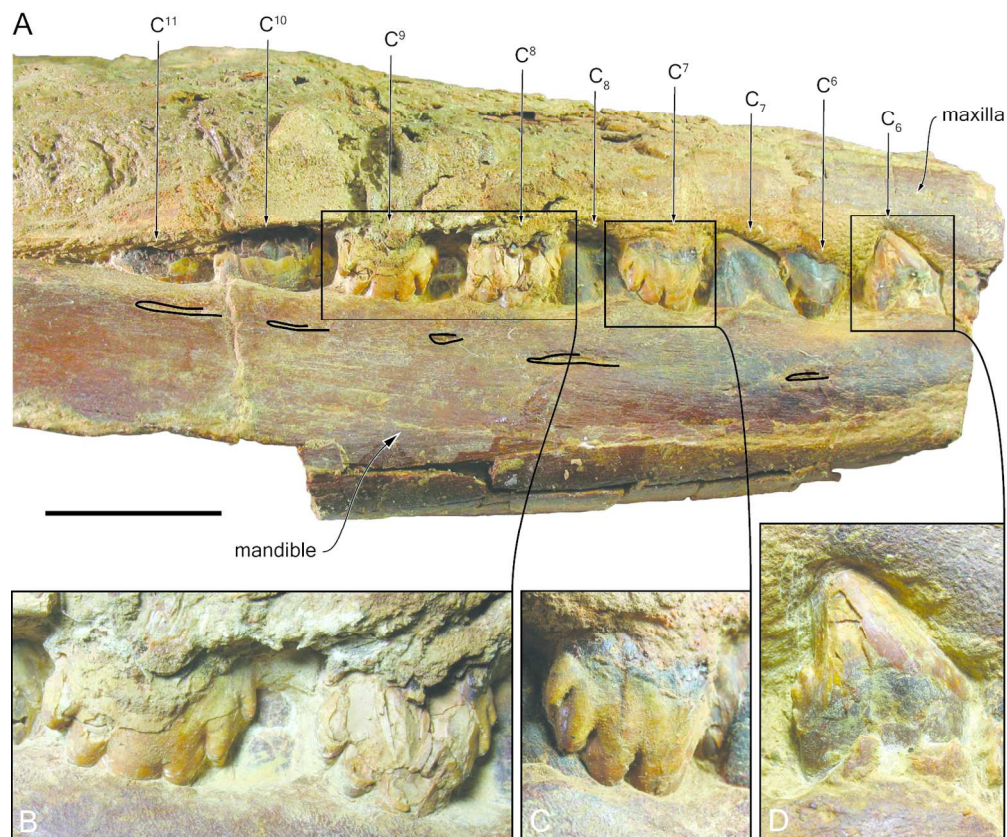


Figure 16. Cranium and mandibles of *Inticetus vertizi* MUSM 1980 (holotype). A, detail of the posterior part of the rostrum and mandible in right lateral view, with anterior part of the rostrum removed; B-D, detail of cheek teeth C⁹, C₈, C⁷, and C₆. Scale bar for A equals 50 mm.

139x116mm (300 x 300 DPI)

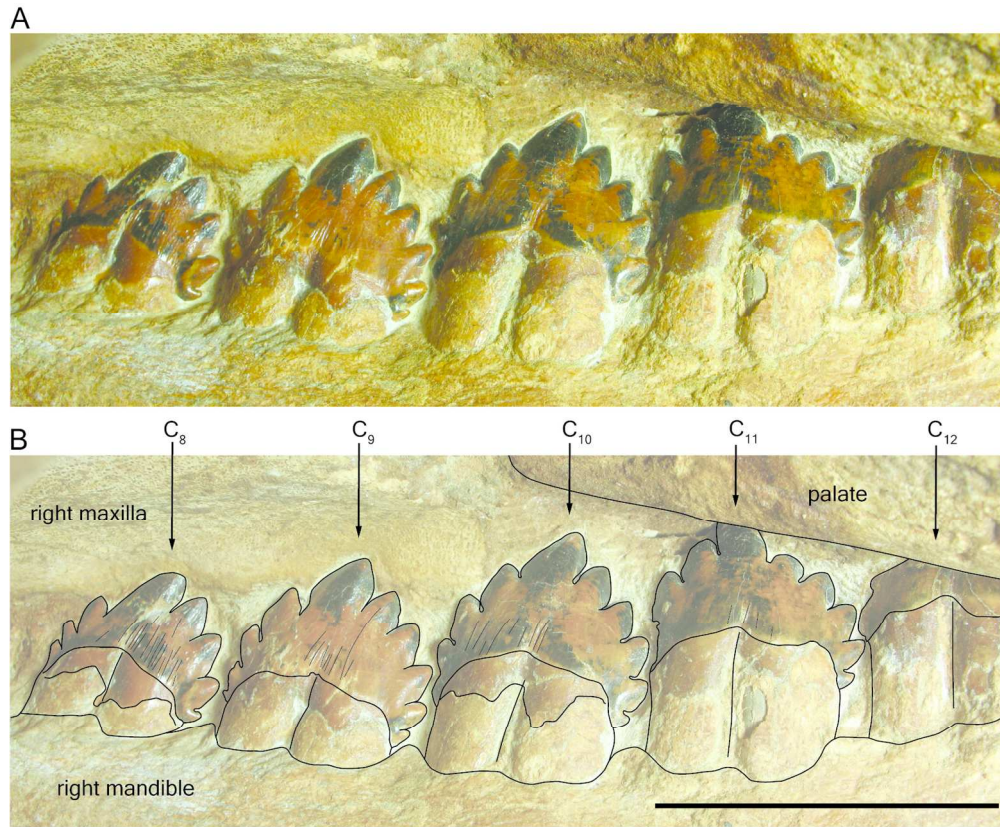


Figure 17. Cranium and mandibles of *Inticetus vertizi* MUSM 1980 (holotype). A, detail of the posterior part of the right lower tooth row including cheek teeth C8-12, in medial view; B, corresponding explanatory linear drawing. Scale bar equals 50 mm.

144x119mm (300 x 300 DPI)

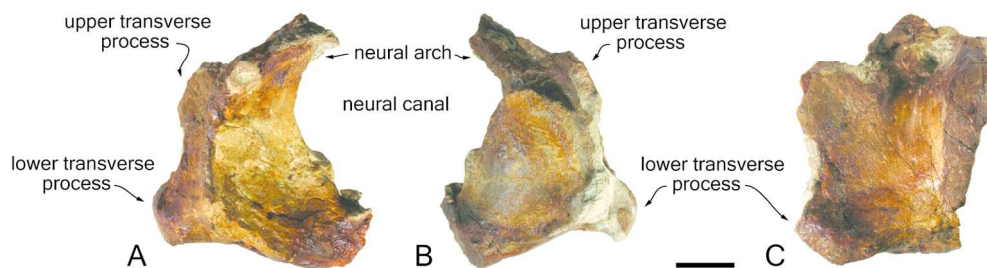


Figure 18. Fragment of the atlas of *Inticetus vertizi* MUSM 1980 (holotype). A, anterior view; B, posterior view. Scale bar equals 20 mm.

143x48mm (300 x 300 DPI)

Review Only

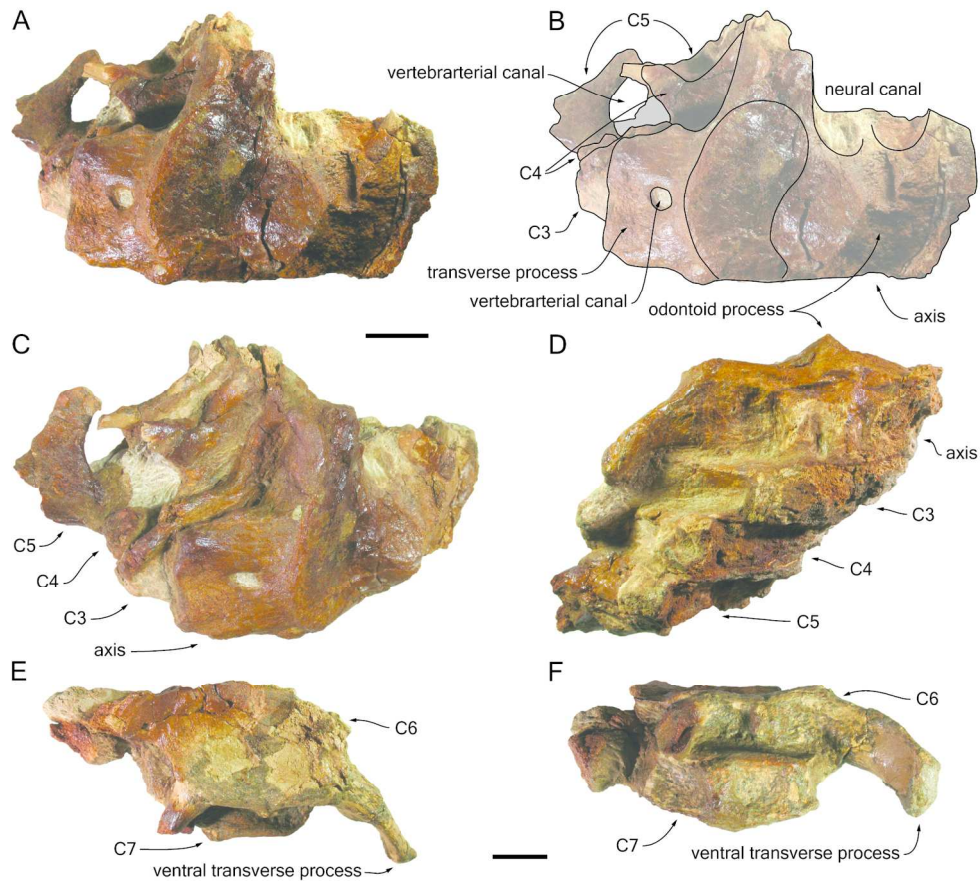


Figure 19. Axis and cervicals C3-C7 of *Inticetus vertizi* MUSM 1980 (holotype). A-D, axis and C3-C5 in anterior view (A), corresponding explanatory linear drawing (B), right anterodorsolateral (C), and ventral (D) view; E-F, C6-C7 in anterior (E) and ventral (F) view. Scale bar equals 20 mm.

157x139mm (300 x 300 DPI)

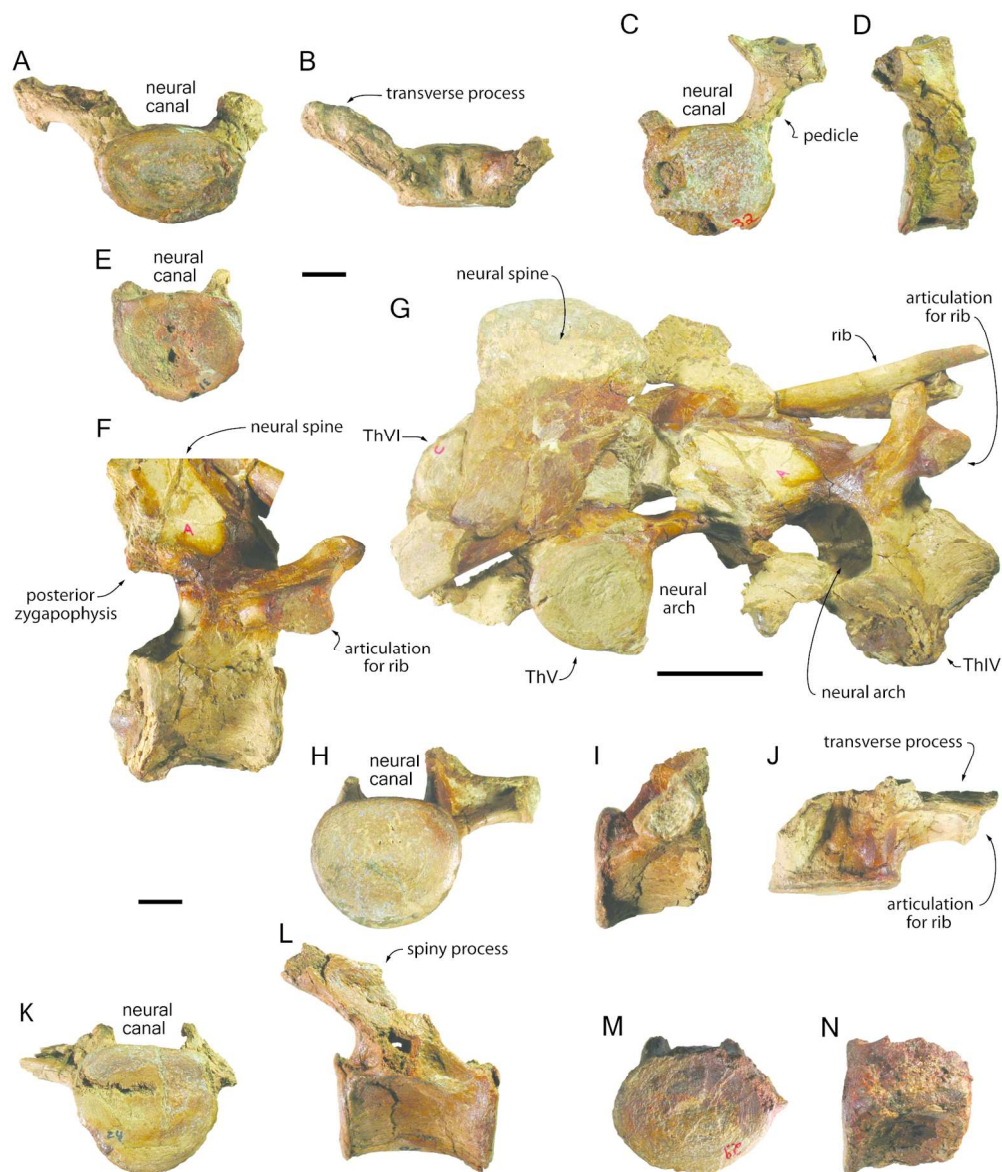
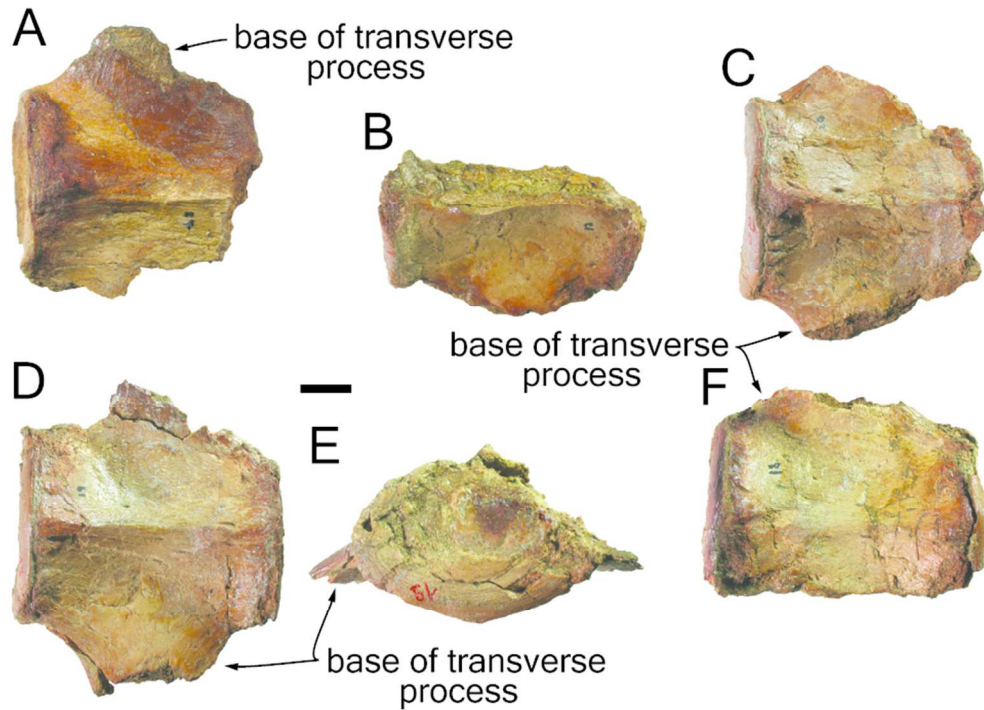


Figure 20. Thoracic vertebrae of *Inticetus vertizi* MUSEM 1980 (holotype). A-B, ThI in posterior (A) and dorsal (B) view; C-D, ThII in anterior (C) and left lateral (D) view; E, ThIII in anterior/posterior view; F, ThIV in right lateral view; G, ThIV-VI in a single block with a rib fragments; H-J, ThVII in posterior (H), right lateral (I), and dorsal (J) view; K, ThIX in right lateral view; L-M, ThXI in anterior/posterior (L) and lateral (M) view. Scale bar equals 20 mm.

155x182mm (300 x 300 DPI)



31 Figure 21. Lumbar vertebrae of *Inticetus vertzi* MUSM 1980 (holotype). A, LuIII in ventral view; B, LuVI in
32 dorsal view; C, LuVII in ventral view; D-E, LuVIII in ventral (D) and anterior/posterior (E) view; F, LuIX in
33 ventral view. Scale bar equals 20 mm.

34 Planned for column width.

35
36 82x58mm (300 x 300 DPI)

37
38
39
40
41
42
43
44
45
46
47
48
49
50
51
52
53
54
55
56
57
58
59
60

Only

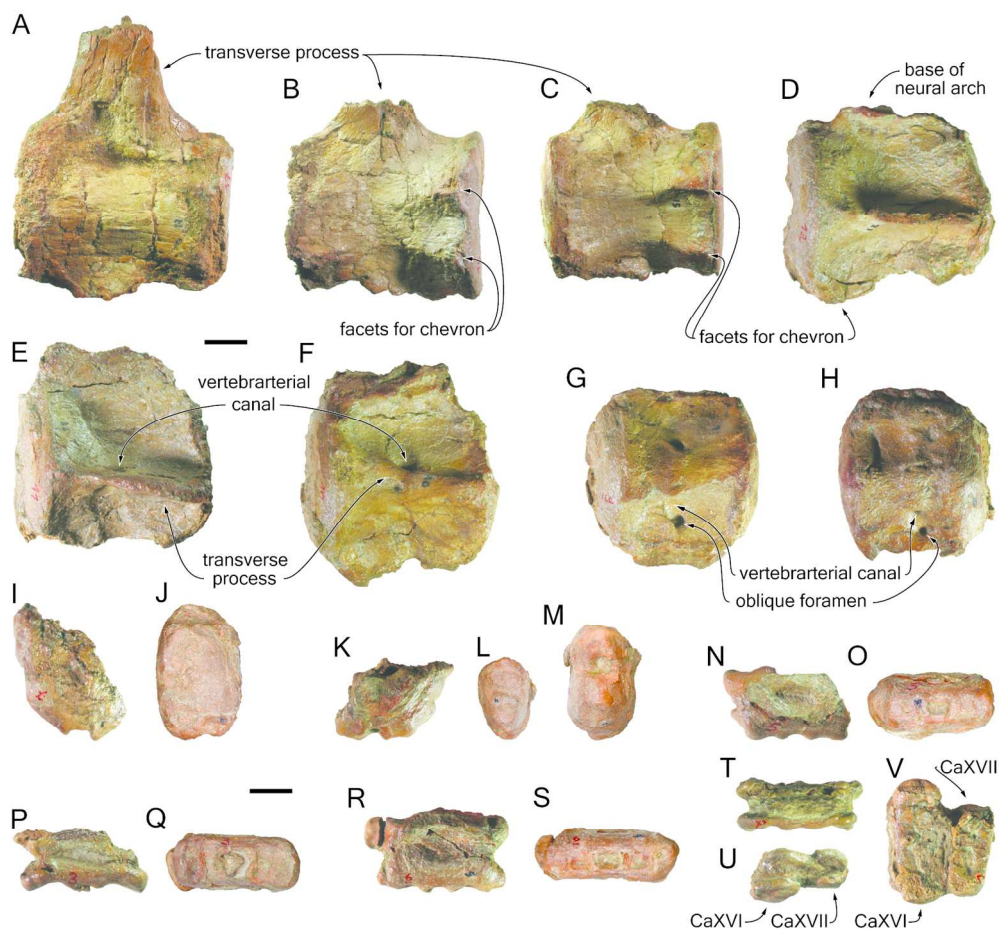


Figure 22. Caudal vertebrae of *Inticetus vertizi* MUSEM 1980 (holotype). A, CaI in ventral view; B, CaII in ventral view; C, CaIII in ventral view; D, CaVI in ?right lateral view; E, CaVII in ?left lateral view; F, CaVIII in ?left lateral view; G, CaIX in lateral view; H, CaX in lateral view; I-J, CaXI in anterior/posterior (I) and lateral (J) view; K-M, CaXII in anterior/posterior (K), lateral (L), and ventral (M) view; N-O, CaXIII in anterior/posterior (N) and ?ventral (O) view; P-Q, CaXIV in anterior/posterior (P) and ?ventral (Q) view; R-S, CaXV in anterior/posterior (R) and ?ventral (S) view; T, CaXVI in anterior view; U-V, CaXVI + CaXVII in left lateral (U) and ventral (V) view. Scale bar equals 20 mm.

154x142mm (300 x 300 DPI)

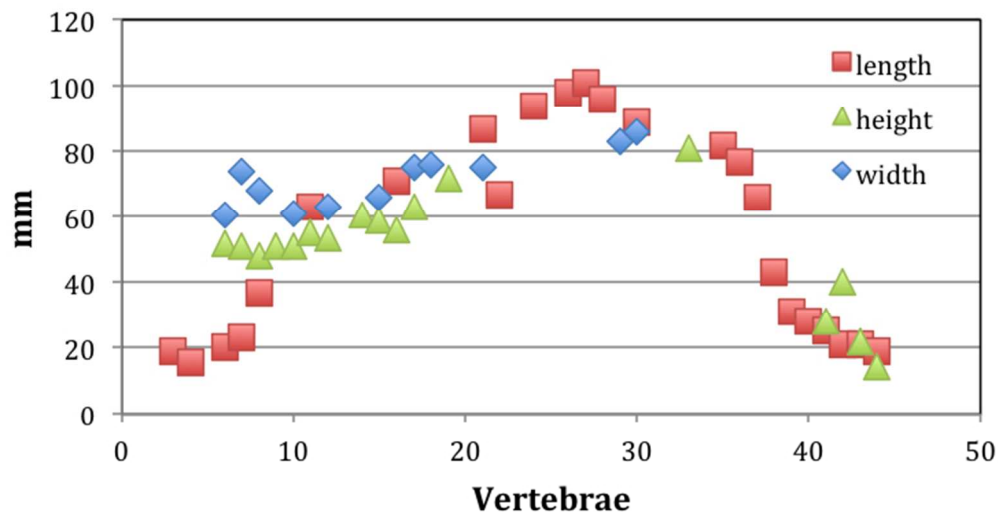


Figure 23. Chart showing changes in the dimensions (in mm) of vertebral central (namely length, height and width) along the vertebral column of *Inticetus vertizi* MUSM 1980 (holotype). Numbers on the horizontal axis correspond to a sequence from cervical C3 on the left to the last preserved caudals on the right, as listed in Table 3. Some vertebrae could be missing and several centra were too incomplete to be measured for one or more of their dimensions.

123x64mm (150 x 150 DPI)

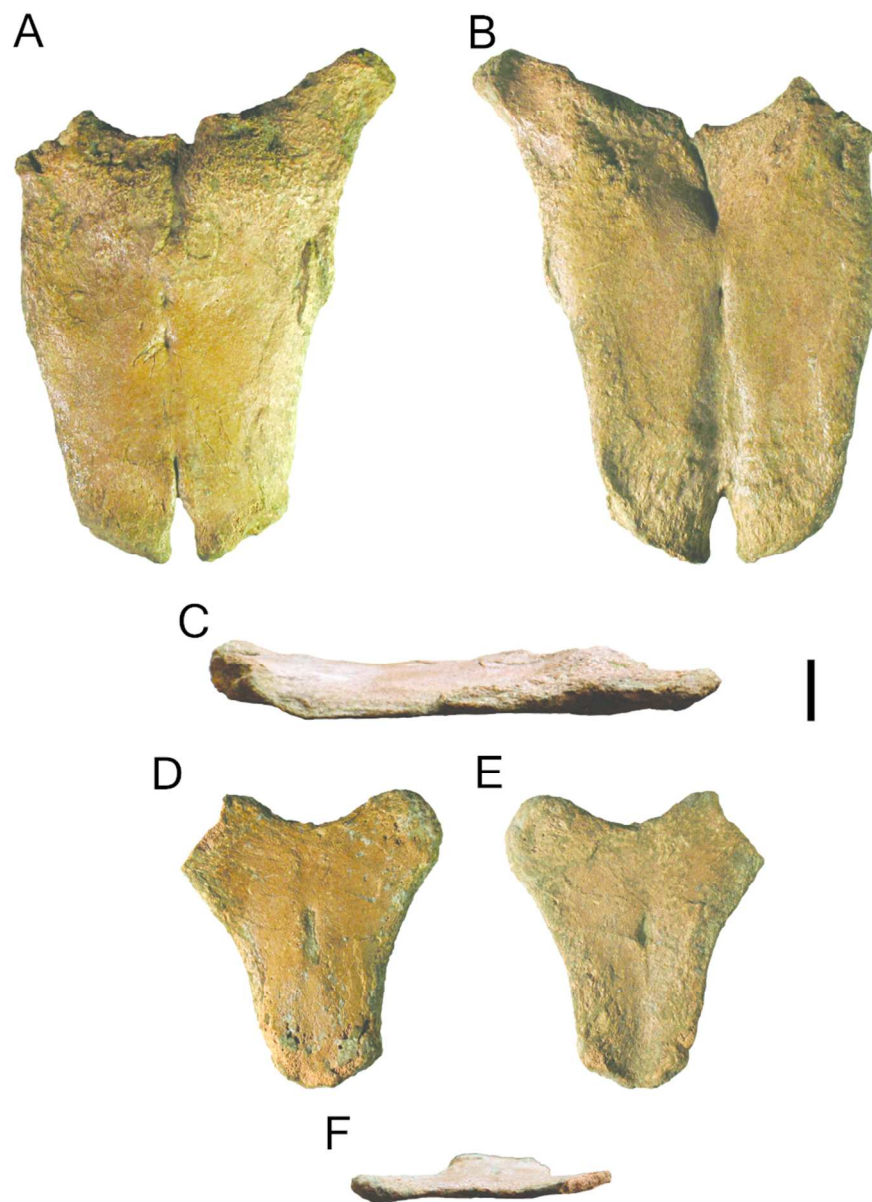


Figure 24. Sternum of *Inticetus vertizi* MUSM 1980 (holotype). A-B, manubrium in dorsal (A), ventral (B), and right lateral (C) view; D-F, second sternebra in ?dorsal (D), ?ventral (E), and anterior (F) view. Scale bar equals 20 mm.

83x109mm (300 x 300 DPI)

1
2
3
4
5
6
7
8
9
10
11
12
13
14
15
16
17
18
19
20
21
22
23
24
25
26
27
28
29
30
31
32
33
34
35
36
37
38
39
40
41
42
43
44
45
46
47
48
49
50
51
52
53
54
55
56
57
58
59
60



Figure 25. Ribs of *Inticetus vertizi* MUSM 1980 (holotype). The rib fragments are organized in an anteroposterior sequence from the lower part of the figure to the top, except for the two lower distal fragments. Scale bar equals 50 mm.

156x168mm (300 x 300 DPI)

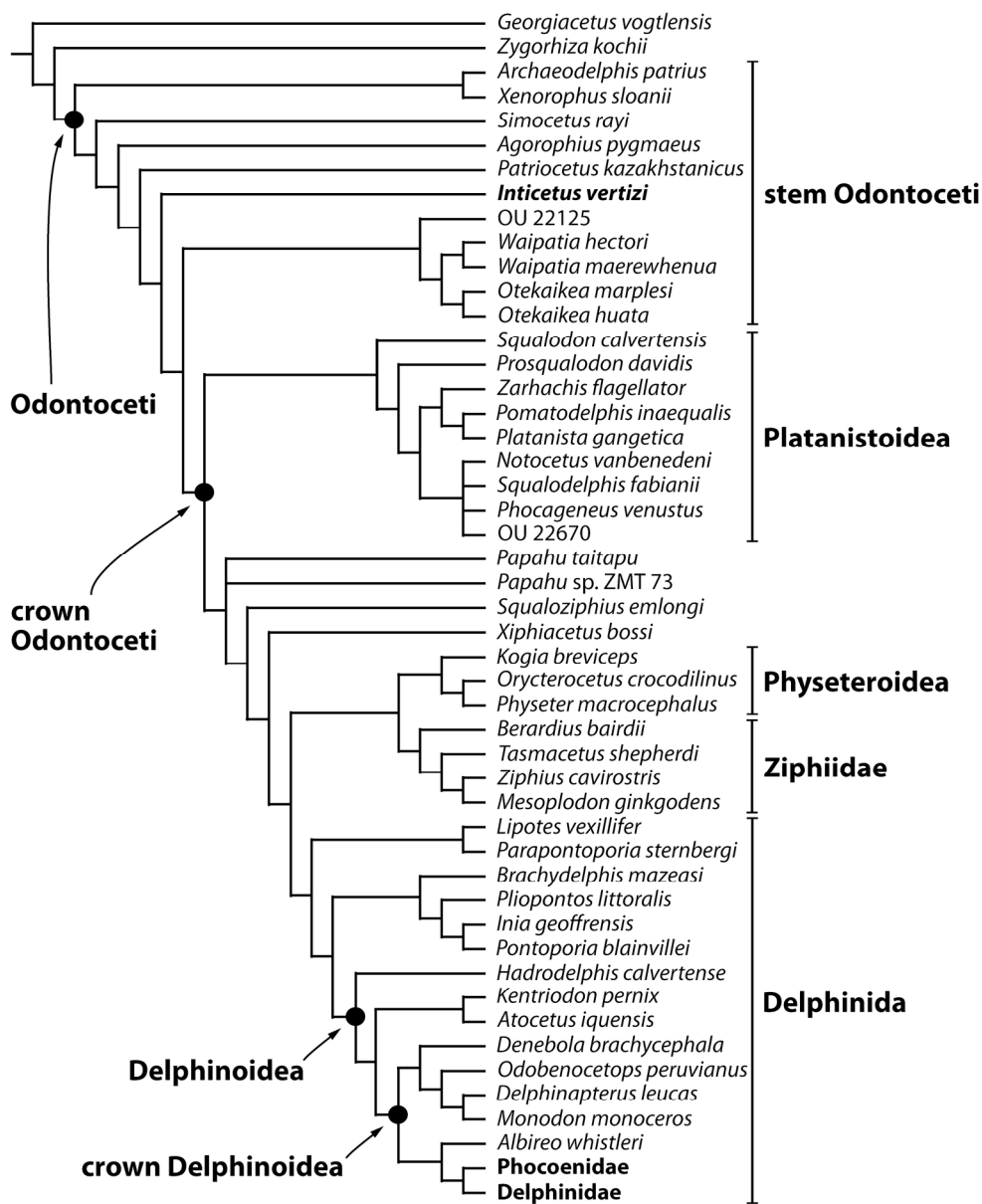


Figure 26. Strict consensus tree for the phylogenetic analysis with equally weighted characters and without molecular constraint (analysis 1), resulting in the placement of *Inticetus vertizi* as a stem Odontoceti.

173x213mm (300 x 300 DPI)

1
2
3
4
5
6
7
8
9
10
11
12
13
14
15
16
17
18
19
20
21
22
23
24
25
26
27
28
29
30
31
32
33
34
35
36
37
38
39
40
41
42
43
44
45
46
47
48
49
50
51
52
53
54
55
56
57
58
59
60

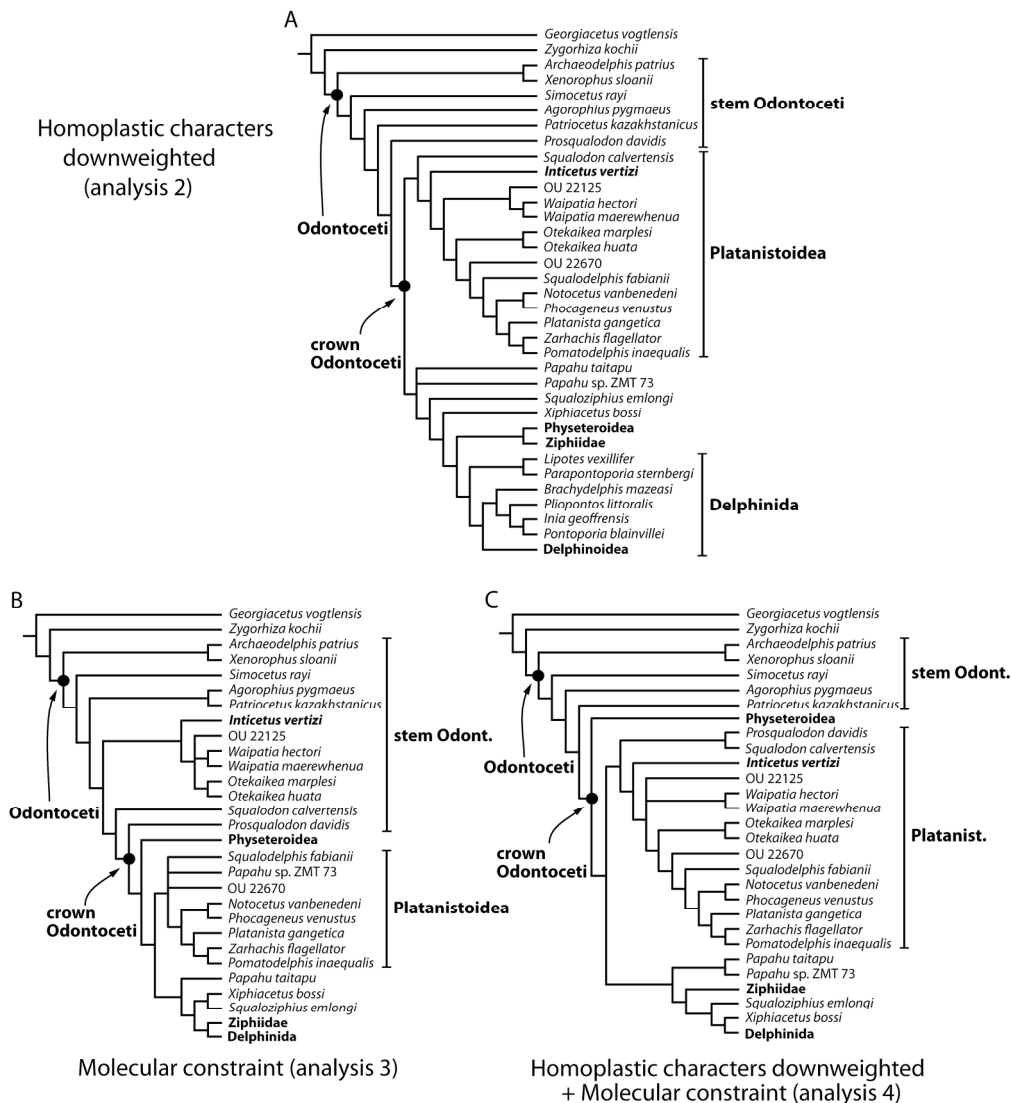


Figure 27. Alternative relationships of *Inticetus vertizi* resulting from other phylogenetic analyses. A, strict consensus tree for the analysis with down-weighted homoplastic characters and without molecular constraint (analysis 2), placing *I. vertizi* in a large Platanistoidea clade; B, strict consensus tree for the analysis with equally weighted homoplastic characters and with molecular constraint (analysis 3), placing *I. vertizi* as a stem Odontoceti; C, strict consensus tree for the analysis with down-weighted homoplastic characters and with molecular constraint (analysis 4), placing *I. vertizi* in a large Platanistoidea clade.

192x211mm (300 x 300 DPI)

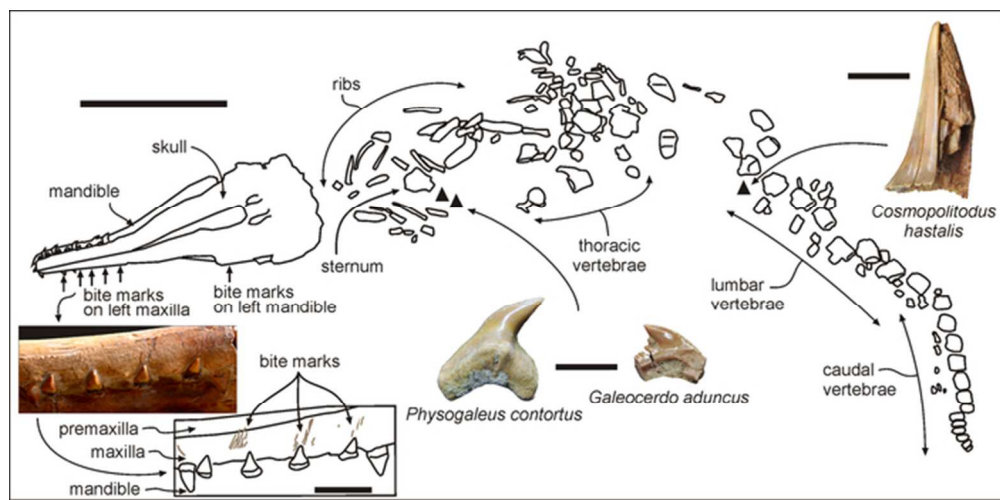


Figure 28. Schematic drawing showing the position of the partly articulated skeleton of *Inticetus vertizi* MUSM 1980 (holotype) as found in the field, together with three shark teeth (black triangles). Detail photograph and interpretive drawing of the rostrum and mandible of MUSM 1980 in left lateral view, with shallow shark bite marks indicated. Scale bar for the skeleton equals 500 mm, scale bar for detail of the rostrum and mandible equals 50 mm, and scale bars for shark teeth equal 10 mm.

59x29mm (300 x 300 DPI)